ARMY RESEARCH LABORATORY

Investigation of the UH-60 Main Rotor Spindle Assembly Retaining Rods P/N 70102-08102/-103

by Scott M. Grendahl

ARL-TR-1585 January 1998

The findings in this report are not to be construed as an official Department of the Army position unless so designated by other authorized documents.

Citation of manufacturer's or trade names does not constitute an official endorsement or approval of the use thereof.

Destroy this report when it is no longer needed. Do not return it to the originator.

Army Research Laboratory
Aberdeen Proving Ground, MD 21005-5066

ARL-TR-1585 **January 1998**

Investigation of the UH-60 Main Rotor Spindle Assembly Retaining Rods P/N 70102-08102/-103

Scott M. Grendahl
Weapons and Materials Research Directorate, ARL

Abstract

The U.S. Army Research Laboratory (ARL) was tasked by the U.S. Army Aviation and Troop Command (ATCOM) to perform a metallurgical examination of main rotor spindle assembly retaining rods fabricated from precipitation hardened (PH 13-8 Mo) stainless steel by three different manufacturers. These components were subjected to prior spectrum load fatigue testing in order to qualify an alternate source. One of the manufacturer's components exhibited only half the fatigue resistance of the other two. The results of fatigue testing (of coupons sectioned from the original rods) showed a dramatic difference between the rods. Metallography was utilized to examine the microstructure and grain size. The structure of each rod was consistent with the prior treatment, and the grain size met the governing requirement. The amount of delta (free) ferrite within the structure varied slightly from rod to rod, but was well within the specified limits. The threads of each rod were examined metallographically, since this was the area of failure as a result of the spectrum load fatigue testing. Although differences in the surface profile of the threads from the different manufacturers were noted, there was no evidence of gross abnormalities such as tear out or chatter. The chemical analysis of each rod varied, but each composition met the governing requirements. Based upon the results of reheat treating, it was concluded that an inadequate prior heat treatment sequence was performed by the manufacturer.

Acknowledgments

The author would like to thank Mr. Victor Champagne and Mr. Marc Pepi (both from the U.S. Army Research Laboratory [ARL], Weapons and Materials Research Directorate [WMRD]) and Dr. Kirit Bhansali (U.S. Army Aviation and Troop Command [ATCOM]) for their fruitful discussions and input concerning this work. Also, the author would like to acknowledge Mr. Jim Catalano, Mr. Joshua Nisenbaum, and Mr. Christopher Singer (all from ARL-WMRD) and Mr. Brad Waterson (Worcester Polytechnic Institute, Worcester, MA) for making data contributions to this work.

INTENTIONALLY LEFT BLANK.

Table of Contents

List of Figures

INTENTIONALLY LEFT BLANK.

List of Tables

INTENTIONALLY LEFT BLANK.

1. Introduction

The purpose of this investigation was to determine the root cause of the differences seen in the fatigue test data of UH-60 main rotor spindle assembly retaining rods from three different vendors.

2. Background

The U.S. Army Aviation and Troop Command (ATCOM) requested the U.S. Army Research Laboratory (ARL), Materials Division (MD) to perform a metallurgical investigation of multiple fatigue-tested main rotor spindle tie rods from the UH-60 Blackhawk helicopter. Sikorsky (SIK) Helicopter had fabricated two of the retaining rods identified as SN C504-00973 (-00973) and D504-00938 (-00938). Purdy Manufacturing Corporation (PUR) had manufactured two retaining rods identified as SNs 33129-177 (-177) and 33129-174 (-174). The remaining rods were fabricated by S&S Precision Machine Corporation and were identified as SNs 34969-2 (-2) and 34969-3 (-3). When tested at the Army Aviation Applied Technology Directorate (AATD) in Fort Eustis, VA, for fatigue performance, the six rods had different cycles to failure, as seen in Table 1. All of the retaining rods failed under cyclic loading during fatigue performance testing as part of a second-source qualification program for these components. This investigation was conducted in an attempt to determine the root cause of the observed difference in fatigue life.

Table 1. Axial Cyclic Fatigue Testing Results From AATD

Specimen No.	No. of Cycles
S&S -2	94,335
S&S -3	131,460
SIK -00938	108,460
SIK -00973	157,274
PUR -174	46,735
PUR -177	54,637

3. Governing Specifications

The following specifications are the governing documents in the fabrication of subject components:

- SIK engineering drawing for P/N 70102-08102/103 [1];
- Aerospace Material Specification (AMS) 5629, "Steel, Corrosion Resistant, Bars, Forgings, Rings, and Extrusions" [2];
- AMS 2315, "Determination of Free Ferrite Content" [3]; and
- MIL-S-8879, "Screw Threads, Controlled Radius Root With Increased Minor Diameter" [4].

4. Visual Examination/Light Optical Microscopy

The as-received condition of the two halves of the failed retaining rods manufactured by SIK -00938 and -00973 are depicted in Figures 1–4, respectively. The as-received condition of the two halves of the failed retaining rods manufactured by PUR -174 and -177 are shown in Figures 5–8, respectively. Figures 9 and 10 depict the as-received failed retaining rods (opposite fracture halves were not received) manufactured by S&S -2 and -3, respectively. Each of the six failed spindle retaining rods was visually examined utilizing light optical microscopy. All six failures originated within the threaded section of the respective rods.

The fracture surfaces of the two failed fatigue rods fabricated by SIK were slightly different in appearance than those manufactured by PUR. The fracture surfaces of the specimens -00938 and -00973 are depicted in Figures 11 and 12, respectively. The most striking difference on the fracture surface was the apparent change in shear angle of the overload region. The two specimens from PUR had shear angles of approximately 40–45°, while the specimens fabricated by SIK had shear angles around 75–80°. The regions of fatigue fracture were noticeably smaller on the SIK specimens, accounting for only approximately 50% of the fracture surface. Additionally, there were far fewer origin sites observed on the SIK specimens, and they were found on different thread roots.

The fracture surface of rod -00973 contained a classic thumbnail crack, as shown in Figure 13. The fracture surfaces of the SIK rods contained at least two competing fatigue crack fronts on each specimen.

It was observed that the two failed specimens fabricated by PUR had relatively flat uniform fracture surfaces indicative of most fatigue failures. The two failed specimens had fracture surfaces that were remarkably similar. Multiple origin sites (greater than 20) were observed on both surfaces, all initiating along the root radius of the same thread. The surface profiles of the threads were examined and compared to those of SIK rods. The roots of the PUR threads were slightly rougher, containing more pronounced tool marks. No other abnormalities were observed along the threads. The fatigue zones covered approximately 80% of the fracture surface of the PUR rods, while the overload regions accounted for only 20% of the fracture surface. The fracture surfaces of the PUR failed specimens -174 and -177 are presented in Figures 14 and 15, respectively. The fatigue cracks propagated on a single plane, and no evidence of competing or secondary cracks was noted.

The fracture surface of S&S rod -2 resembled that of both SIK rods. Fracture propagated on two competing crack fronts, giving a total fatigue region of approximately 40% as depicted in Figure 16. This specimen had an initial shear angle of 75–80° that progressed onto another shear plane of approximately 40–45°. The fracture surface of S&S specimen -3, in comparison, appeared similar to the PUR rods as shown in Figure 17. The fatigue region appeared fairly flat and uniform, although two competing crack fronts were observed, totaling 70% of the fracture surface. A classic thumbnail feature that comprised the secondary fracture, is depicted in Figure 18. Like both PUR specimens, specimen -3 had a 40–45° shear angle.

4.1 Dimensional Inspection. The threads of each specimen were inspected utilizing an optical comparison. According to the governing specification, the thread dimensions should conform to MIL-S-8879. *Table III, Fine Thread Series* of MIL-S-8879 references the dimensional acceptance criteria for thread characteristics. Table 2 outlines the acceptance criteria for the threads along with the data acquired for the six test specimens for the external thread, UNJF Class 3A. The values indicated are the average of three measurements obtained. Except for the root radii of SIK -00938

Table 2. Retaining Rod Thread Dimensional Analysis Data

Specimen No.	Basic Size	Threads Per Inch	Major Diameter		Pitch Diameter		Minor Diameter		Root Radius	
MIL-S-8879	1.25	12	Min.	Max.	Min.	Max.	Min.	Max.	Min.	Max.
			1.2386	1.2500	1.1913	1.1959	1.1442	1.1538	0.0125	0.0150
SIK -00938	1.25	12	1.2445		1.19525		1.1463		**0.01082**	
SIK -00973	1.25	12	1.2464		1.19433		1.1487		0.0135	
PUR -174	1.25	12	1.2491		1.19446		1.1480		**0.0217**	
PUR -177	1.25	12	1.2487		1.19506		1.1491		0.0142	
S&S -2	1.25	12	1.2429		1.1951		1.1511		0.0146	
S&S -3	1.25	12	1.2409		1.1941		1.1501		0.0146	

NOTE: The **bold** data indicate a value out of tolerance.

and PUR -174, all measurements are within the specified limits. It was determined that neither radius discrepancy greatly affected that outcome of the fatigue performance testing.

4.2 Surface Roughness. Each of the six failed retaining rods was examined with respect to surface roughness. Both the thread roots and the outside surface finishes were examined. ARL contacted Lasertec USA Inc., for scanning confocal laser (SCL) analysis (with the use of a 1LM21W laser scanning microscope) of the thread roots of the rods. SCL analysis is a sophisticated technique utilized to determine the surface characteristics of small areas. Lasertec evaluated one typical thread root from SIK -00938, S&S -3, and PUR -177. Linear scans were conducted at 500x and 1,250x magnification. A three-dimensional (3-D) color profile was also generated at 1,250x magnification for each rod thread root for comparison. The linear scans for the SIK, S&S, and PUR rod thread roots can be seen in Figures 19–24 respectively. The laser line scan was generated along the horizontal white line at 0.00 µm in the figures (indicated by the arrows). The output produced is represented by the jagged curved lines in the figures. An approximated depth is provided in micrometers. All of the generated output is then presented over an image of the thread roots precisely where the scan was taken. The laser provides less accurate information where the thread root walls become very steep (the darker regions within Figures 19–24). Although, it is quite evident from other analyses (optical microscopy and scanning electron microscopy [SEM]) that the deep "gouges" recorded by the line scan in the darker areas of the figures are fictitious, this technique allows for a quantitative comparison of the relative surface roughness within the thread roots that is unavailable by other means. It is clearly demonstrated in the figures that the S&S thread root is much "smoother" than either the SIK or PUR thread roots. The 3-D color profiles generated for the three samples from SIK, S&S, and PUR are depicted in Figures 25–27, respectively. While these scans do not provide much quantitative data, it is clearly demonstrated that the S&S thread root is the smoothest and best formed. It must be understood that the light-blue "mountains" on the color images are asperities (dirt and dust) on the surfaces and are not of concern. The "U" shape of the thread root and the overall "waviness" of the surface are the crucial factors.

Measurements of the surface finish were taken along the end of the rods (region A, Figure 28) and the unpainted shank (region B, Figure 28). The surface profile was measured utilizing a Mitutoyo Surftest Analyzer in three places along the part in the locations noted in Figure 28.

Table 3 presents the data obtained during surface roughness testing. The data were measured as root mean square (RMS), in microinches. Five readings were taken at each region as presented. The governing specification requires a surface finish of 125-µin maximum. The results in Table 3 show that although the surface finish values of the components from each vendor were well within the requirements, the SIK components were slightly smoother than the PUR and much smoother than the S&S components in both regions A and B (Figure 28).

Table 3. Surface Finish Results

Specimen No.	Region A	Average Requirement	Region B	Average Requirement
70102-08102/103	—	(<125 µin)	—	(<125 µin)
S&S -2	60-60-66	62.0	52-45-54	50.3
S&S -3	100-104-104	102.7	87-91-83	87
SIK -00938	25-26-26-25-25	25.4	25-21-21-16-18	20.2
SIK -00973	15-13-18-21-25	18.4	8-12-16-16-12	12.8
PUR -174	43-43-43-43-42	42.8	21-18-34-30-24	25.4
PUR -177	45-45-46-47-46	45.8	10-16-14-12-14	13.2

5. Mechanical Testing

5.1 Hardness. Specification AMS 5629 and SIK part drawing 70102-08102 designate a hardness of 40–44 HRc for the H1050 heat-treat condition of precipitation hardened (PH) 13-8 material. Surface macrohardness was determined from Rockwell C scale measurements directly on the part utilizing a 150-kg major load. A total of 10 readings was obtained from each specimen. The

data acquired were corrected according to the standard round work correction for cylindrical specimens. These data are presented in Table 4. In addition, the typical hardness of the H1000, H1050, and H1100 conditions as received from Armco Steel Corporation [5] are listed. The hardness values obtained conformed to the governing specifications. The values obtained from the SIK components were generally higher than the respective components fabricated by S&S and PUR; however, the S&S hardness values more closely resembled the SIK values than the PUR values. Additionally, both the SIK and S&S specimens exhibited a hardness that exceeded the minimum standards for AMS 5629 H1025 conditions. This suggested the SIK and S&S rods were heat-treated closer to an AMS 5629 H1025 condition rather than the required H1050. Although the minimum hardness requirement does not differ much between the H1050 and H1000 conditions, the hardness values of the SIK and S&S components were closer to the typical values of H1000 than the PUR components. The relative difference in hardness between the SIK, S&S, and PUR samples was consistent with their respective tensile properties. The highest hardness values were from SIK, which also had the highest tensile strength (see section 5.2).

5.2 Tensile Testing. Specification AMS 5629 outlines the requirements for the tensile properties of PH 13-8 material heat-treated to the H1050 condition. A tensile specimen was fabricated from each of the six retaining rods in order to confirm the mechanical properties of the H1050 heat treatment. Only one tensile specimen was fabricated from each retaining rod, since a heavier priority was placed on fatigue testing (see section 5.3). Cylindrical rods were sectioned from the components by wire electrical discharge machining (EDM), and final machining was performed to achieve the dimensions schematically illustrated in Figure 29. Figure 30 shows a representative tensile and fatigue specimen. Table 5 presents the results of ARL-MD tensile testing. Also listed are the minimal values of this given alloy in the H1000, H1025, and H1050 condition when tested in the longitudinal direction as stipulated within AMS 5629. In addition, the typical tensile properties of the H1000 and H1050 conditions as received from Armco Steel Corporation [6] are listed. The results indicated that the S&S material had been heat-treated to the H1050 condition, meeting both the minimal tensile properties of AMS 5629 and the typical properties established by Armco Steel. The results of the SIK specimens also conformed to the minimal and typical values of PH 13-8 in the H1050 condition. The PUR specimens met the minimal values of the tensile

Table 4. Macrohardness (Corrected) HRc Hardness Values 150-kg Major Load

SIK -00938	SIK -00973	PUR -174	PUR -177	S&S -2	S&S -3
41.9	42.2	40.7	40.4	41.7	42.5
41.9	42.3	40.9	40.9	41.0	42.7
43.4	40.7	40.6	41.3	41.7	41.2
41.2	42.3	40.3	41.1	42.0	40.8
42.5	41.2	40.8	41.1	39.8	42.5
41.8	40.6	40.2	40.7	41.7	42.2
40.8	42.3	40.4	39.8	40.3	41.1
42.4	42.0	40.5	40.7	41.1	41.4
43.0	42.2	40.4	40.0	41.9	42.2
43.4	42.1	40.2	40.5	41.6	43.0
Avg. 42.2	41.8	40.5	40.7	41.2	42.0

AMS 5629 H1000	43 min
AMS 5629 H1025	41 min
AMS 5629 H1050	40 min
Typical H1000 [5]	45
Typical H1050 [5]	41
Typical H1100 [5]	35

properties of H1050, but the values were much lower than the typical values of this condition. This difference in tensile properties may be related to the difference in fatigue properties (presented in the next section) noted both from the actual components and the specimens fabricated by ARL-MD. It is interesting that both the SIK and S&S specimens met the minimum tensile strength requirement for the H1025 condition, while the specimens fabricated by PUR did not.

Table 5. Tensile Testing Results

Specimen No.	Area (in^2)	0.2% YS (psi)	UTS (psi)	RA (%)	EL (%)
S&S -2	0.0495	185,100	195,800	65.7	13.8
S&S -3	0.0495	187,700	194,000	65.1	13.2
SIK -00938	0.0499	201,000	203,610	64.6	14.0
SIK -00973	0.0495	180,000	189,170	69.8	15.0
PUR -174	0.0491	178,710	180,340	65.0	16.0
PUR -177	0.0495	178,200	182,660	67.6	14.4
AMS 5629 H1000	(Long.)	190,000	205,000	50.0	10.0
AMS 5629 H1025	(Long.)	175,000	185,000	50.0	11.0
AMS 5629 H1050	(Long.)	165,000	175,000	50.0	12.0
Typical H1000 [6]	(Long.)	205,000	215,000	55.0	13.0
Typical H1050 [6]	(Long.)	180,000	190,000	55.0	15.0

Notes: YS = yield strength.
UTS = ultimate tensile strength.
RA = reduction in area.
EL = elongation.

5.3 Fatigue Testing. Fatigue specimens were fabricated and tested such that the results of the testing could be directly compared (i.e., all specimens were similarly machined with identical surface finishes). This would alleviate comparison of fatigue results of the actual components processed by different vendors, utilizing different tooling, methods, etc. In addition, the actual component fatigue failures occurred within the threads of each component, raising questions concerning the thread dimensions, surface finish, etc. The fatigue testing performed and presented within this work was accomplished in a manner that eliminated this variability. Two fatigue specimens were fabricated from SIK -00973, PUR -177, and one each from the S&S -2 and -3 retaining rods, to the dimensions shown schematically in Figure 31 and depicted pictorially in Figure 30. Testing was conducted on a Model 8502 Instron servohydraulic test machine, with an R (ratio of minimum stress to maximum stress in a fatigue cycle) value of 0.1 and a frequency of 25 Hz. As dictated by ATCOM, a stress

level of 170 ksi was utilized. The results revealed a definite material difference, as listed in Table 6. The PUR specimens failed at 83,020 and 168,567 cycles, respectively, while the SIK and S&S specimens did not fail after a total of 3 million cycles.

Table 6. ARL-MD Fatigue Testing Results

Specimen No.	Area (in^2)	Stress (ksi)	R	Frequency (Hz)	Cycles to Failure
S&S -2	0.0184	170	0.1	25	3,000,000+
S&S -3	0.0184	170	0.1	25	3,000,000+
SIK -00973	0.0184	170	0.1	25	3,000,000+
SIK -00973	0.0184	170	0.1	25	3,000,000+
PUR -177	0.0184	170	0.1	25	168,567
PUR -177	0.0184	170	0.1	25	83,020

6. Metallography

Alloy PH 13-8 Mo is a martensitic precipitation hardenable stainless steel with a composition balanced to prevent the formation of delta ferrite in the structure, low carbon content to minimize grain boundary carbide precipitation and double vacuum melting to reduce alloy segregation [7]. AMS 5629 lists two requirements as follows, with respect to the microstructure of this alloy.

- Microstructure - The product shall contain not more than 2% free ferrite, determined in accordance with AMS 2315 (3.4.1.2).

- Grain Size - Shall be five or finer for a product up to 3.00 in in nominal cross-sectional thickness with occasional grains as large as three determined by comparison of a polished and etched specimen with the chart in ASTM E 112 (3.4.2.1.3).

Metallographic samples representing the SIK, S&S, and PUR components were mounted in phenolic powder with edge retention and rough-polished with silicon carbide papers ranging in grit from 180 to 1,200. The samples were subsequently fine-polished utilizing 1-μ diamond suspension, followed by 0.05-μ colloidal silica. The structure of the samples was consistent with vacuum induction plus consumable electrode melted material in that there was no evidence of gross inclusions or anomalies in the as-polished condition. The samples were then etched using Vilella's reagent to compare the microstructural features. At low magnification, banding was noted within the structure of the PUR and, to a lesser degree, the S&S samples. The SIK samples contained relatively little banding. Banding is caused by chemical segregation and becomes increasingly prominent as the size of the original ingot increases. Figures 32–34 show examples of the structural banding noted within the PUR, S&S, and SIK samples, respectively. It should be noted that the banding shown for the SIK sample was the only region where any banding was observed and was not representative of the overall structure of the SIK samples. At higher magnification (100×, Figure 35), significant stringers of free (delta) ferrite were noted within the bands of the PUR samples. In addition, the free ferrite stringers were of greater length within the PUR samples. In comparison, samples of SIK and S&S exhibited considerably less delta ferrite, as shown in Figures 36 and 37. Delta ferrite forms within the bands due to the elements present from the prior segregation. Elements such as titanium, silicon, molybdenum, and chromium increase the tendency of delta ferrite formation [8]. Although an increased amount of free ferrite stringers was noted within the PUR samples, the total free ferrite was well below the AMS 5629 requirement of 2% maximum as determined by AMS 2315. As determined by visual examination, the total amount of free ferrite within a representative PUR sample was approximately 0.5%, as measured from a microphotograph. The region analyzed was representative of the overall PUR material. For comparative purposes, the regions of heaviest free ferrite content within the SIK and S&S samples were analyzed. These regions were not representative of the remaining SIK or S&S material; these were the only areas where significant free ferrite was noted. These regions contained approximately 0.05% free ferrite. Figures 38–40 represent typical stringers of free ferrite within the structure of the PUR, S&S, and SIK material, respectively.

At higher magnification (1,000×), the structures of the PUR, S&S, and SIK samples were compared in both the longitudinal and transverse directions. An attempt was made to characterize the heat treatment by microstructural analysis. However, during conversation with Armco representatives, it was confirmed that there is not much microstructural difference between these three conditions [5]. The structure of the SIK, S&S, and PUR material was similar, consisting of precipitated compounds within a martensitic matrix. The grain sizes of all the materials were similar in size and geometry in the longitudinal and transverse directions, when etched with a modified Vilella's reagent (additional HCl). Figures 41–46 show the structure and grain size of the PUR, S&S, and SIK samples in the longitudinal and transverse direction, respectively. The grain size of each sample was much finer than the "five" required by AMS 5629.

It was unknown whether the differences in hardness, tensile properties, and corresponding fatigue strength alone were enough to account for their response to the spectrum load fatigue tests. Therefore, closer examination of other material processing parameters was warranted. This led to an analysis of the external threads of the actual tie rods. Each of the three manufacturers was compared. Figures 47–49 are montages of a tapered cross-sectional metallographic sample taken through the threads of the S&S, SIK, and PUR tie rods, respectively. A light-etching cold-worked layer, a result of the thread-cutting operation, can be observed. In general, the layer on all three manufacturers tie rods was thickest at the thread roots and near the crest. The SIK white layer contained areas that were much thicker than either the S&S or PUR material. The PUR white layer appeared to be discontinuous in areas. Another observation made was the resistance to etching. The SIK material had a very high resistance to etching, taking several minutes before an acceptable microstructure appeared, while the PUR and S&S material etched much more quickly. These differences can be attributed in part to subtle differences in chemistry and/or heat treatment.

The uniformity of the machined surface of the threads was also examined metallographically. Figures 50–52 show as-polished metallographic samples taken perpendicular to the threads. These low-magnification photographs clearly show the surface condition of the machined threads. The machined surfaces of the S&S threads are by far the smoothest, while the that of PUR are the roughest. Figures 53–55 are scanning electron macrographs also showing the relative surface

condition of the threads for all three manufacturers. Figure 53 is a typical thread root representative of the S&S tie rods. The machine marks remnant from the thread-cutting operation are quite discernible and appear uniform. There was no evidence of chatter or gross abnormalities such as tear out on either of the S&S tie rods. Similar findings for SIK and PUR tie rods were observed. However, a relative ranking of "smoothness" in the thread area is quite easily discerned. As in the findings presented earlier by Lasertec, the S&S is the smoothest, followed by SIK and, finally, PUR.

7. Chemical Analysis

Chemical Analysis was performed by ARL-MD to verify the elemental composition of the SIK, S&S, and PUR retaining rods. The chemical composition was governed by AMS 5629. The material designated was PH 13-8, heat-treated to the H1050 condition. Inductively coupled plasma/atomic emission spectroscopy was utilized to determine the weight-percent of each element. Samples were sectioned from each of the six rods under investigation; SIK -00938 and -00973, S&S -2 and -3, and PUR -174 and -177. Table 7 lists the results of this testing as well as the required composition. Each sample conformed to specification AMS 5629, with the addition of several trace elements for the SIK and PUR samples, as listed in Table 7.

These elements were most likely the remnants of previous heats within the melt. Although the material from all vendors was within specification, small differences were noted in the manganese, silicon, chromium, nickel, and molybdenum content. In each case, the S&S samples contained a slightly higher percentage of these elements. The overall effect of a higher composition of these particular elements is an increase in the tensile strength and hardness of the material. It is indeterminate whether the small increases would have a significant impact on the overall performance of the rods under fatigue, but the S&S rods did have a higher hardness and tensile strength than the PUR rods. Additionally, the PUR material had a higher content of manganese than the SIK material, and higher phosphorus and cobalt than the SIK and S&S material. The cobalt composition is a function of the purity of the nickel, and compositions of up to 0.15% have been shown to have no effect on mechanical properties [5]. It is believed that the small difference in phosphorus content would also have no effect on the mechanical properties.

Table 7. Chemical Composition of the S&S, SIK, and PUR Material

Element	S&S -2	S&S -3	SIK -00938	SIK -00973	PUR -175	PUR -177	AMS 5629
Carbon	0.040	0.040	0.050	0.034	0.040	0.043	0.05 max.
Manganese	0.05	0.04	<0.01	<0.01	0.03	0.03	0.10 max.
Silicon	0.07	0.06	<0.01	<0.01	<0.01	<0.01	0.10 max.
Chromium	12.65	12.71	12.38	12.32	12.36	12.47	12.25–13.25
Nickel	8.21	8.27	7.93	7.82	7.94	7.81	7.5–8.5
Phosphorus	0.008	0.008	0.007	0.008	0.010	0.010	0.01 max.
Sulfur	<0.005	<0.005	0.002	0.002	0.001	0.001	0.008 max.
Molybdenum	2.18	2.17	2.15	2.09	2.11	2.06	2.0–2.5
Aluminum	0.96	1.02	1.05	1.08	1.14	1.15	0.9–1.35
Nitrogen	0.003	0.004	0.003	0.004	0.005	0.004	0.01 max.
Copper	<0.01	<0.01	<0.01	0.02	0.01	0.01	—
Vanadium	<0.01	<0.01	<0.01	<0.01	<0.01	<0.01	—
Titanium	<0.01	<0.01	0.01	0.02	0.01	0.01	—
Niobium	<0.01	<0.01	<0.01	<0.01	<0.01	<0.01	—
Cobalt	<0.01	<0.01	<0.01	<0.01	0.06	0.06	—
Magnesium	<0.01	<0.01	<0.01	<0.01	<0.01	<0.01	—
Iron	rem.	rem.	rem.	rem.	rem.	rem.	rem.

8. SEM

The fracture surfaces of the original failed tie rods were examined by SEM to determine the nature of failure and to investigate any possible fracture mode differences between the components fabricated by the three vendors. Figures 56–61 are schematics that illustrate the fracture surfaces and all the significant characteristics of SIK rods -00938, -00973, PUR rods -174, -177, and S&S rods

-2 and -3, respectively. As shown in Figure 56, the -00938 sample contained seven origins. One of the origins (right side of schematic) was on a different fracture plane than the remaining six origins. Fatigue progressed approximately 40% of the fracture surface as indicated by the transgranular fracture morphology, until final fast fracture occurred. This fast fracture was characterized by shear lips containing ductile dimples, indicative of tensile overload. Figures 62–70 are SEM micrographs that represent the fracture morphology of each of the regions illustrated in Figure 56. Figures 62 and 63 represent the origins, while Figure 64 shows the transgranular morphology characteristic of the fatigue zone. Figure 65 represents the fatigue and ductile interface, while Figure 66 represents typical striations on the fracture surface at low magnification. Figures 67–70 also represent the fatigue striations contained within the fracture surface at higher magnification.

SIK tie rod -00973 also contained seven origins, as shown in Figure 57. These origins were located on three different fracture planes. Fatigue progressed approximately 60% of the fracture surface until final fast fracture occurred. Figures 71 and 72 are representative of typical origins on the fracture surface. Figure 73 shows a transgranular/ductile morphology, while Figure 74 shows the transgranular morphology noted within the fatigue region. Figure 75 shows ductile dimples representative of the overload region. Figures 70–79 represent typical striations observed in the fatigue region.

The fracture surfaces of the PUR rods were markedly different from those of the SIK rods. The most notable differences were that the PUR rods contained a far greater number of origins, and these origins were all located on one plane. For example, rod -174 contained 24 origins (Figure 58), while rod -177 contained 32 origins (Figure 59). For each fracture surface, these origins were located on one plane. The origins of rod -177 were evenly dispersed along the periphery of the fatigue zone, while the origins of rod -174 were heavily grouped in one region. Another fractographic difference was the distinct zones on the PUR fracture surfaces compared to the SIK surfaces. The PUR surfaces contained a transgranular zone, followed by a transgranular/ductile zone, a ductile zone cyclic overload zone, and, finally, the shear lip region. For both the PUR rods, fatigue progressed approximately 75% of the fracture surface.

Figures 80–82 show low-magnification SEM micrographs of typical origins noted on the -174 fracture surface. Figures 83–86 represent the different morphologies noted on this fracture surface. Figure 82 shows the cyclic overload to shear transition region, while Figure 83 shows an example of cyclic overload. Figure 85 shows a cyclic overload morphology mixed with tearing, while Figure 86 is a morphology consisting of striations, tearing and ductility. Figures 87–91 represent the morphology within the fatigue regime.

Figure 92 shows a low-magnification SEM micrograph of a typical origin noted on the PUR -177 fracture surface (Figure 59), while Figure 93 depicts the typical transgranular cyclic fatigue morphology. Figure 92 shows a morphology consisting of tearing with striations. Figure 94 shows a morphology consisting of tearing and a transgranular mode, as well as slight ductility. Figure 95 contains striations mixed with ductility, as well as cyclic overload, while Figure 96 shows ductile dimples with evidence of incremental loading. Figure 97 shows these ductile dimples at higher magnification. Figures 98–102 represent typical fatigue striation differences noted on the fracture surface of the PUR specimens.

As shown in Figure 60, the S&S -2 sample contained 34 origins. Seven of the origins (bottom of schematic) were on a different fracture plane than the remaining origins. Fatigue progressed approximately 40% of the fracture surface as indicated by the transgranular fracture morphology, until final fast fracture occurred. This fast fracture was characterized by shear lips containing ductile dimples, indicative of tensile overload. Figures 103–106 are SEM micrographs that represent the fracture morphology of each of the regions of S&S rod -2 illustrated in Figure 60. Figure 103 represents a typical origin, while Figure 104 shows the transgranular morphology characteristic of the fatigue zone. The directional tearing in the shear region of S&S rod -2 is depicted in Figure 105. Figure 106 depicts the typical striation marking of the fatigue region in PH 13-8 Mo.

Tie rod S&S -3 contained 40 origins, as shown in Figure 61. These origins were located on three different fracture planes. Fatigue progressed approximately 80% of the fracture surface until final fast fracture occurred. Figure 107 is representative of a typical origin on the fracture surface. Figure 108 shows a transgranular morphology noted within the fatigue region of rod -3. Figure 109

shows ductile dimples representative of the overload region, while Figure 110 exhibits the 45° shear plane. Figure 111 represents the typical striation morphology of the fatigue region in the S&S rods.

The fracture surfaces of the S&S rod were markedly different from each other. Specimen -2 possessed origins on two different planes. The large shear zone with its steep angle makes it closely comparable to the SIK rods. Sample -3, on the other hand, was decidedly similar to the PUR specimens. Fatigue accounted for the majority of the fracture surface, while shearing was minimal. There is a clear cyclic overload zone that accounts for approximately 20% of the overall surface. Again, both samples developed a number of origins, 34 and 36, evenly dispersed along the periphery of the fatigue zone. The PUR rods followed with 24 and 32, respectively. Each SIK rod, however, only contained seven origins randomly located along the edge of the tie rod.

9. Discussion

9.1 Fracture Surfaces. The fracture surfaces of the failed S&S rod -2 and S&S rod -3 were markedly different. The main differences were the sizes of the fracture fatigue region and the angle of the resultant shear lips. S&S rod -2 had a small fatigue region resembling those regions found in the SIK rods. In contrast, S&S rod -3 had a fatigue region that covered 80% of its fracture surface, similar to the PUR specimens. The difference in shear angle was surprising, since shear angle is usually inherent in certain materials tested under similar loading conditions. However, a slight difference between the microstructures of the S&S rods did exist; banding was more prevalent on rod -2. This suggested that heat treatment of this material affects the shear angles more than chemical composition or other variables.

While S&S -2 resembled the SIK rods and -3 resembled the PUR rods, the fracture surfaces of both the failed SIK and PUR tie rods were markedly different from each other. The main difference was the angle of the resultant shear lips and the total size of the fatigue region. If the same material shears at drastically different angles under similar loading conditions, it may be characteristic of

slight changes or differences in matrix distortion on an atomic level, which would in turn modify the slip system of the material.

9.2 Tensile and Fatigue Testing. There was a general correlation between the tensile properties and fatigue resistance among the three manufacturers. Those specimens (S&S and SIK) that had a higher tensile strength and hardness also showed greater values of fatigue in both actual component and laboratory specimen fatigue testing. The S&S material satisfied both the minimal and typical values for tensile properties as listed in Table 5. The tensile and hardness data indicate that the PUR material, although satisfying the minimal requirements for yield strength and UTS, falls short of satisfying the "typical" values for the H1050 condition listed within Table 5. These "typical" values were provided to ARL-MD by Armco Steel Corporation, the developer of the PH 13-8 Mo alloy. The SIK material not only meets the minimal and typical values of UTS, but of the two tensile specimens tested, one actually exhibited a UTS value 13 ksi higher than the typical value and fell close to the minimal requirement for the H1000 condition. Additional tension and fatigue testing would be required to obtain a greater understanding of the exact relationship between the difference in UTS and fatigue behavior observed in each material. However, it can be stated from the data obtained, that material that only satisfied minimal tensile properties was most likely to fail the fatigue criteria, while material meeting the typical tensile properties was most likely to pass fatigue testing.

9.3 Microstructural Differences. The PUR material contained more extensive banding and delta ferrite stringers than the SIK material. The material specification AMS 5629 limits the amount of delta ferrite to 2%. Delta ferrite can adversely affect the fatigue resistance of this alloy in concentrations greater than 5% [7]. The S&S rods contained limited banding and delta ferrite stringers. One rod had a microstructure comparable to that found in the SIK rods, while the other more closely resembled the PUR microstructure. However, it has been deduced by metallography that the amount of free ferrite in the S&S material is much less than 2%. It was not thought that the difference in amount of free ferrite observed would solely account for the difference in the mechanical performance of the material form the three different vendors.

A cold-worked layer formed as a result of the thread-cutting operation on the external threads of the tie rods. Moreover, the surface finish differed between each manufacturer in the threaded region. These differences can attribute to differences in fatigue behavior. The magnitude of its effects is not quantifiable by metallurgical evaluation.

10. Conclusions

- A significant difference in the mechanical performance of the material from the three different vendors was observed and verified.

- The difference in performance could not be directly linked to any metallographic variance noticed due to the similarity of the microstructures.

- The most likely explanation for the difference observed in the mechanical performance of the materials lies within a variation of the heat treatment utilized by the three different vendors.

- Surface Profile: The average surface profile for all vendors was well below the 125-µin maximum specified on the engineering drawing (SIK 70102-08102/103).

- Hardness: The hardness of all three materials satisfied the material specification AMS 5629 of HRc 40 minimum.

- Tensile Properties: The data recorded from the tensile specimens indicated that the S&S and SIK tie rods met the minimal values contained in AMS 5629 for the H1050 condition and the typical values established by Armco Steel Corporation.

- Fatigue Testing: Two S&S and SIK fatigue specimens tested at a level of 170 ksi with an R value of 0.1 and a frequency of 25 Hz did not fail after 3 million cycles.

- Metallography: All three materials were clean, having no gross inclusions or inherent material defects, consistent with a vacuum induction plus consumable electrode melted stainless steel. The AMS 5629 requirement of 2% maximum free ferrite was easily met by the all three materials. Only slight banding and traces of free ferrite stringers were observed on the S&S and SIK materials. The grain size of all three materials was much finer than the "five" required by AMS 5629.

- Tie Rod Threads: The surface finish of the S&S thread roots was much smoother than the other manufacturers, while the PUR finish was the roughest. The cold-worked layer of the SIK thread roots contained regions much thicker than the others, and that of PUR showed the most discontinuities.

- Fractography: The two S&S tie rods broken in fatigue exhibited a markedly different fatigue and shear zones. One resembled that of the SIK tie rods (small fatigue, large shear zone), the other of PUR (large fatigue, small shear zone). Numerous origins occurring on three main crack fronts were observed.

11. Recommendations

In order to obtain a greater understanding of the effects of prior heat treatment and cold-working in the threaded regions, a number of tie rods should be reheat-treated in accordance with the governing specification and subjected to spectrum fatigue testing.

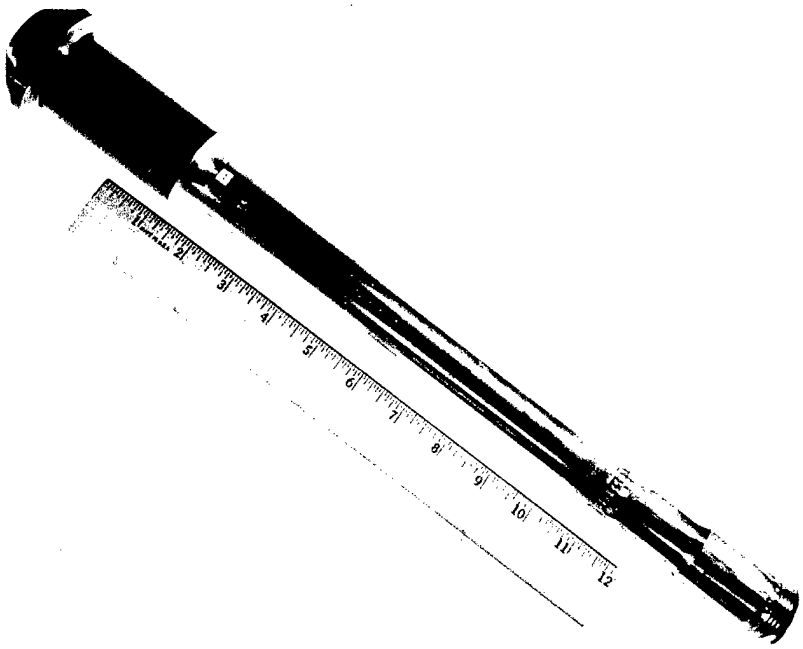

Figure 1. Failed SIK Rod -00938 in the As-Received Condition (Reduced 75%).

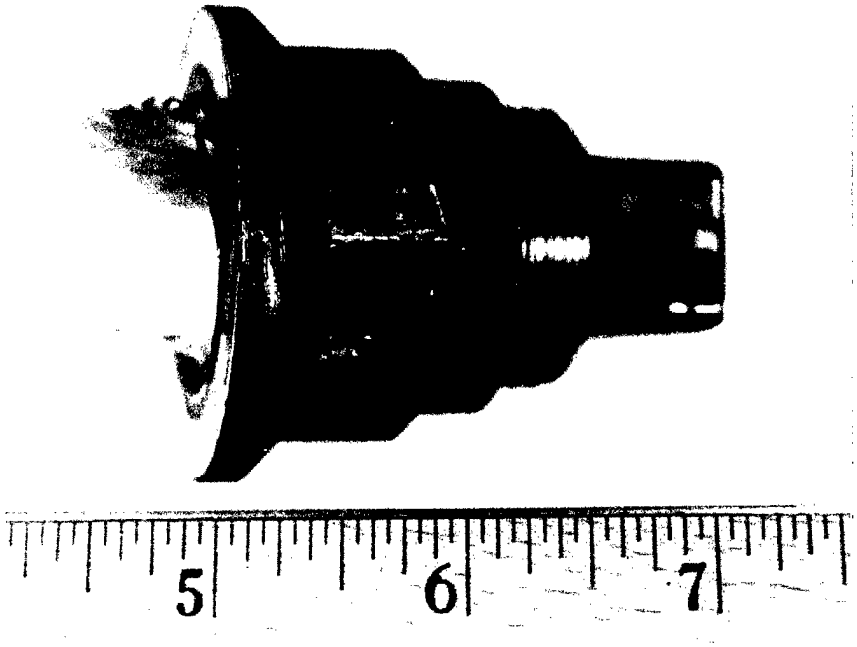

Figure 2. Failed Threaded End of SIK Rod -00938 in the As-Received Condition (Mag. 1.25x).

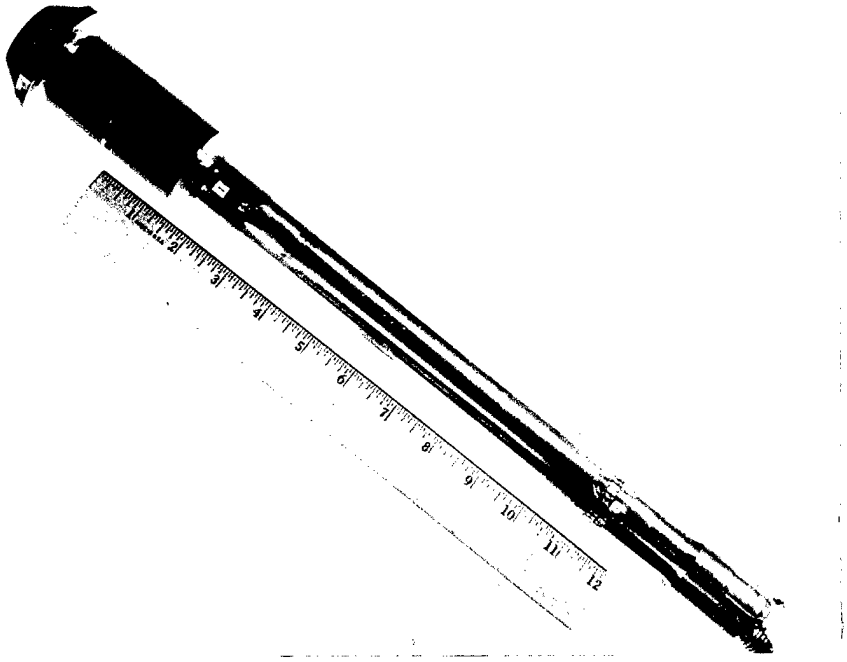

Figure 3. Failed SIK Rod -00973 in the As-Received Condition (Reduced 75%).

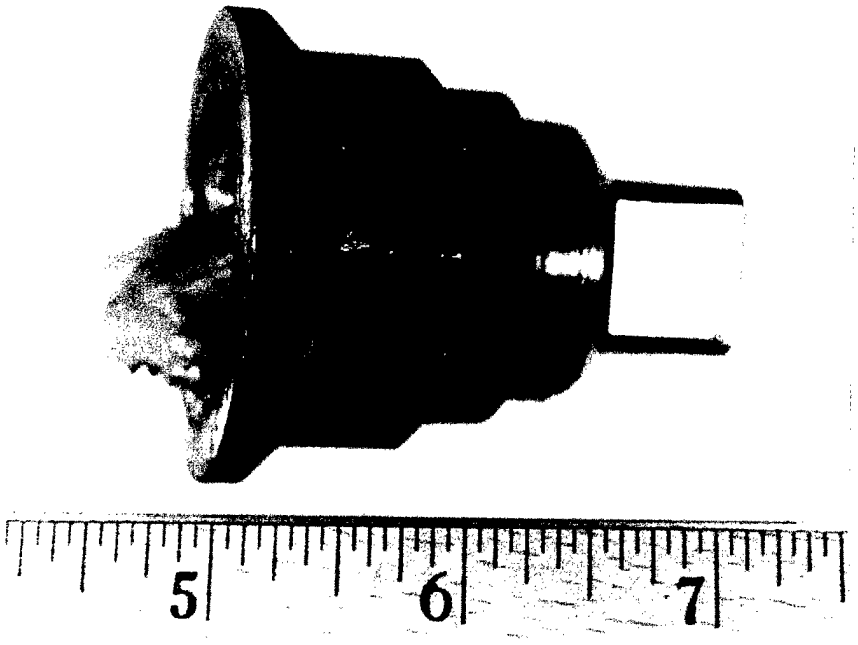

Figure 4. Failed Threaded End of SIK Rod -00973 in the As-Received Condition (Mag. 1.25x).

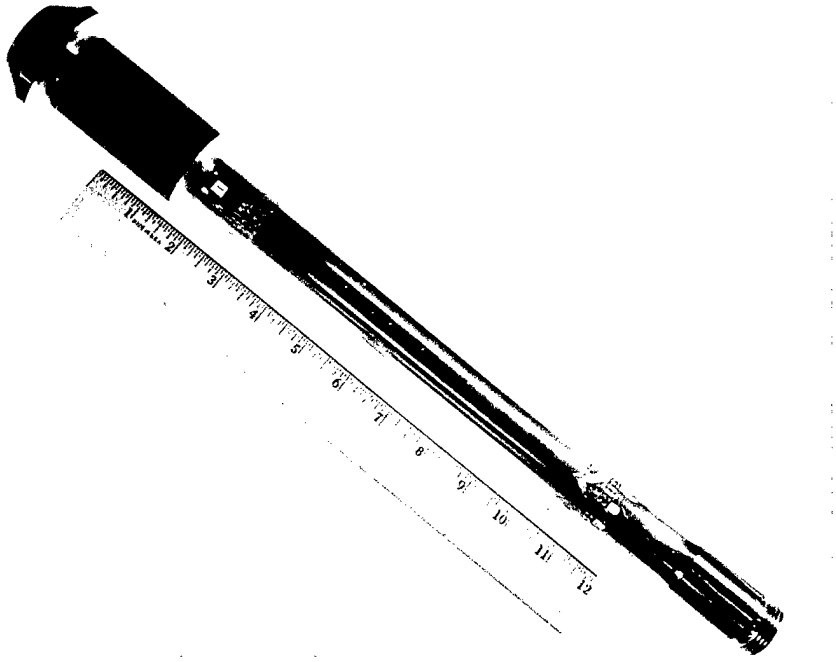

Figure 5. Failed PUR Rod -174 in the As-Received Condition (Reduced 75%).

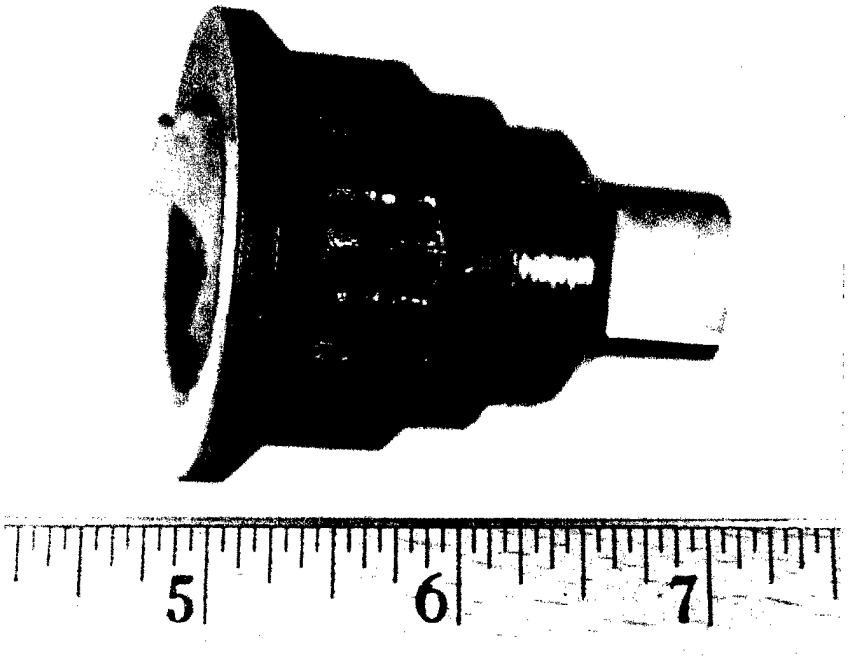

Figure 6. Failed Threaded End of PUR Rod -174 in the As-Received Condition (Mag. 1.25x).

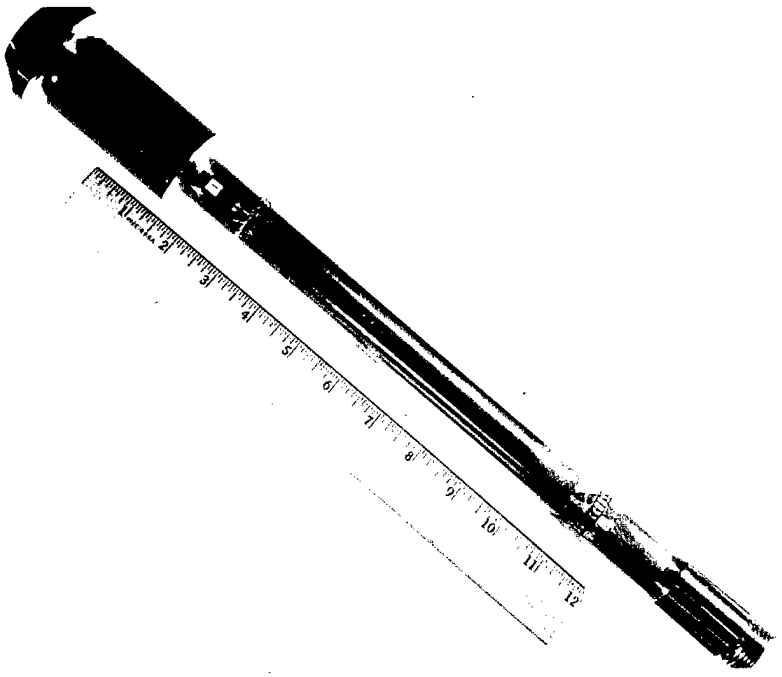

Figure 7. Failed PUR Rod -177 in the As-Received Condition (Reduced 75%).

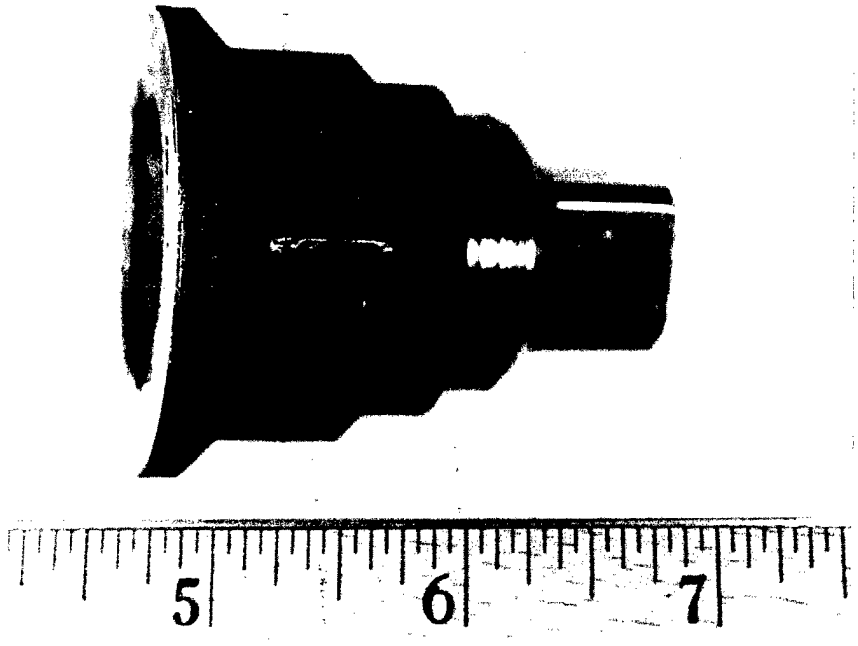

Figure 8. Failed Threaded End of PUR Rod -177 in the As-Received Condition (Mag. 1.25x).

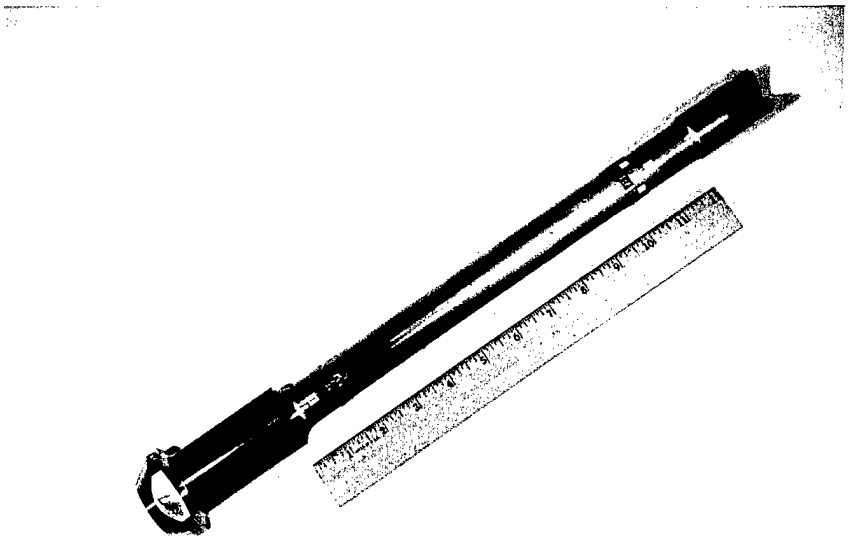

Figure 9. Failed S&S Rod -2 in the As-Received Condition (Reduced 80%).

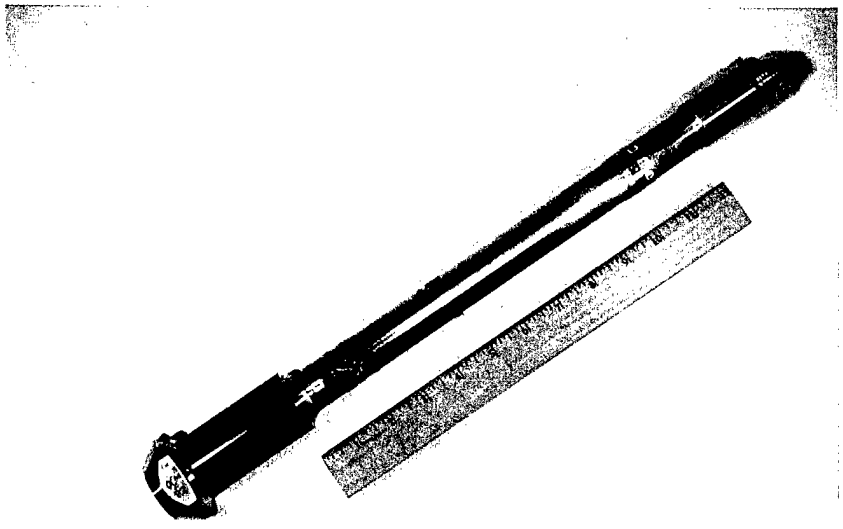

Figure 10. Failed S&S Rod -3 in the As-Received Condition (Reduced 80%).

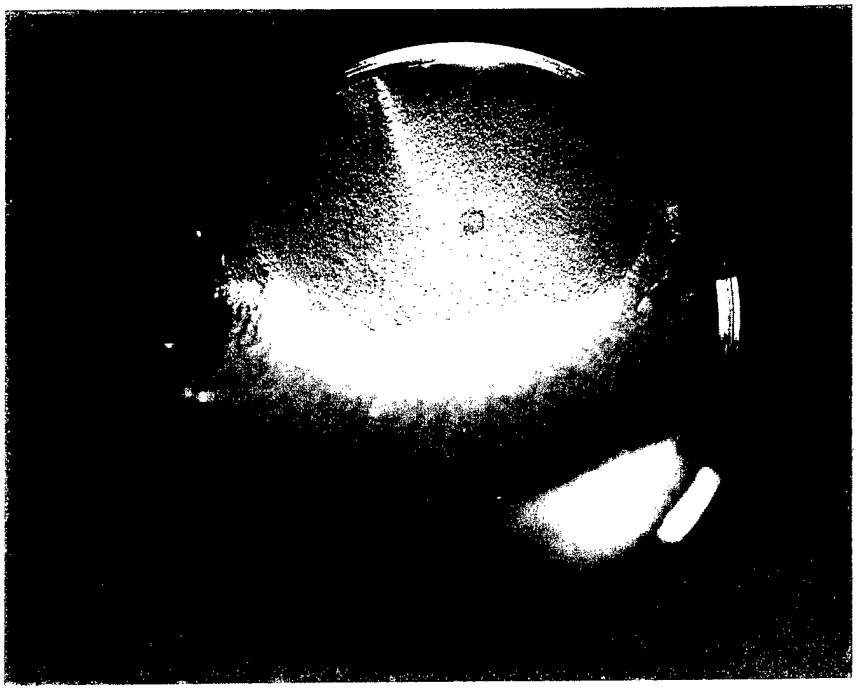

Figure 11. Fracture Surface of SIK Rod -00938 in the As-Received Condition. The Fatigue Region Is Within Focus (The Depth of Field Was Distorted by the Angled Shear Lips) (Mag. 2x).

Figure 12. Fracture Surface of SIK Rod -00973 in the As-Received Condition. Again, the Fatigue Region Is Within Focus. Note the Two Planes of Fatigue Crack Propagation (Mag. 2x).

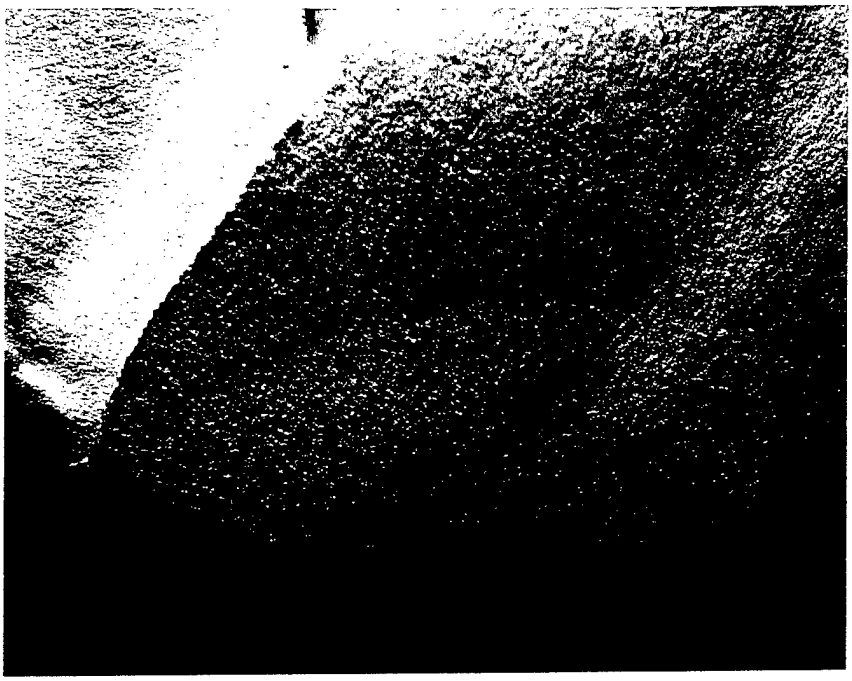

Figure 13. A Thumbnail Crack Noted on the Fracture Surface of SIK Rod -00973 (Mag. 7.5x).

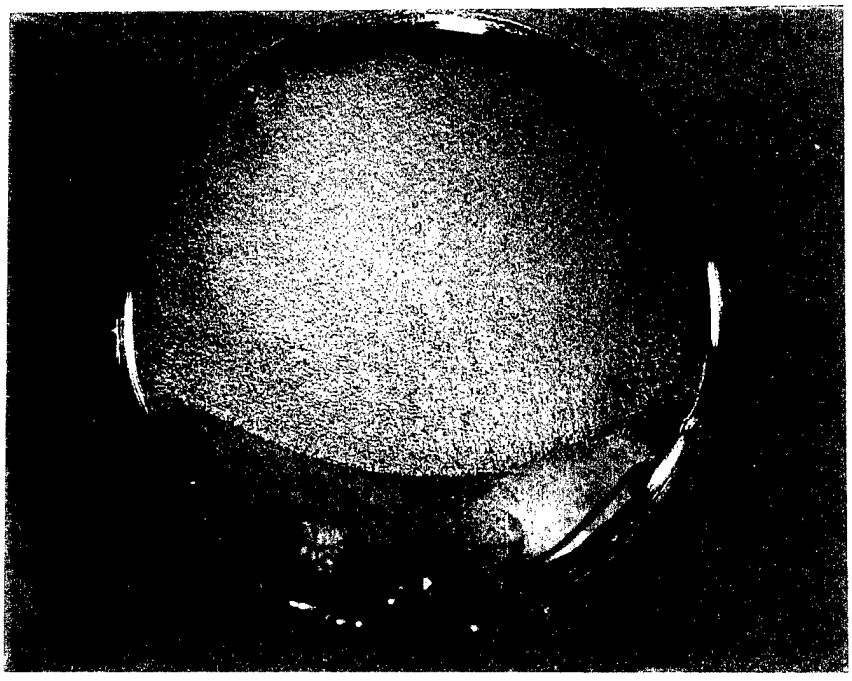

Figure 14. Fracture Surface of PUR Rod -174 in the As-Received Condition. Note the Increased Fatigue Zone as Opposed to the Fracture Surfaces of the SIK Rods (Mag. 2x).

Figure 15. Fracture Surface of PUR Rod -177 in the As-Received Condition. Note the Increased Fatigue Zone as Opposed to the Fracture Surfaces of the SIK Rods (Mag. 2x).

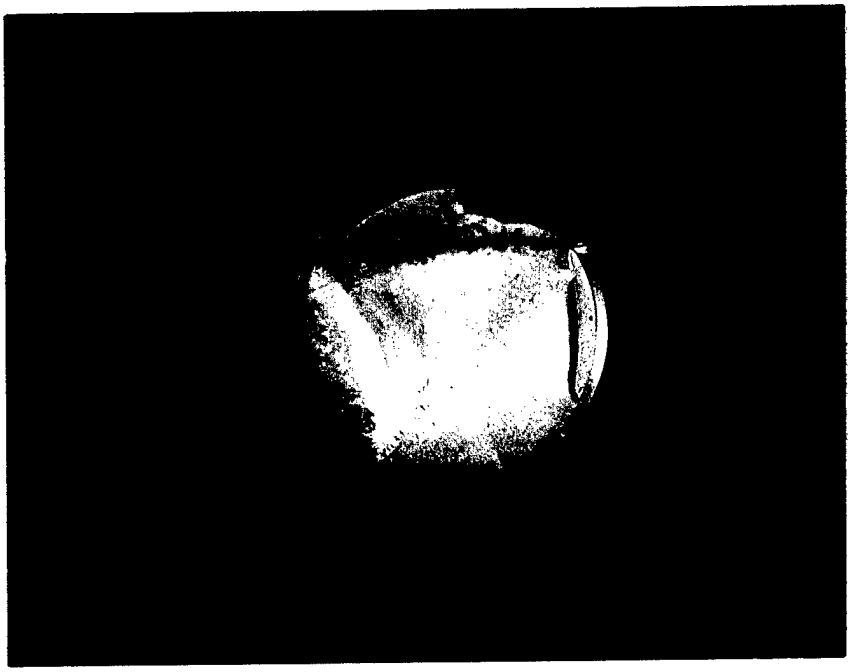

Figure 16. Fracture Surface of S&S Rod -2 in the As-Received Condition. The Fatigue Region Is Within Focus (Mag. 1.2x).

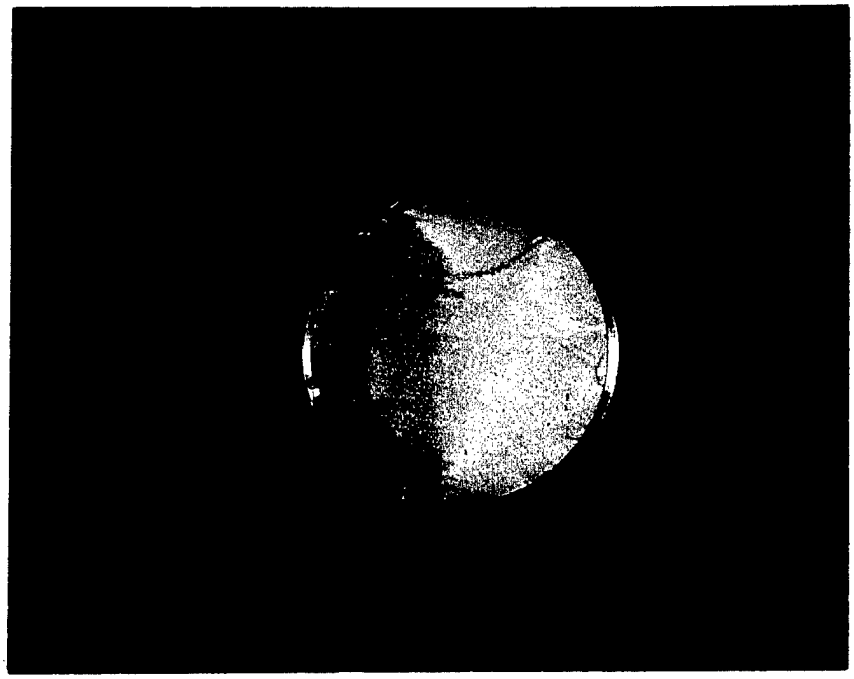

Figure 17. Fracture Surface of S&S Rod -3 in the As-Received Condition. Again, the Fatigue Region Is Within Focus. Note the Large Flat Fatigue Plane Similar to the PUR Samples (Mag. 1.2x).

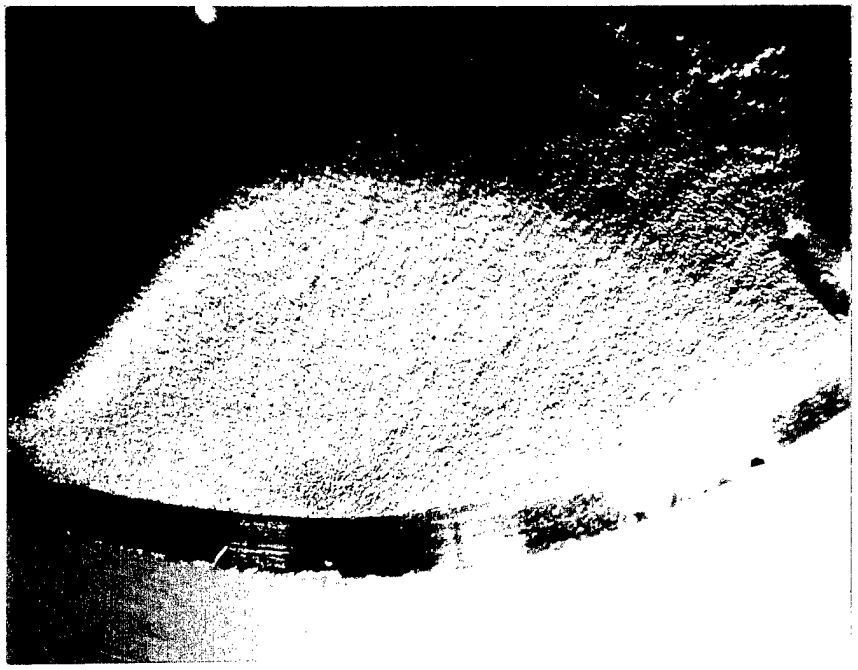

Figure 18. A Thumbnail Crack Noted on the Fracture Surface of S&S Rod -3 (Mag. 10x).

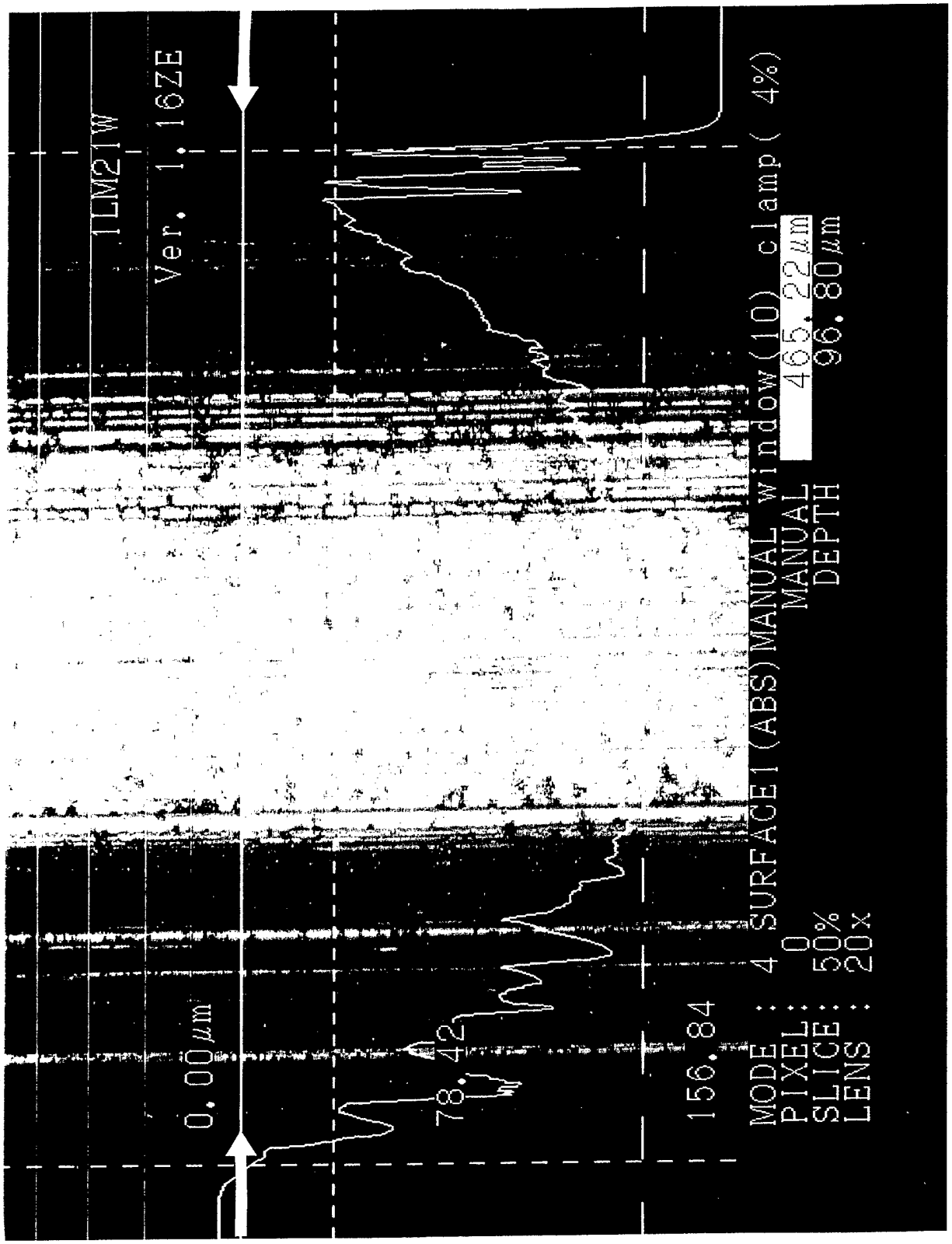

Figure 19. Lasertec Linear Scan Profile of SIK -00938 Rod Typical Thread Root (Mag. 500x).

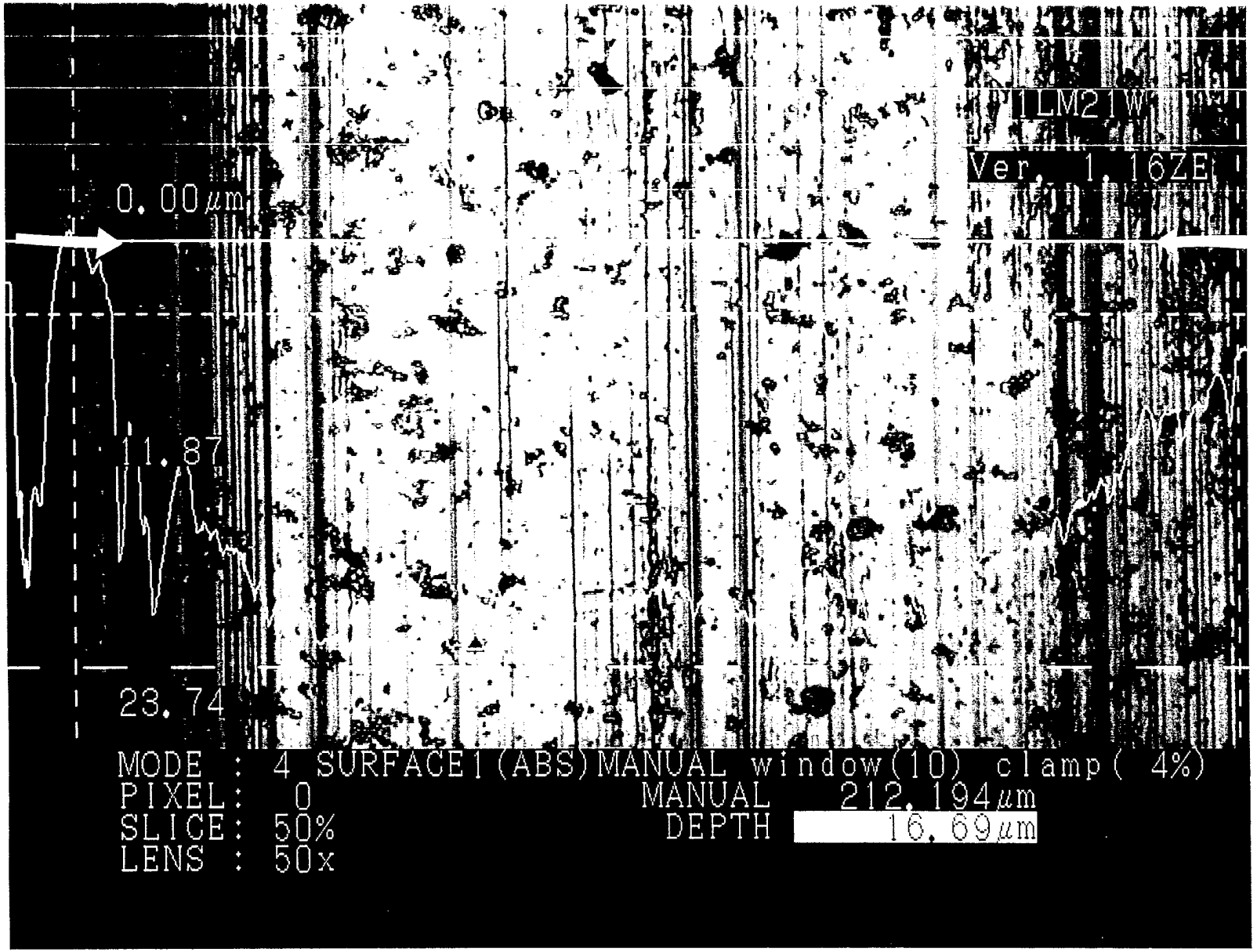

Figure 20. Lasertec Linear Scan Profile of SIK -00938 Rod Typical Thread Root (Mag. 1,250x).

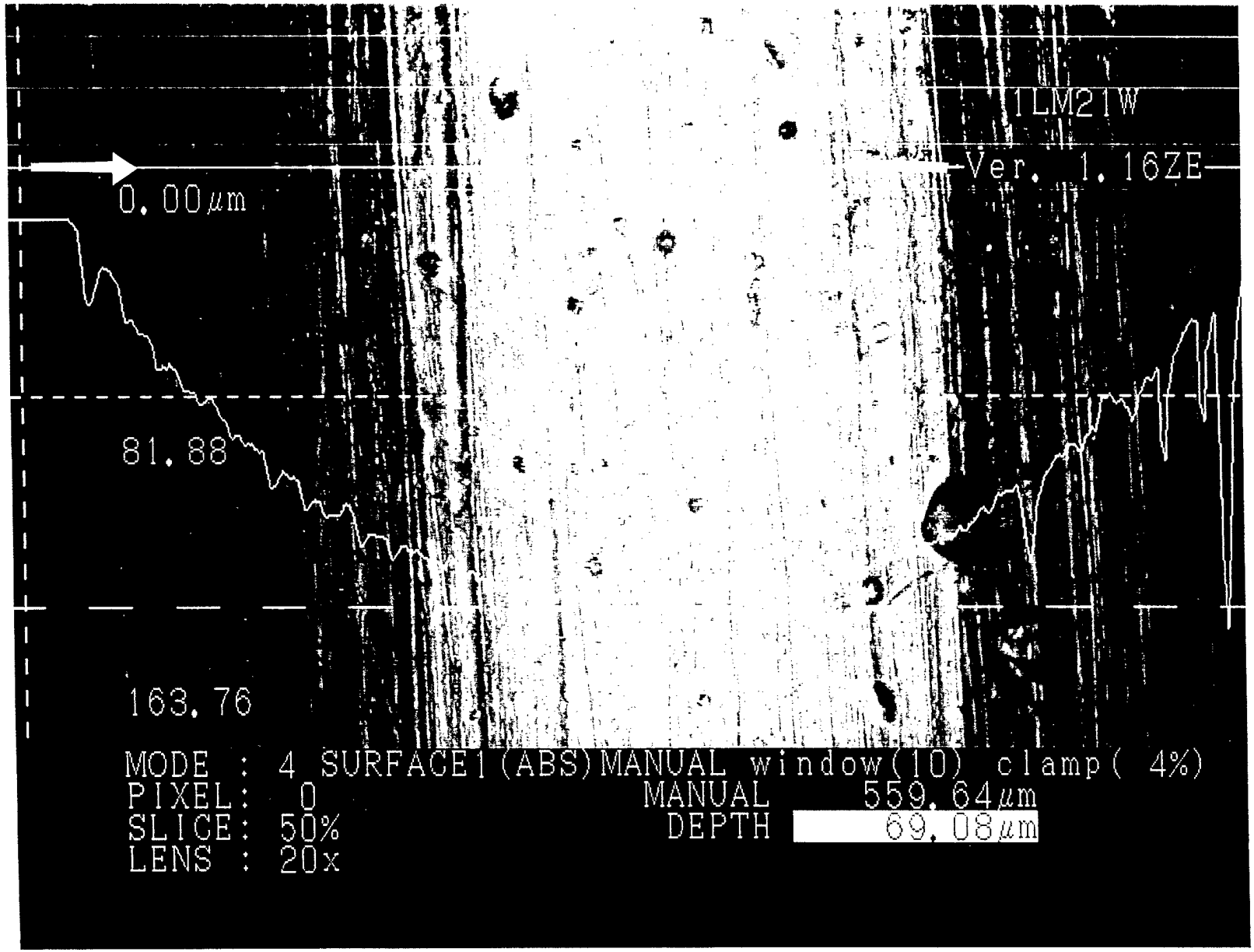

Figure 21. Lasertec Linear Scan Profile of S&S -3 Rod Typical Thread Root (Mag. 500x).

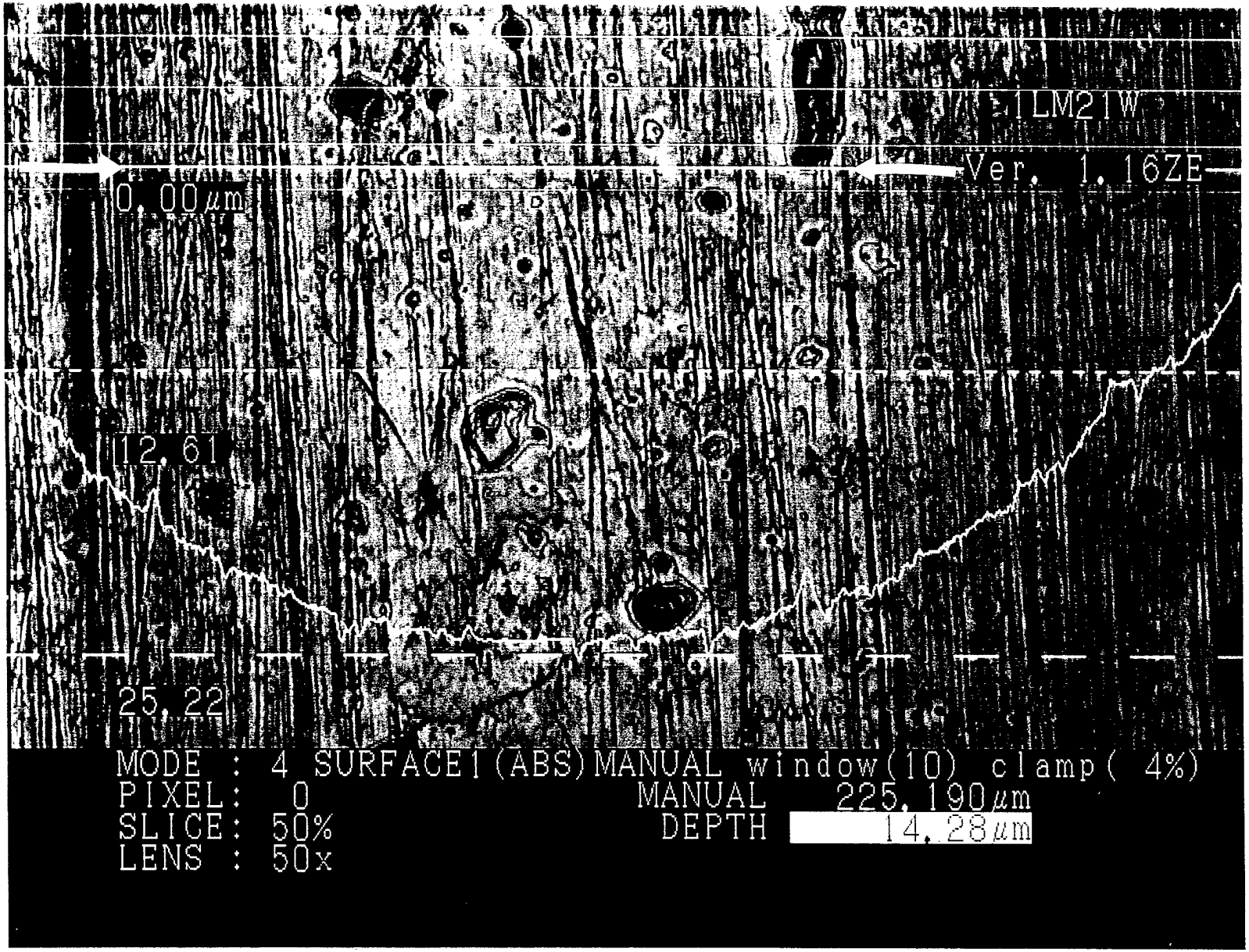

Figure 22. Lasertec Linear Scan Profile of S&S -3 Rod Typical Thread Root (Mag. 1,250x).

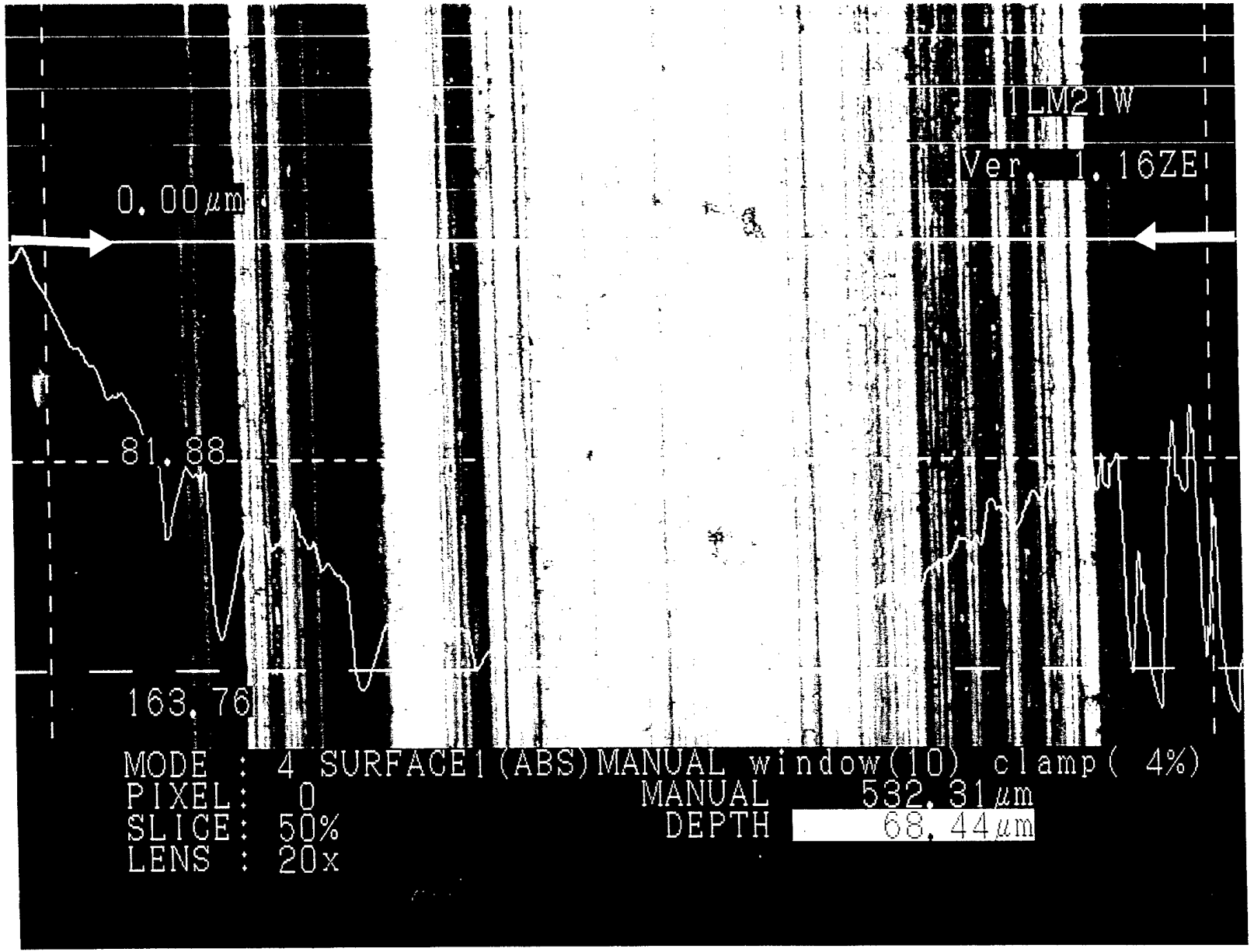

Figure 23. Lasertec Linear Scan Profile of PUR -177 Rod Typical Thread Root (Mag. 500x).

Figure 24. Lasertec Linear Scan Profile of PUR -177 Rod Typical Thread Root (Mag. 1,250x).

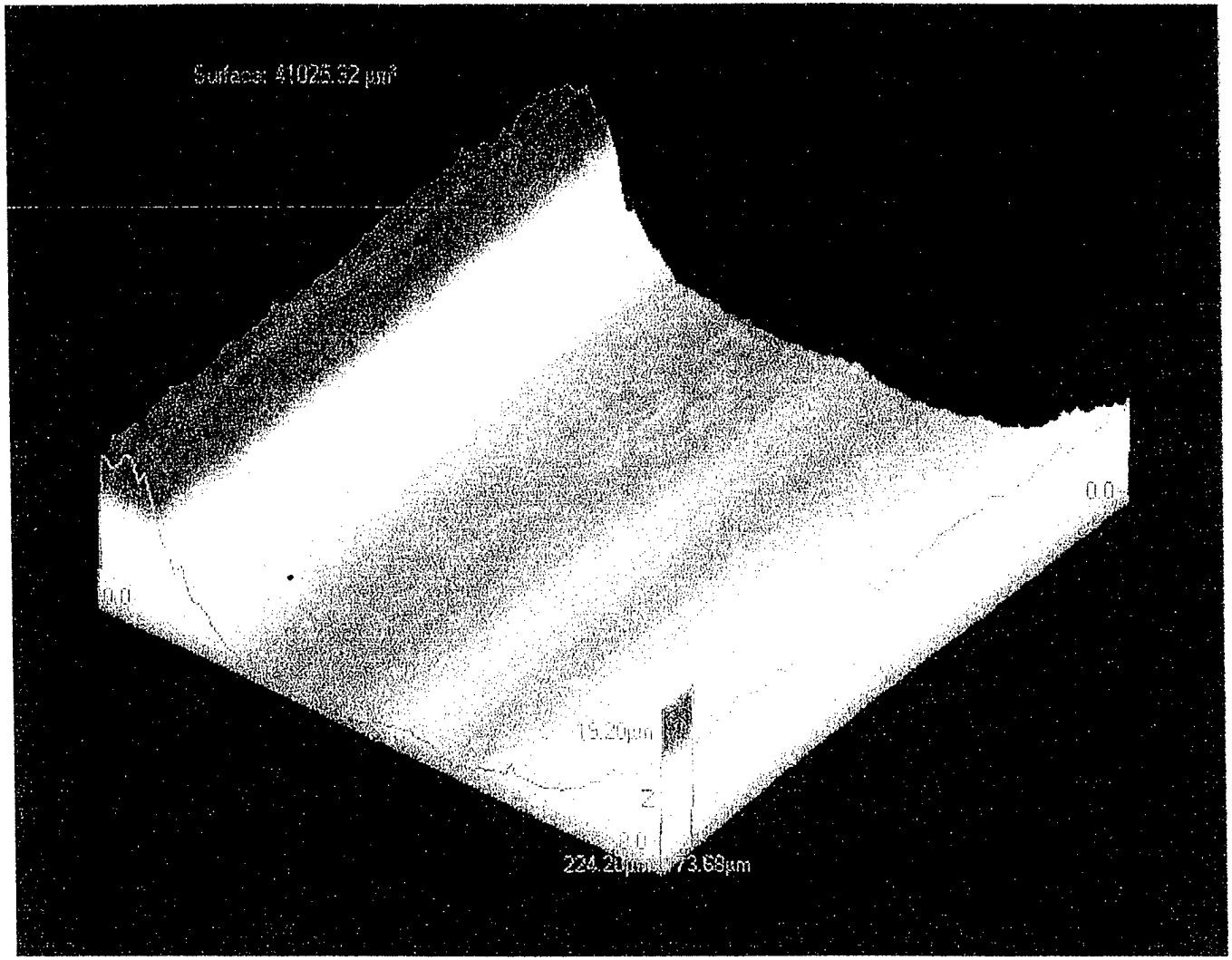

Figure 25. Color 3-D Scan of SIK Specimen -00938 (Mag. 1,250x).

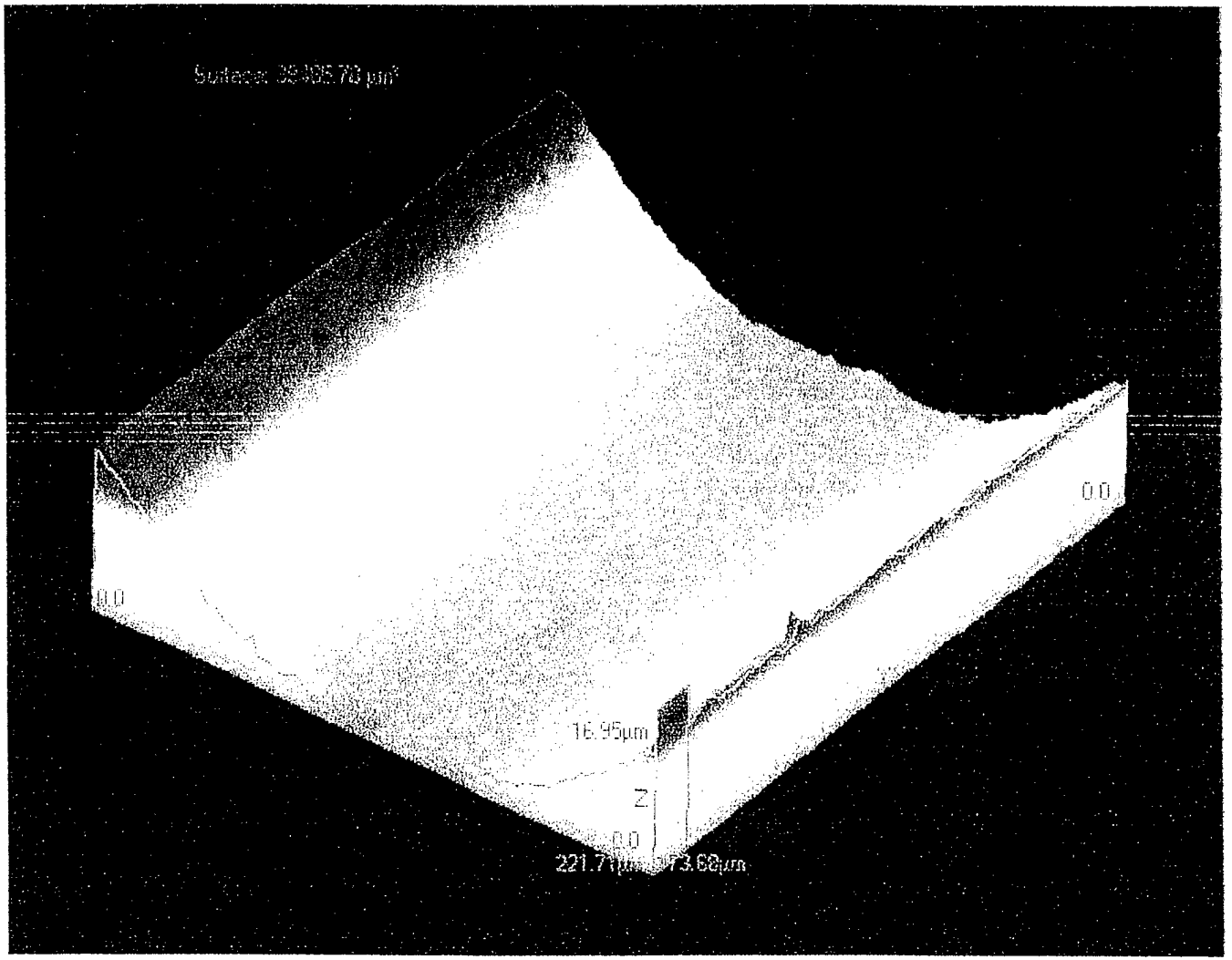

Figure 26. Color 3-D Scan of S&S Specimen -3 (Mag. 1,250x).

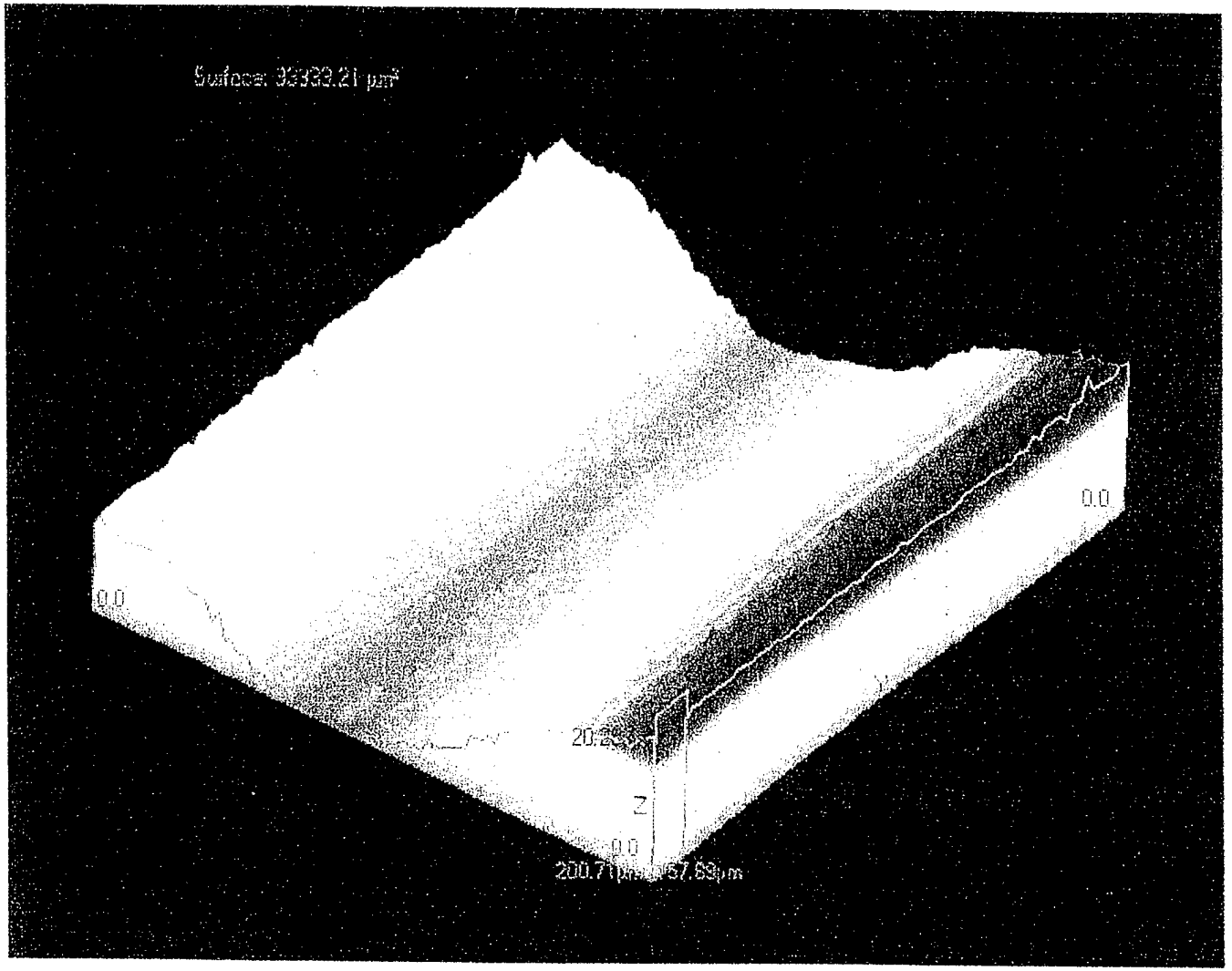

Figure 27. Color 3-D Scan of PUR Specimen -177 (Mag. 1,250x).

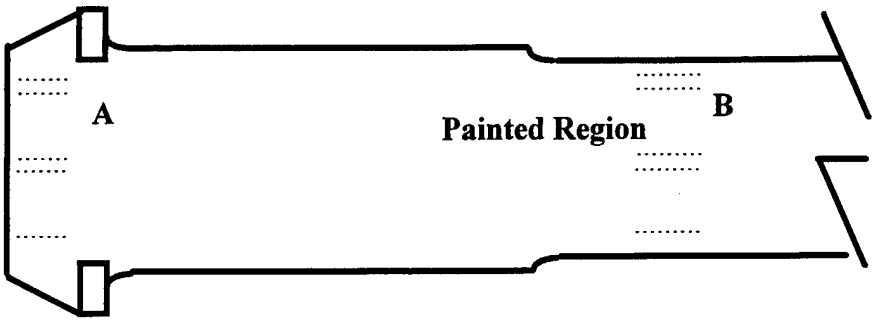

Figure 28. Typical Tie Rod Surface Finish Schematic.

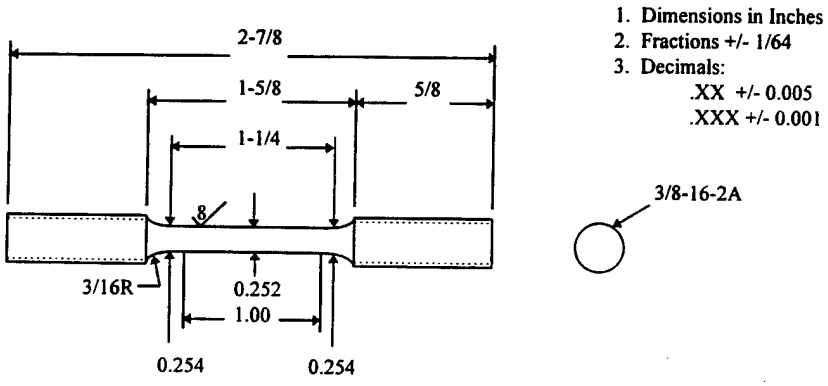

Figure 29. Schematic Illustrating the Dimensions of the Tensile Specimens Tested by ARL-MD.

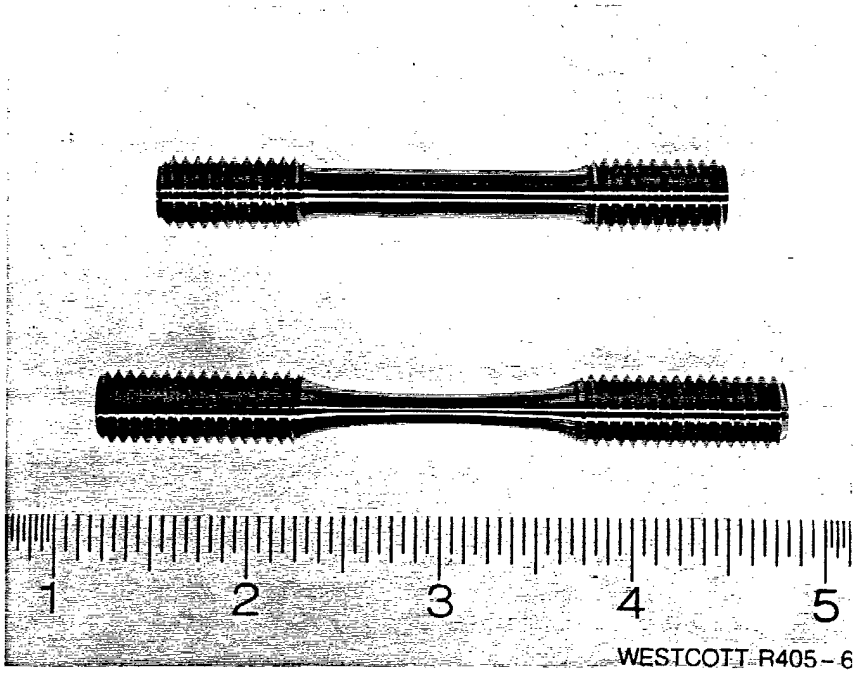

Figure 30. Representative Tensile (Top) and Fatigue (Bottom) Specimens Tested by ARL-MD.

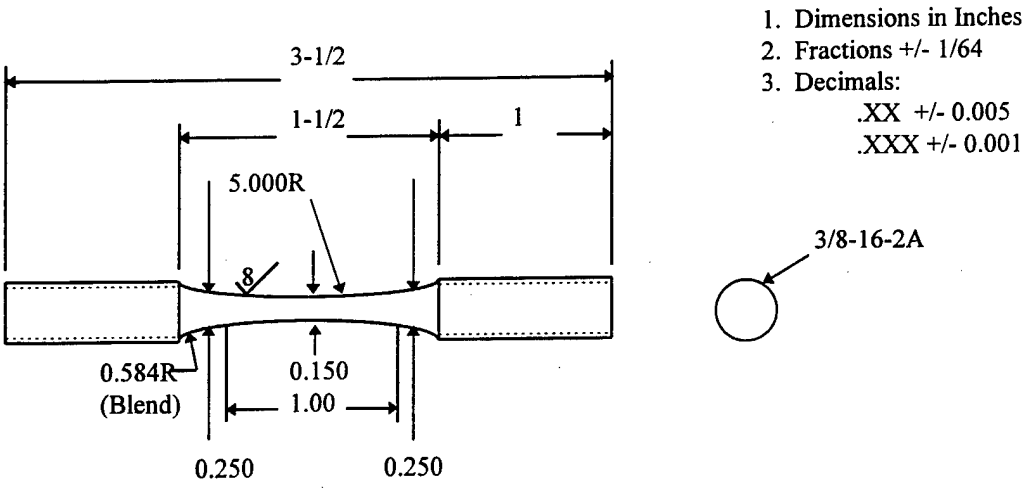

Figure 31. Schematic Illustrating the Dimensions of the Fatigue Specimens Tested by ARL-MD.

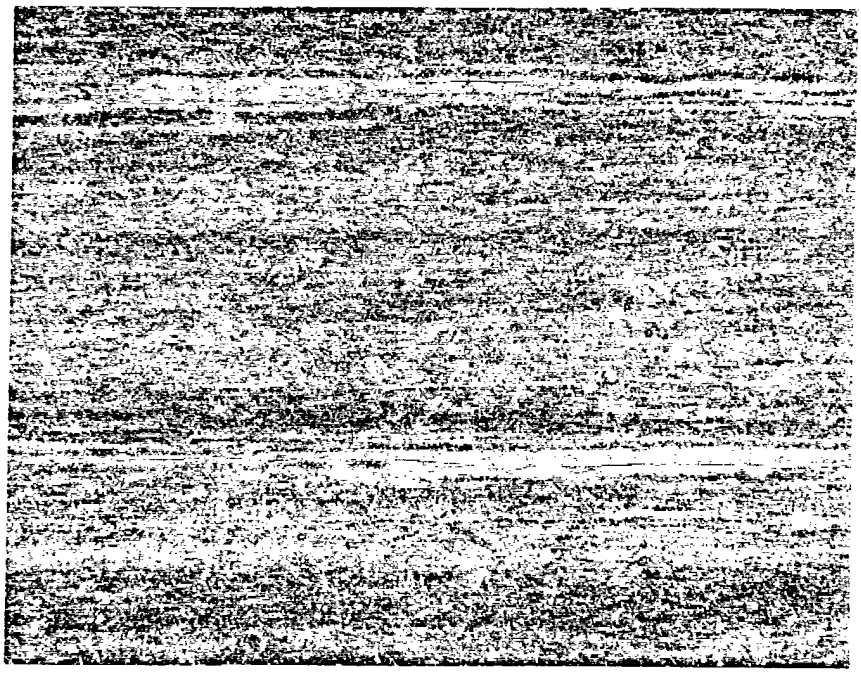

Figure 32. Structure of PUR -174 in the Longitudinal Direction Showing Heavy Banding. This Region Was Representative of the Entire Sample. Vilella's Reagent (Mag. 50x).

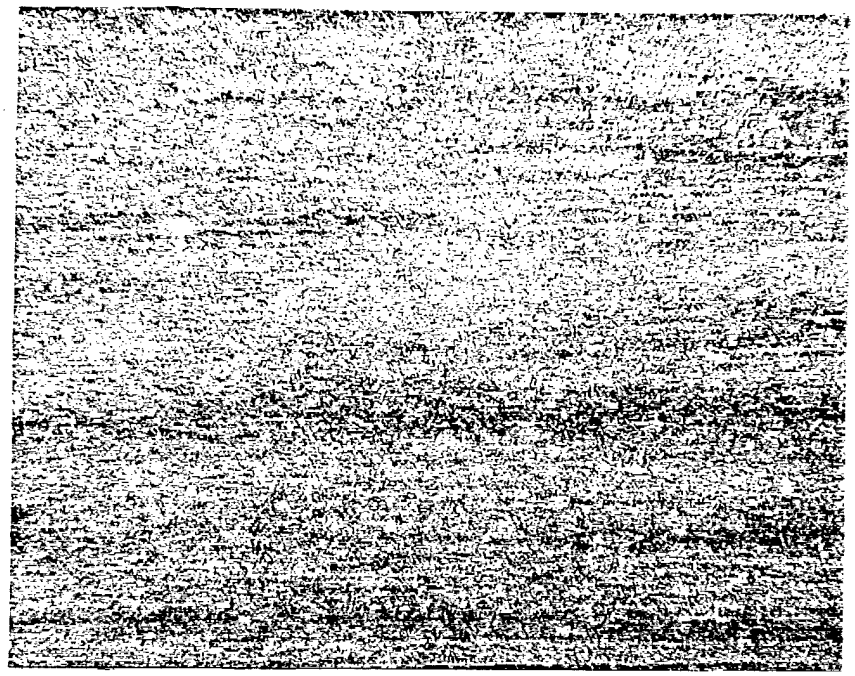

Figure 33. Structure of S&S Sample -2 in the Longitudinal Direction Showing Minimal Banding. This Region Was Representative of the Entire Sample. Vilella's Reagent (Mag. 50x).

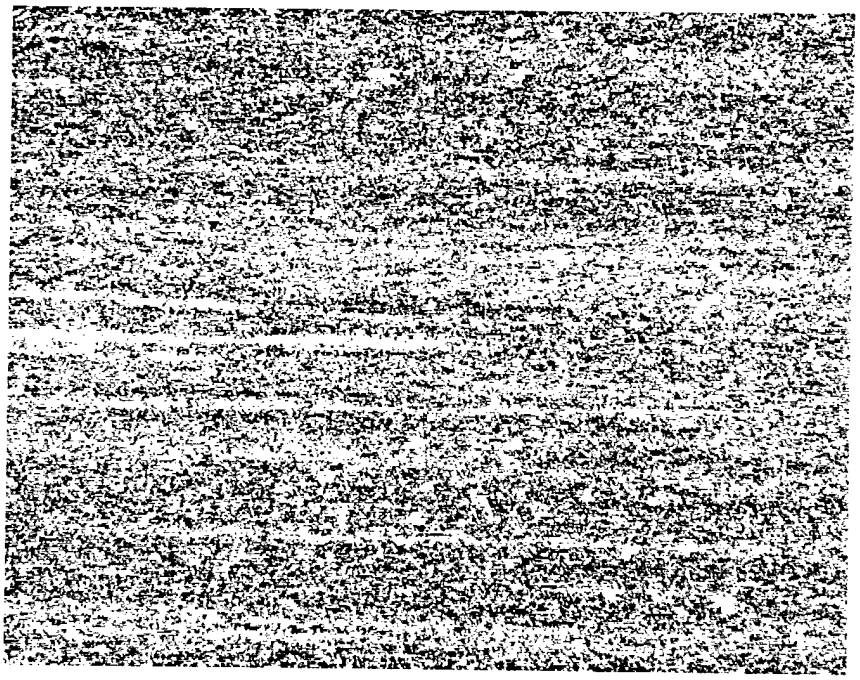

Figure 34. Structure of SIK -00973 in the Longitudinal Direction Showing Minimal Banding. Note: This Region Was Not Representative of the Entire Sample, as Most of the Structure Was Free of Banding. Vilella's Reagent (Mag. 50x).

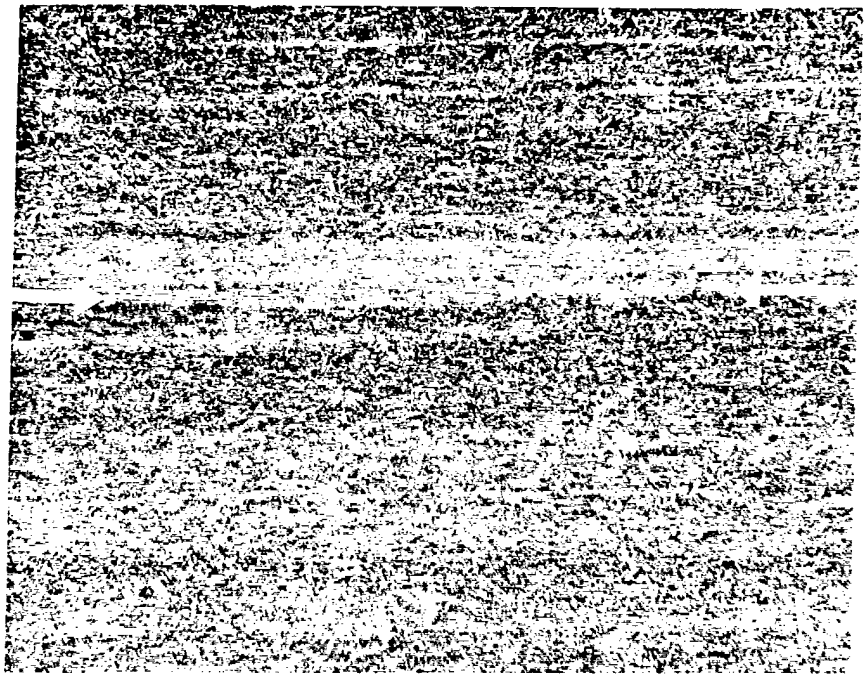

Figure 35. Structure of PUR -174 in the Longitudinal Direction Showing Delta Ferrite Within the Banding. Note the Length of the Ferrite Stringer That Extends the Length of the Micrograph. Vilella's Reagent (Mag. 100×).

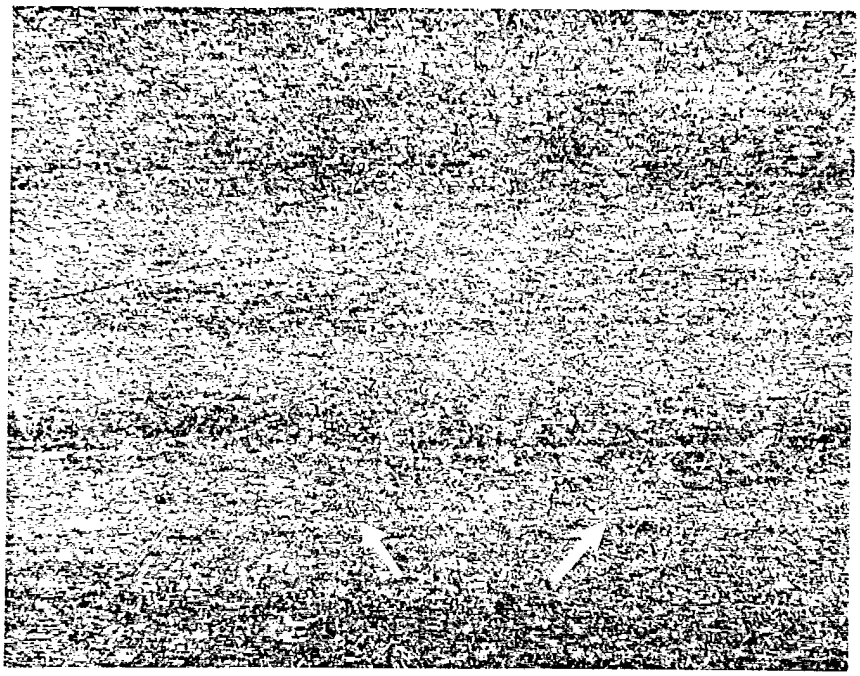

Figure 36. Structure of S&S Sample -2 in the Longitudinal Direction Showing Minimal Delta Ferrite Within the Banding. Vilella's Reagent (Mag. 100×).

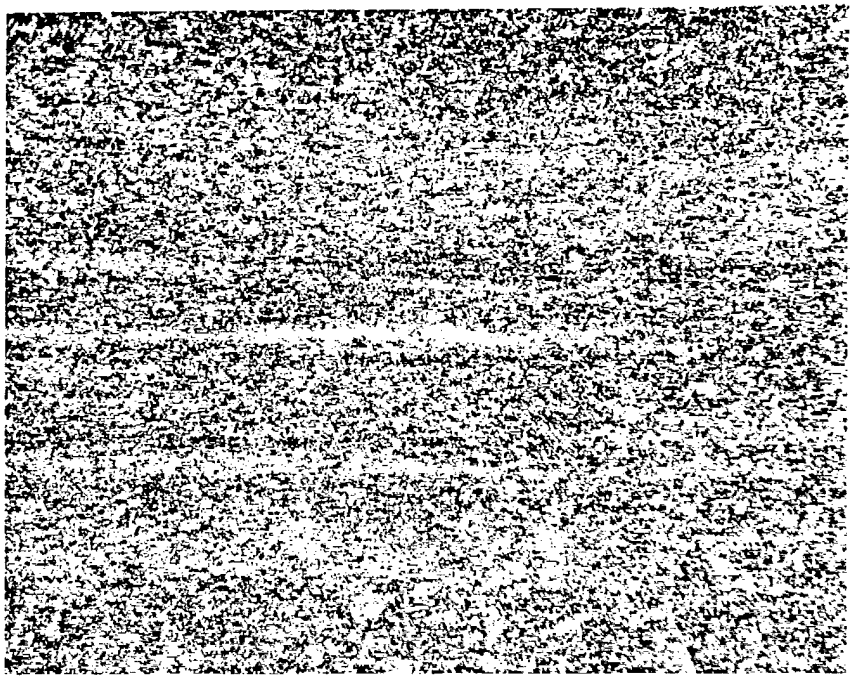

Figure 37. Structure of SIK -00973 in the Longitudinal Direction Showing Minimal Delta Ferrite Within the Banding. This Was the Only Delta Ferrite Noted Within the Structure of the SIK Samples. Vilella's Reagent (Mag. 100×).

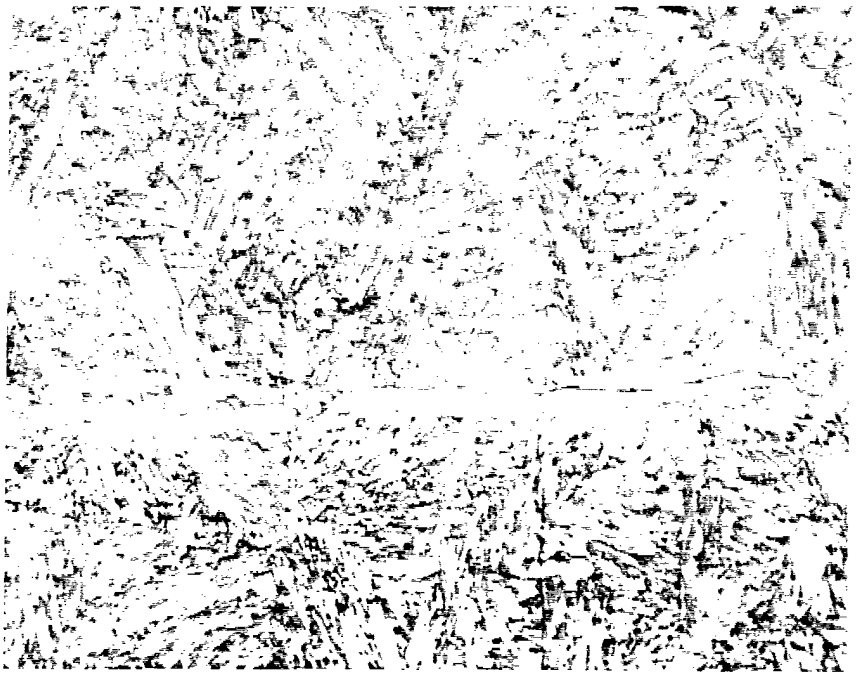

Figure 38. Enlarged View of a Ferrite Stringer Noted Within PUR Sample -174. Vilella's Reagent (Mag. 1kx).

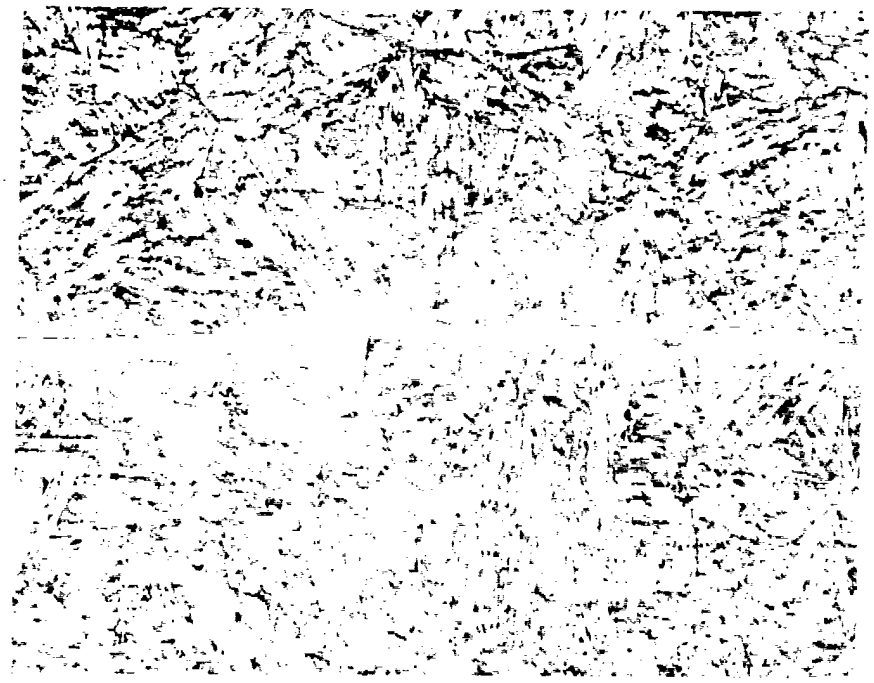

Figure 39. Enlarged View of the Ferrite Stringer Noted Within S&S Sample -2. Vilella's Reagent (Mag. 1kx).

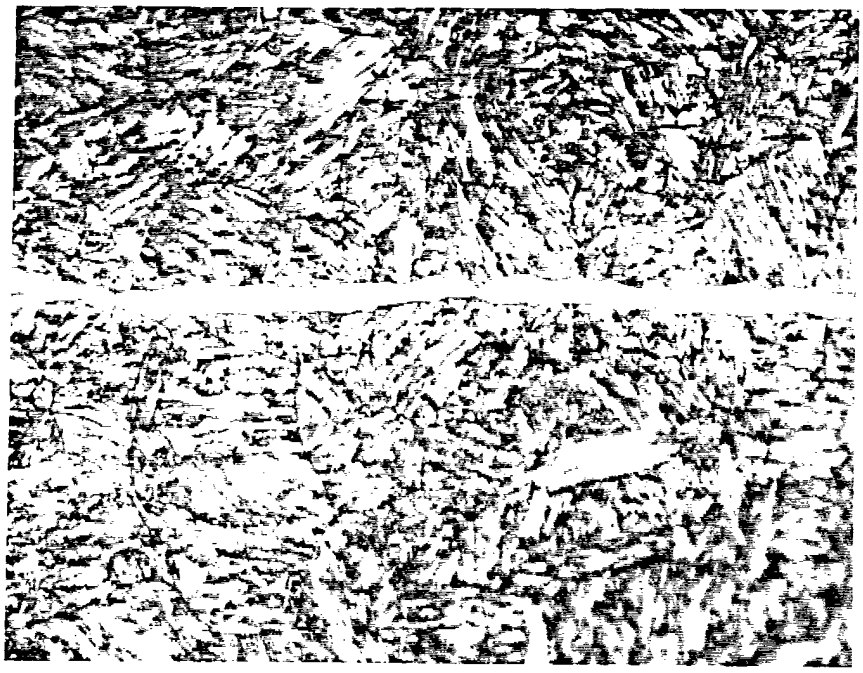

Figure 40. Enlarged View of the Ferrite Stringer Noted Within SIK Sample -00973. Vilella's Reagent (Mag. 1kx).

Figure 41. Structure of PUR Sample -174 in the Longitudinal Direction. Vilella's Reagent (Mag. 1kx).

Figure 42. Structure of PUR Sample -174 in the Transverse Direction. Vilella's Reagent (Mag. 1kx).

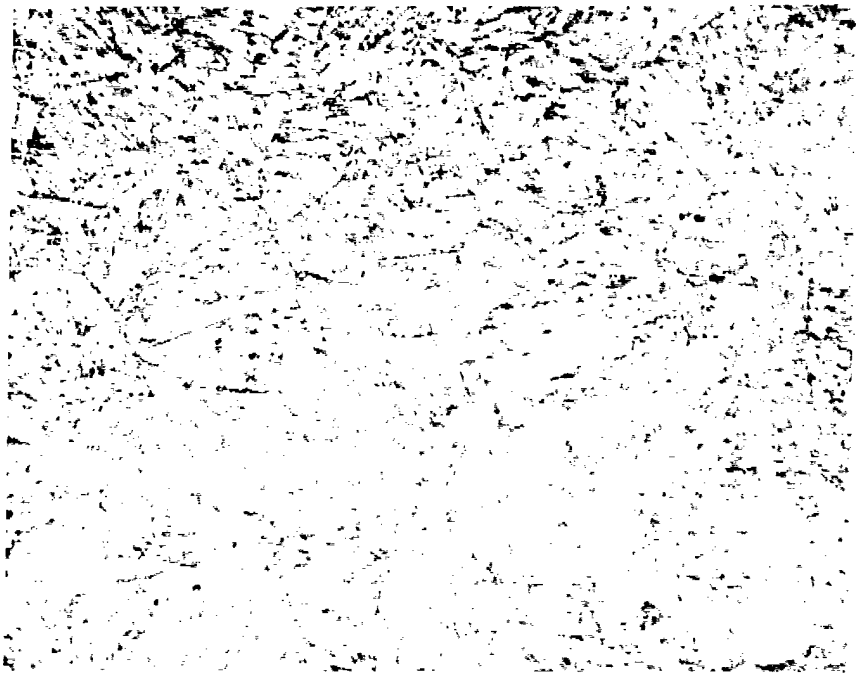

Figure 43. Structure of S&S Sample -2 in the Longitudinal Direction. Vilella's Reagent (Mag. 1kx).

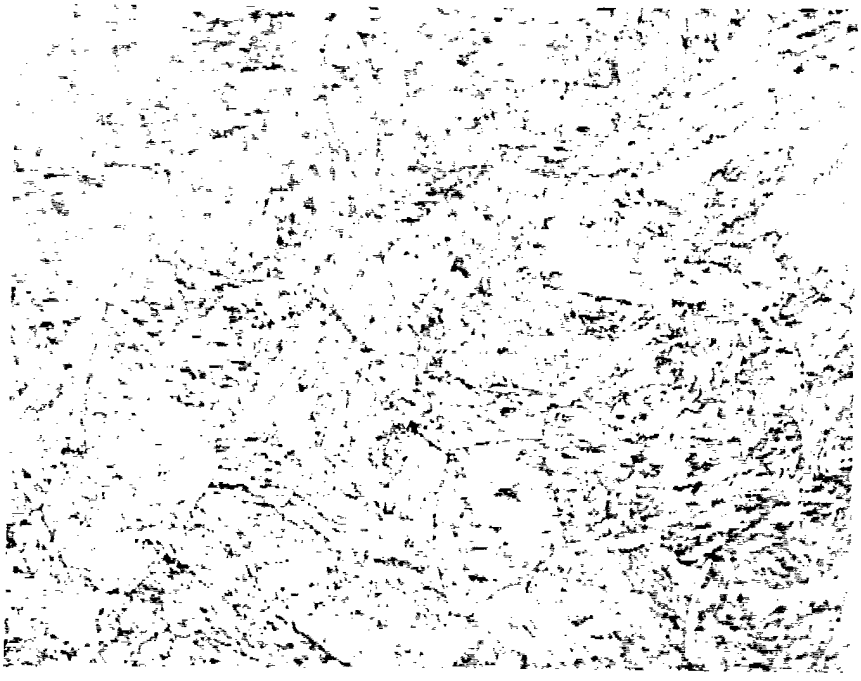

Figure 44. Structure of S&S Sample -2 in the Transverse Direction. Vilella's Reagent (Mag. 1kx).

Figure 45. Structure of SIK Sample -00973 in the Longitudinal Direction. Vilella's Reagent (Mag. 1kx).

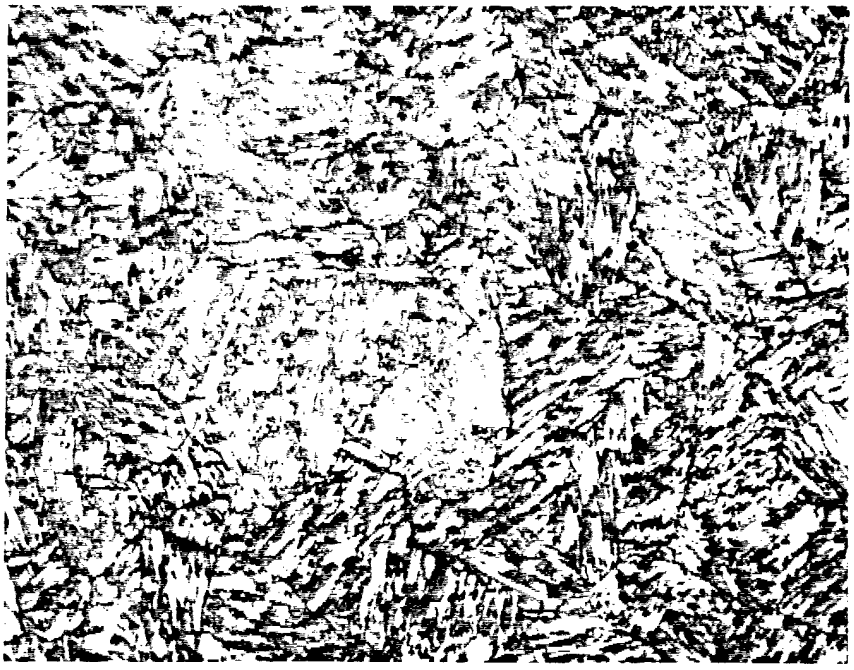

Figure 46. Structure of SIK Sample -00973 in the Transverse Direction. Vilella's Reagent (Mag. 1kx).

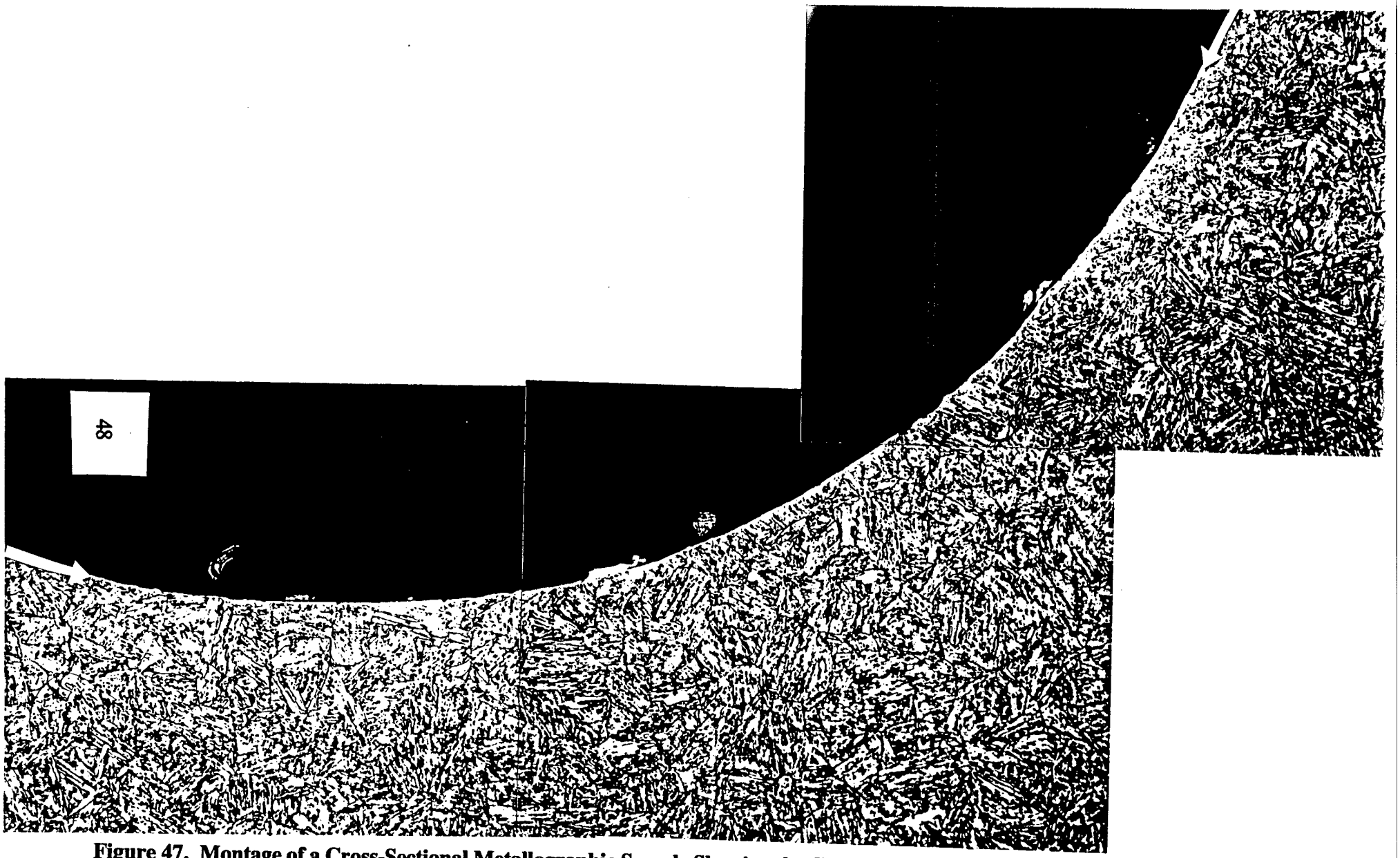

Figure 47. Montage of a Cross-Sectional Metallographic Sample Showing the Cold-Worked Layer on the External Surface of an S&S Thread (Mag. 500x).

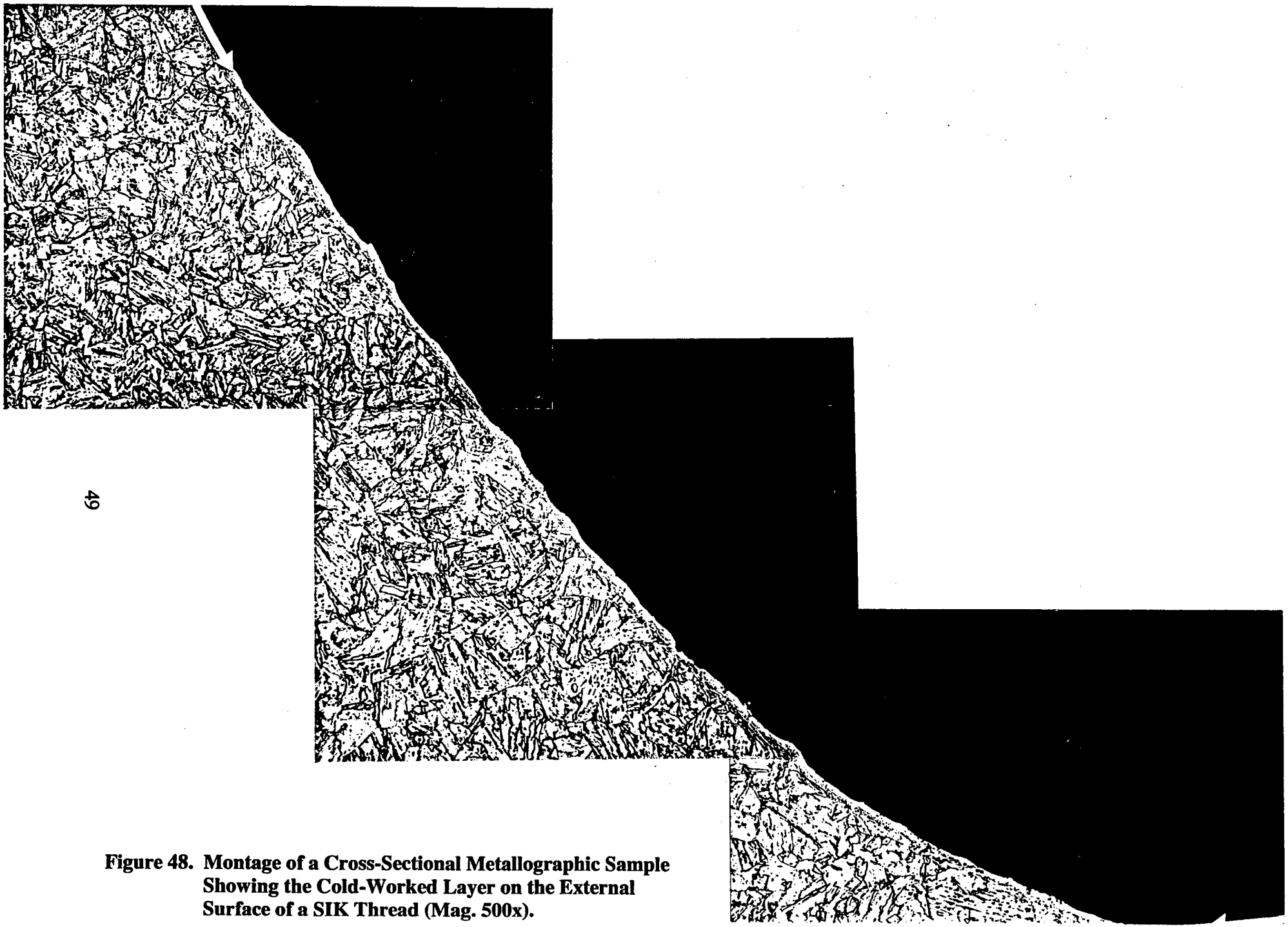

Figure 48. Montage of a Cross-Sectional Metallographic Sample Showing the Cold-Worked Layer on the External Surface of a SIK Thread (Mag. 500x).

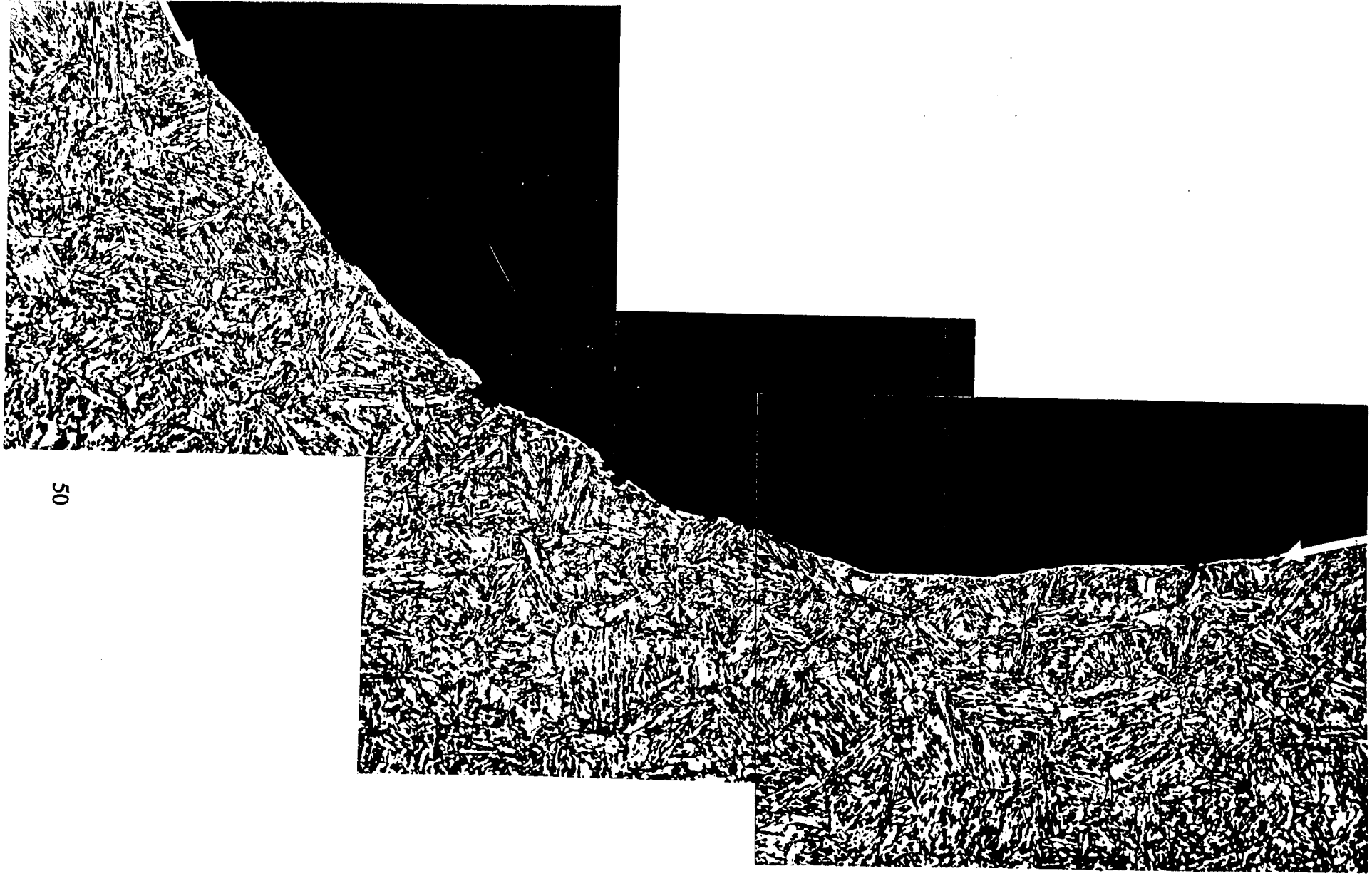

Figure 49. Montage of a Cross-Sectional Metallographic Sample Showing the Cold-Worked Layer on the External Surface of a PUR Thread (Mag. 500x).

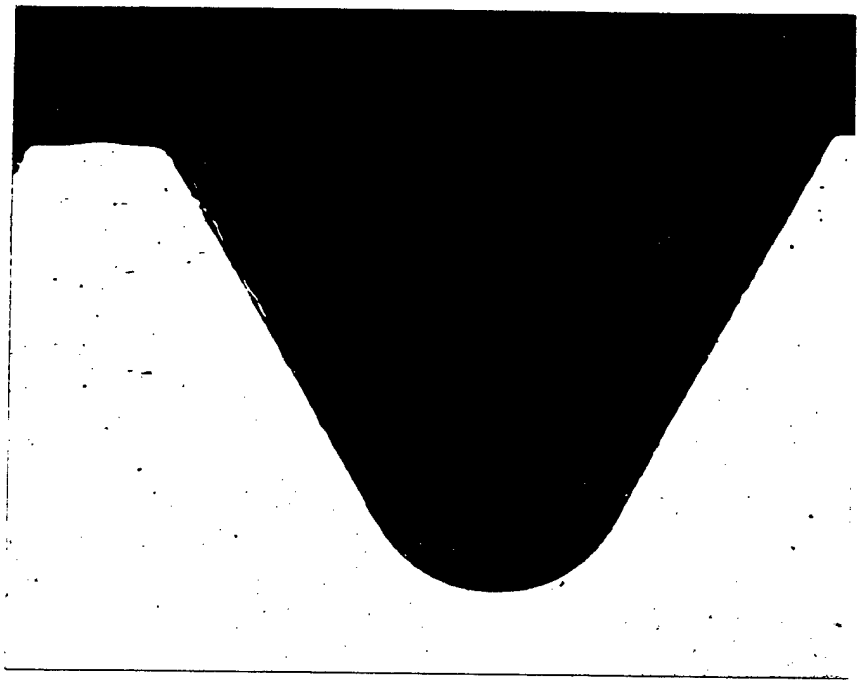

Figure 50. Cross Section of a Typical S&S Thread Showing a Smooth Profile (Mag. 50x).

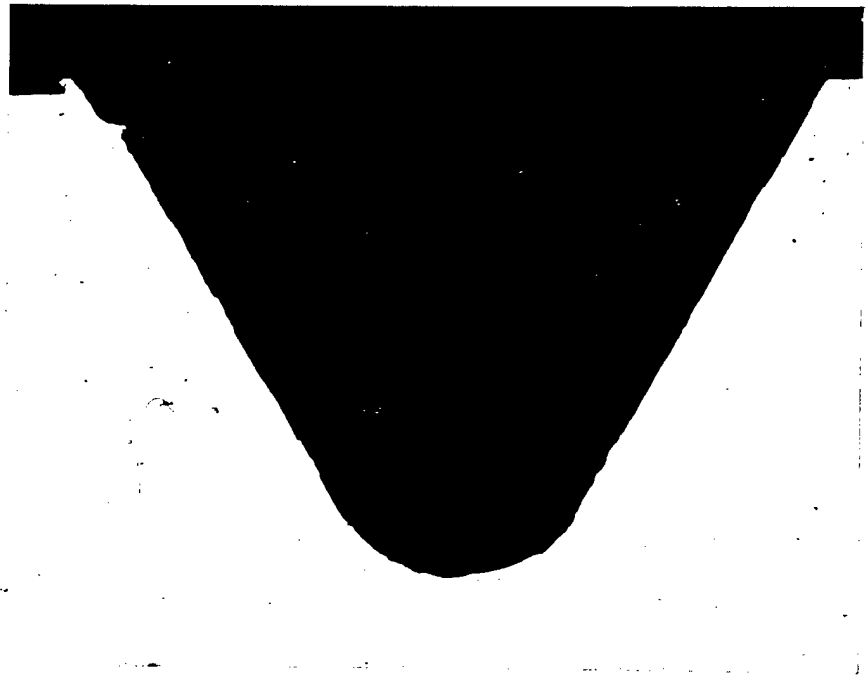

Figure 51. Cross Section of a Typical PUR Thread Showing the Roughest Profile (Mag. 50x).

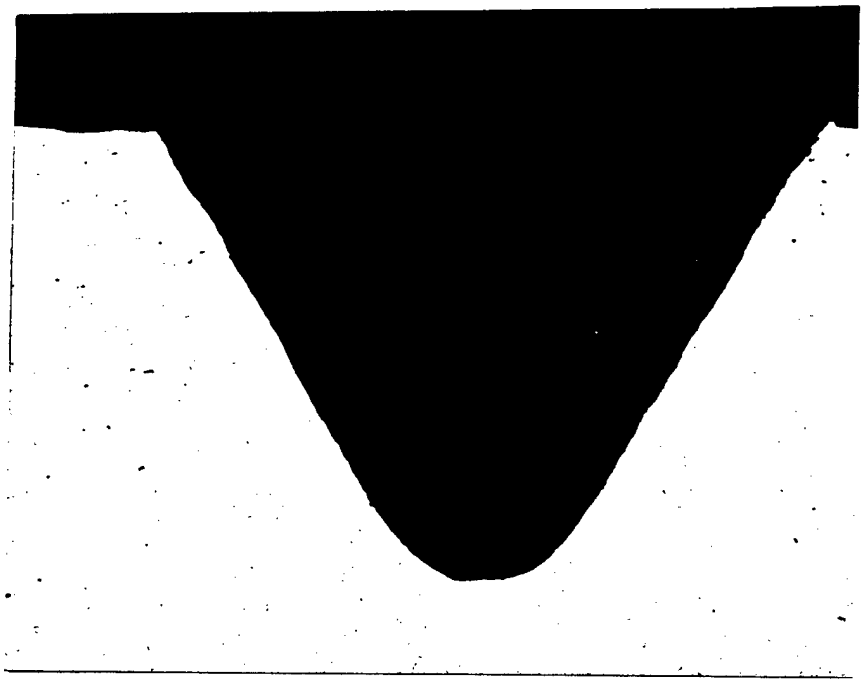

Figure 52. Cross Section of a Typical SIK Thread Showing a Somewhat Rough Profile (Mag. 50x).

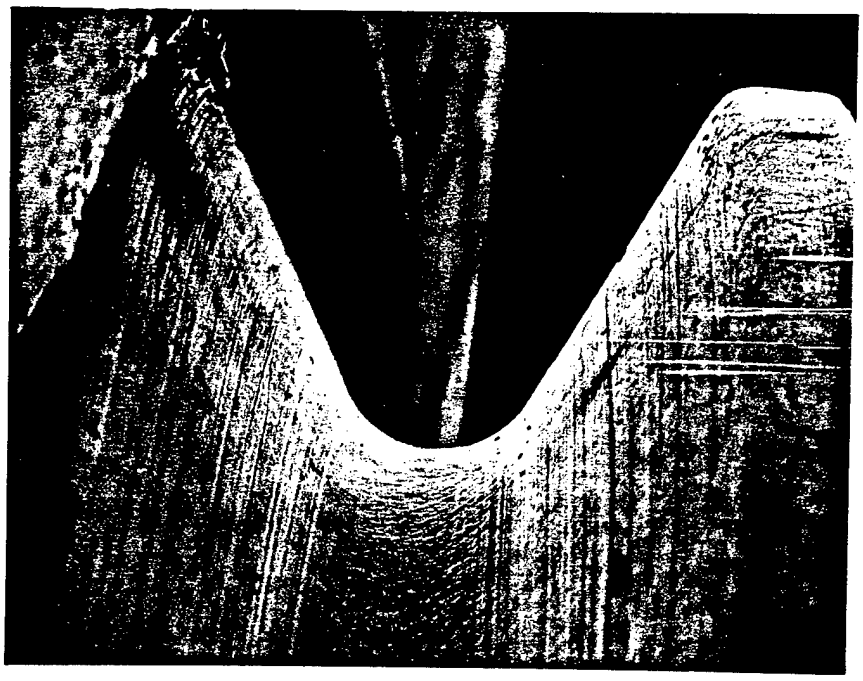

Figure 53. SEM Micrograph Depicting the Smoothness of an S&S Thread Root (Mag. 50x).

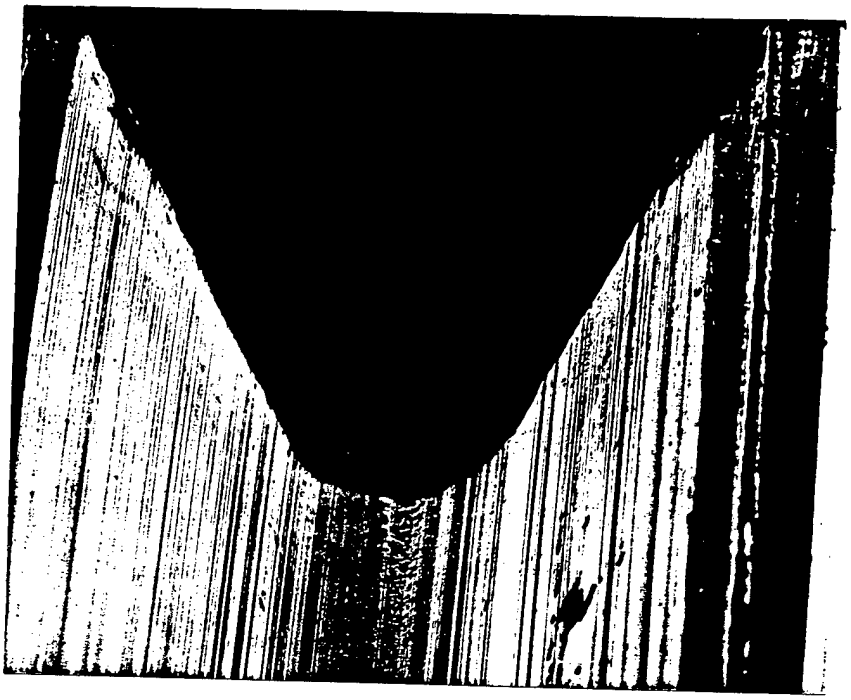

Figure 54. SEM Micrograph Depicting the Somewhat Rough SIK Thread Root (Mag. 50x).

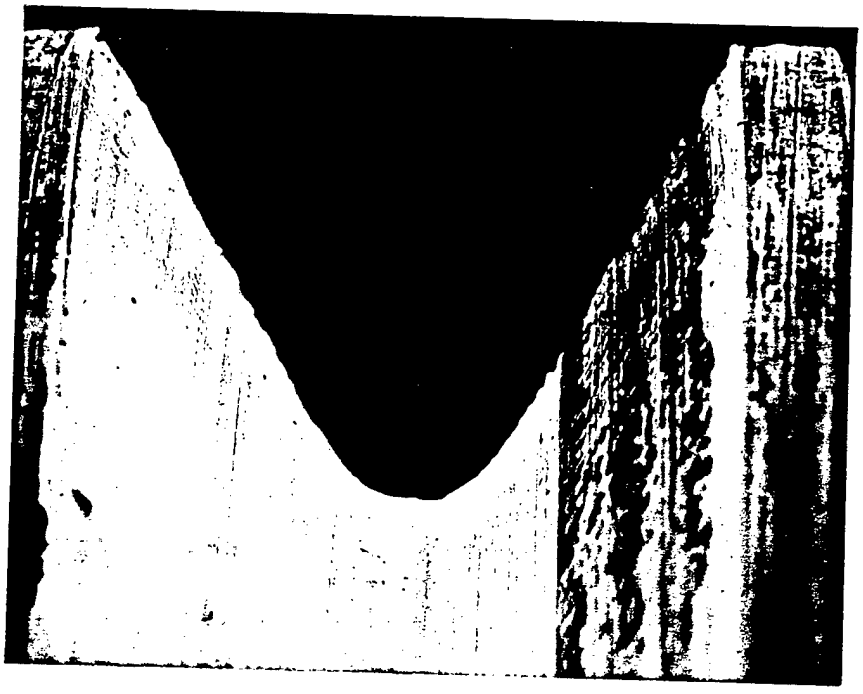

Figure 55. SEM Micrograph Depicting the Rough PUR Thread Root (Mag. 50x).

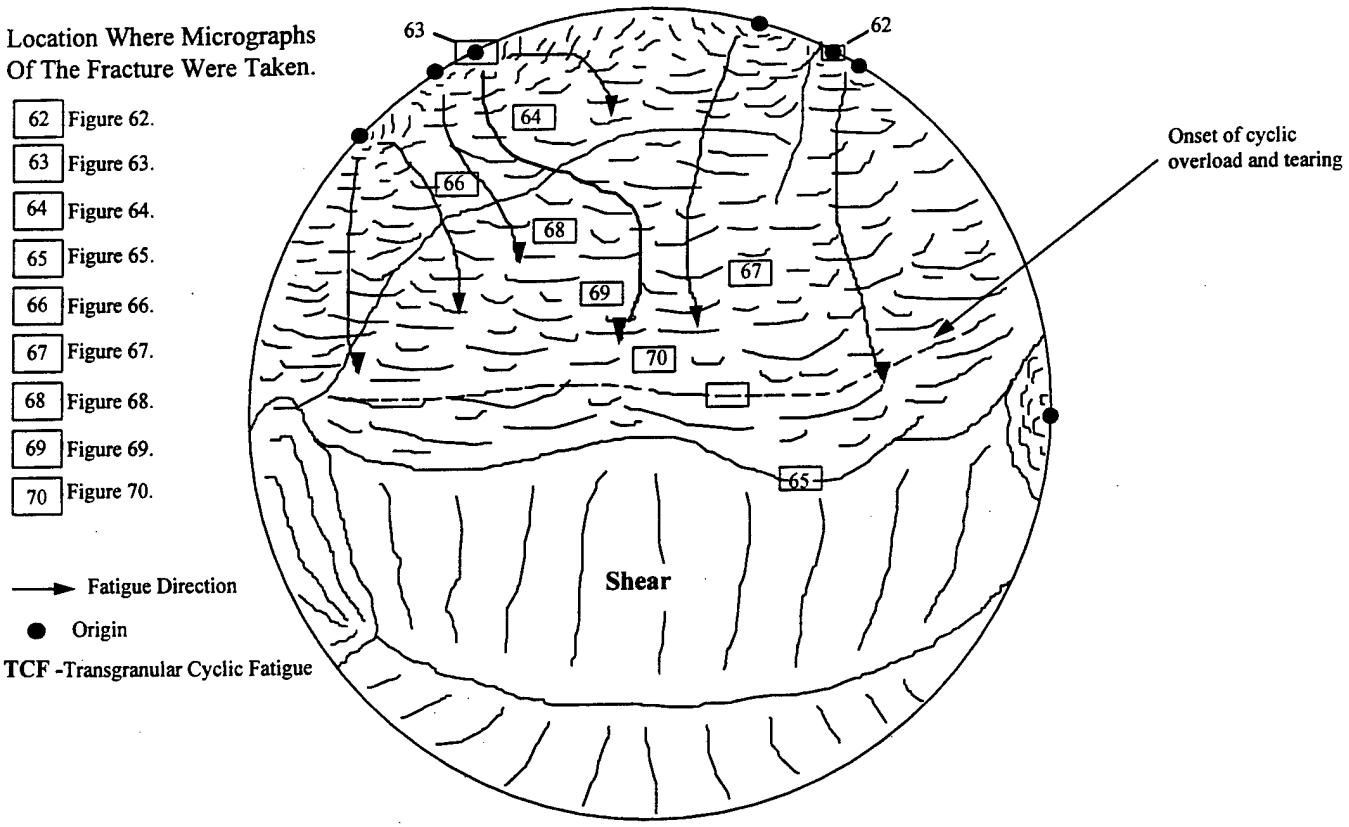

Figure 56. Schematic of the Fracture Surface of SIK Tie Rod -00938.

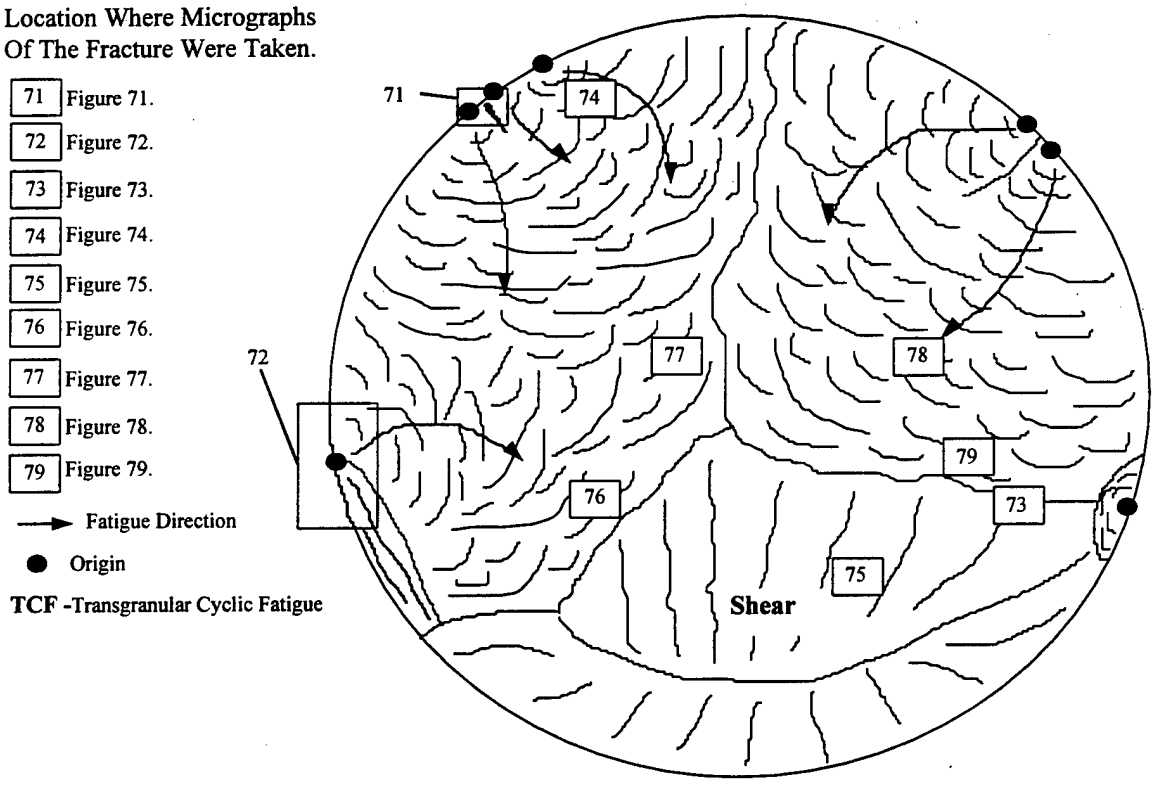

Figure 57. Schematic of the Fracture Surface of SIK Tie Rod -00973.

Location Where Micrographs Of The Fracture Were Taken.

80	Figure 80.	86	Figure 86.
81	Figure 80.	87	Figure 87.
82	Figure 82.	88	Figure 88.
83	Figure 83.	89	Figure 89.
84	Figure 84.	90	Figure 90.
85	Figure 85.	91	Figure 91.

→ Fatigue Direction

● Origin

TCF Transgranular Cyclic Fatigue

D Ductility

CO Cyclic Overload

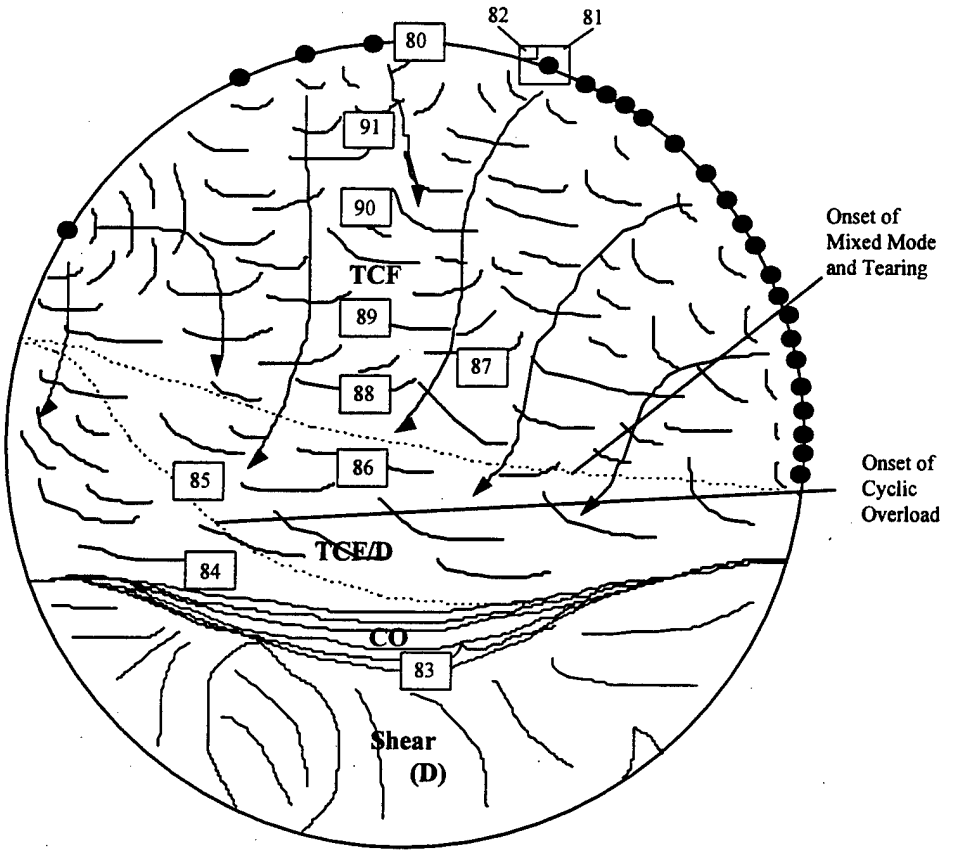

Figure 58. Schematic of the Fracture Surface of PUR Tie Rod -174.

Location Where Micrographs Of The Fracture Were Taken.

92	Figure 92.
93	Figure 93.
94	Figure 94.
95	Figure 95.
96	Figure 96.
97	Figure 97.
98	Figure 98.
99	Figure 99.
100	Figure 100.
101	Figure 101.
102	Figure 102.

→ Fatigue Direction

● Origin

TCF Transgranular Cyclic Fatigue

D Ductility

CO Cyclic Overload

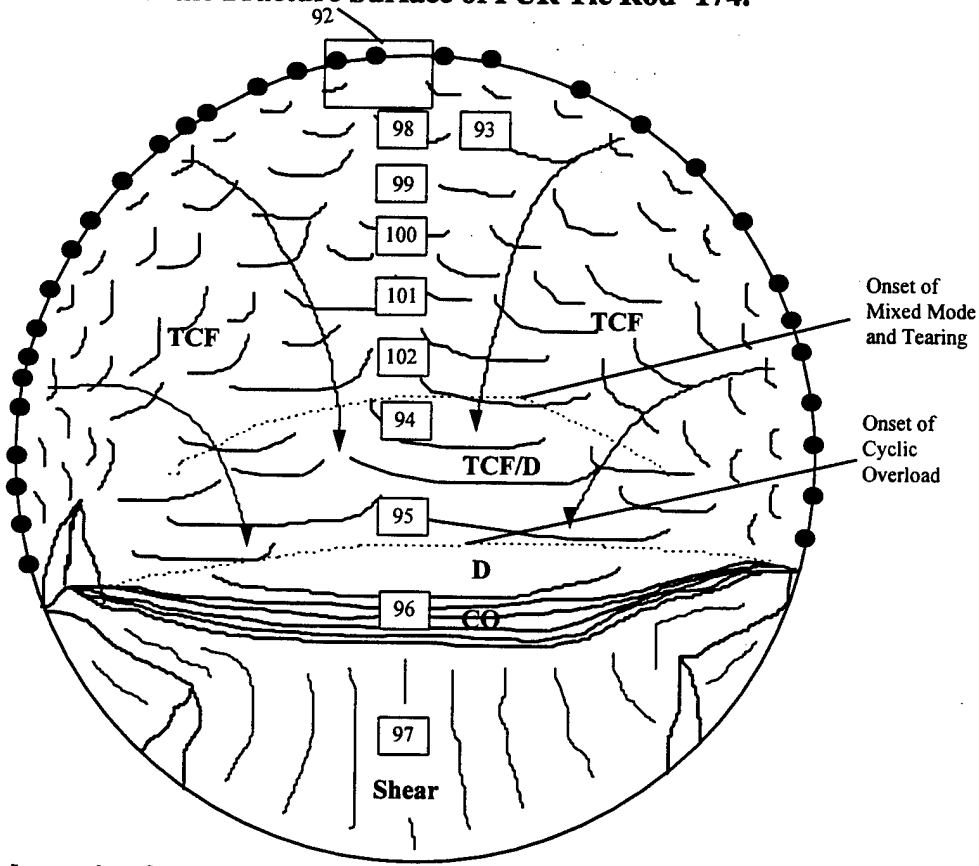

Figure 59. Schematic of the Fracture Surface of PUR Tie Rod -177.

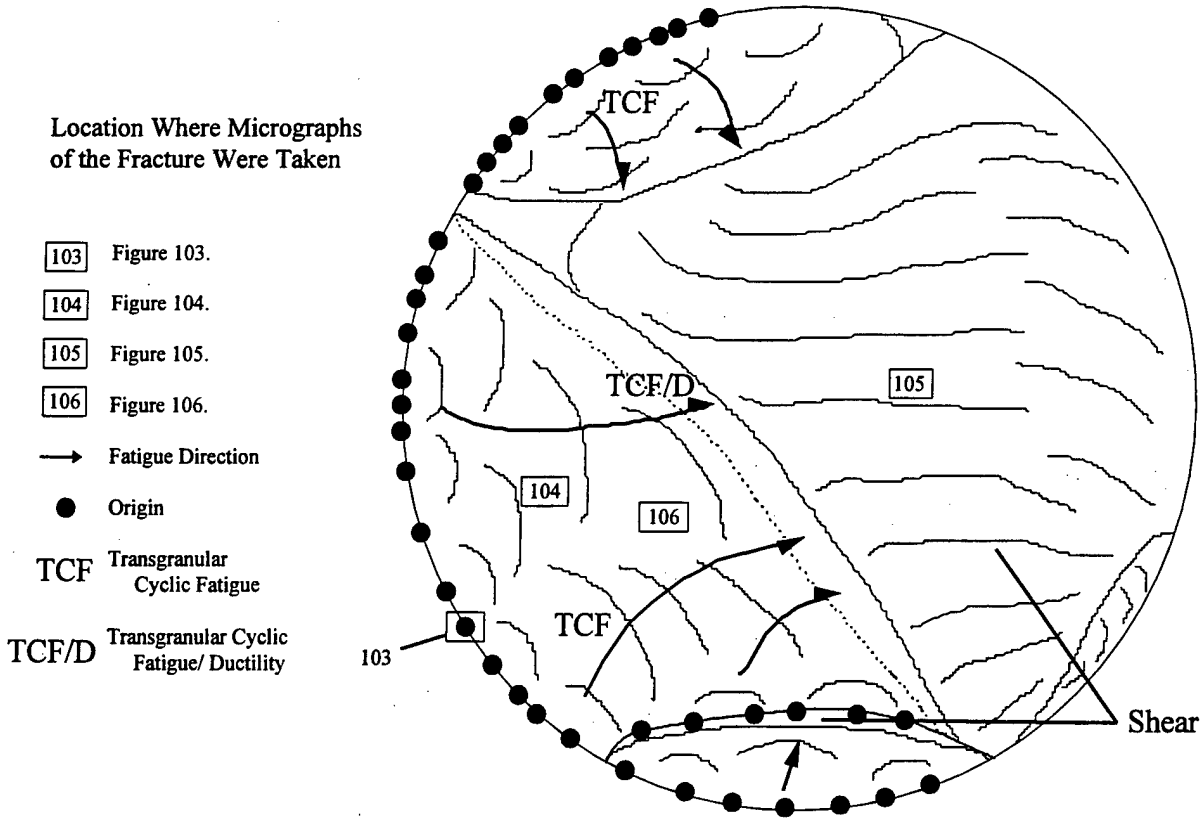

Figure 60. Schematic of the Fracture Surface of S&S Tie Rod -2.

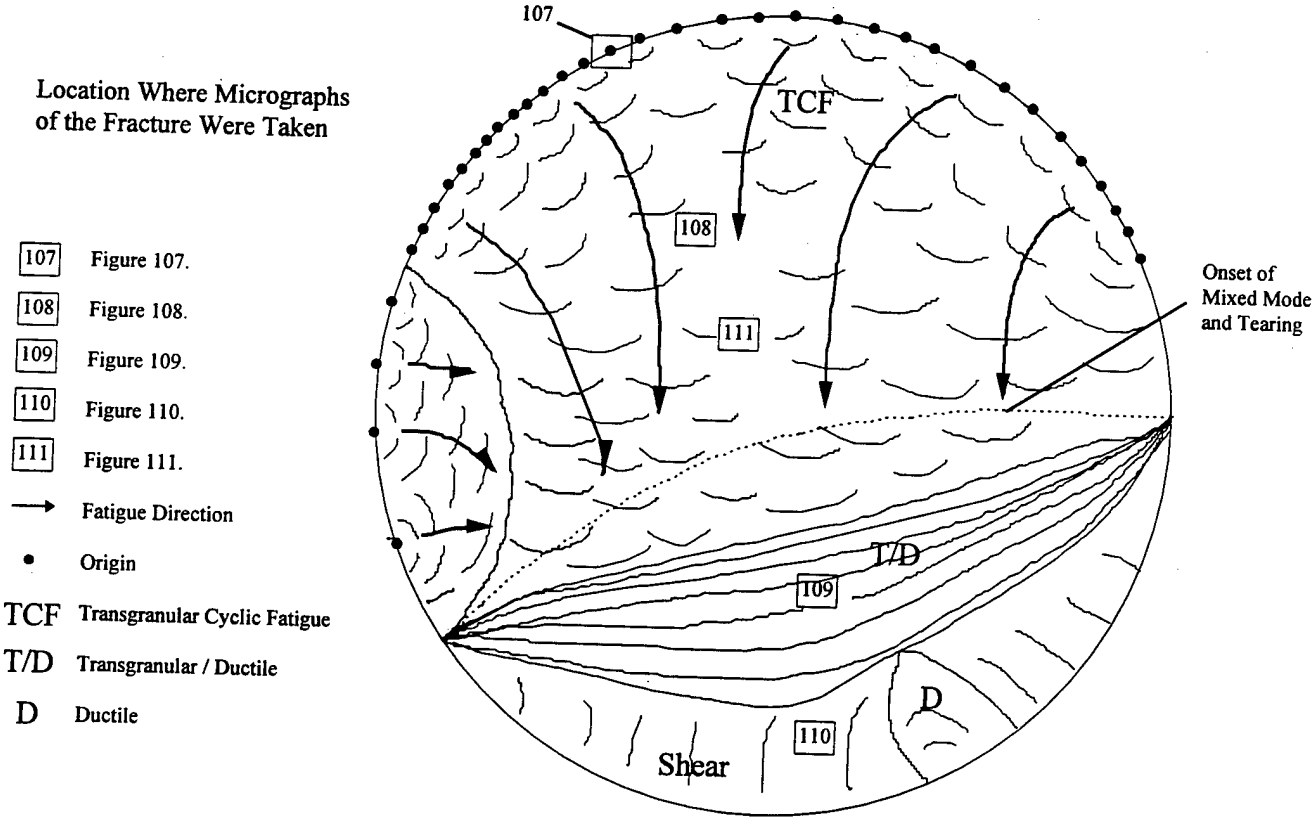

Figure 61. Schematic of the Fracture Surface of S&S Tie Rod -3.

Figure 62. A Typical Origin on the Fracture Surface of SIK Rod -00938 (Mag. 500x).

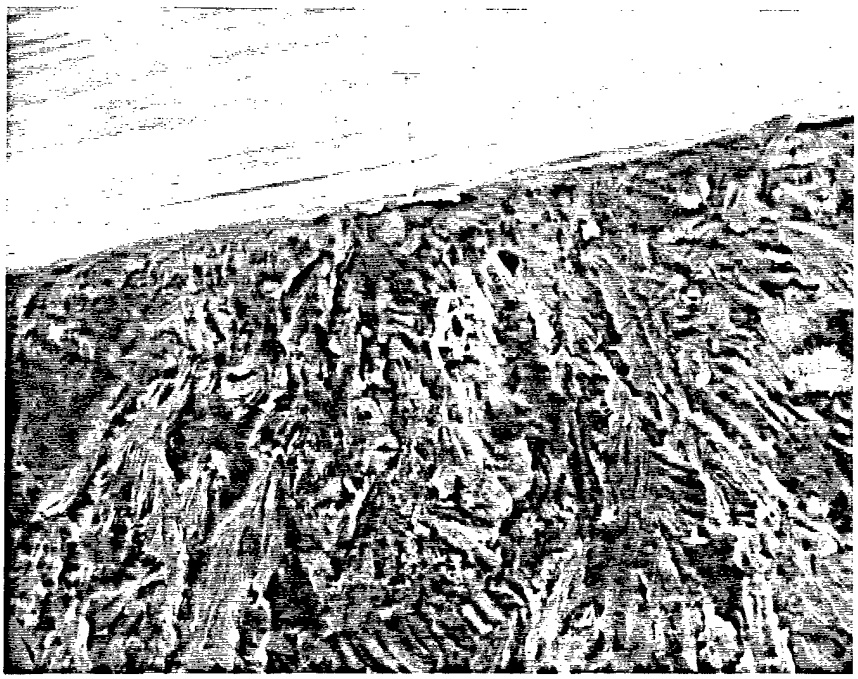

Figure 63. Another Origin on the Fracture Surface of SIK Rod -00938 (Mag. 1kx).

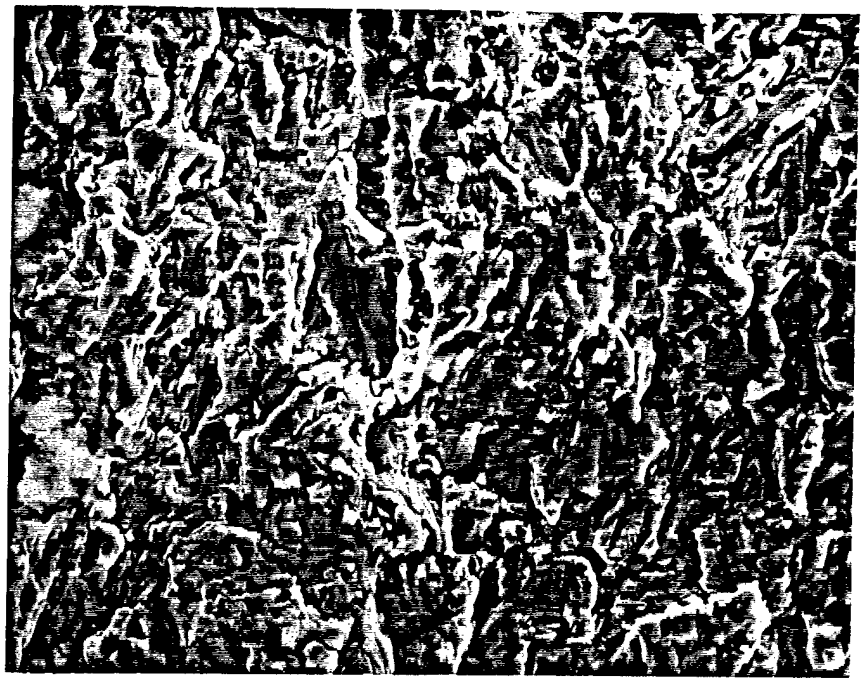

Figure 64. Typical Transgranular Morphology of SIK Rod -00938. This Morphology Was Characteristic of the Fatigue Region (Mag. 1kx).

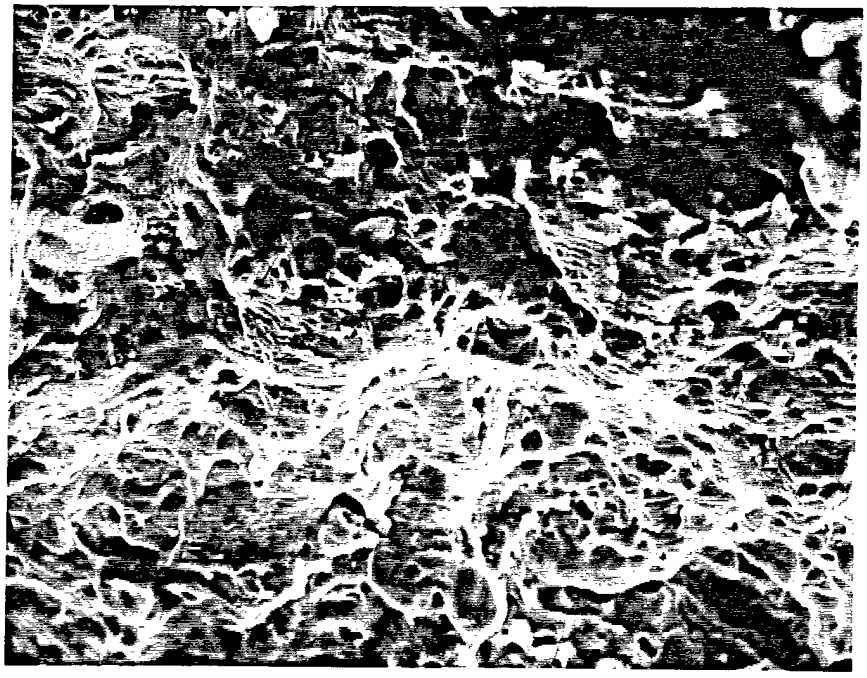

Figure 65. The Morphology of SIK Rod -00938 at the Interface of Fatigue and Overload (Mag. 1kx).

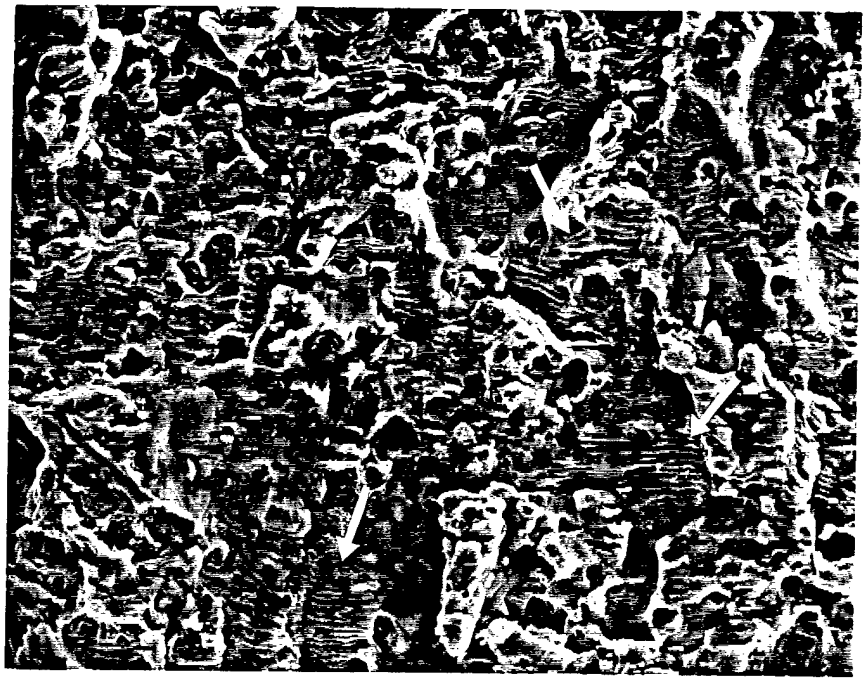

Figure 66. Typical Striations on the Fracture Surface of SIK Rod -00938 (Mag. 1kx).

Figure 67. Striations Noted on the Surface of SIK Rod -00938 (Mag. 25kx).

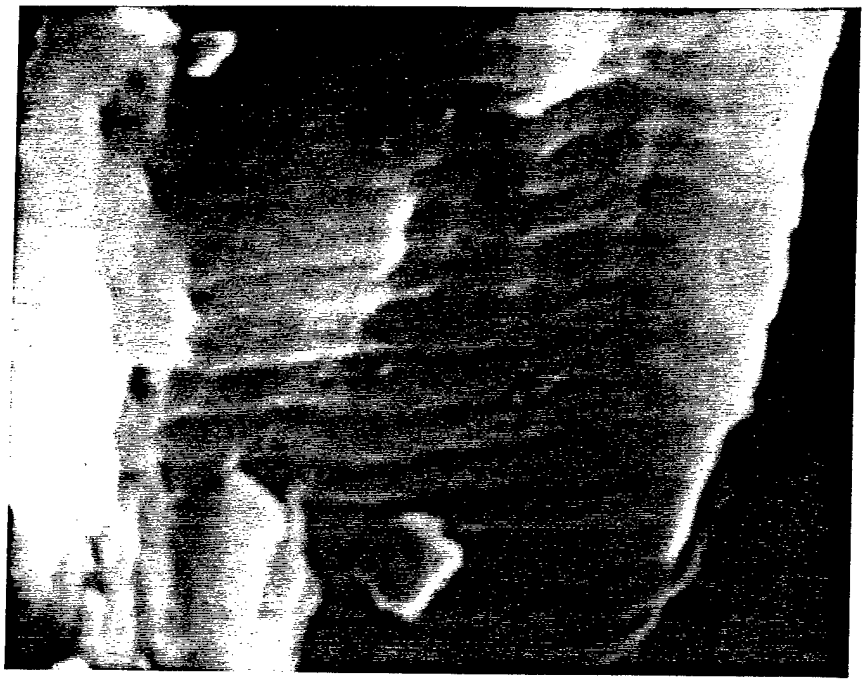

Figure 68. Additional Striations Noted on the Surface of SIK Rod -00938 (Mag. 25kx).

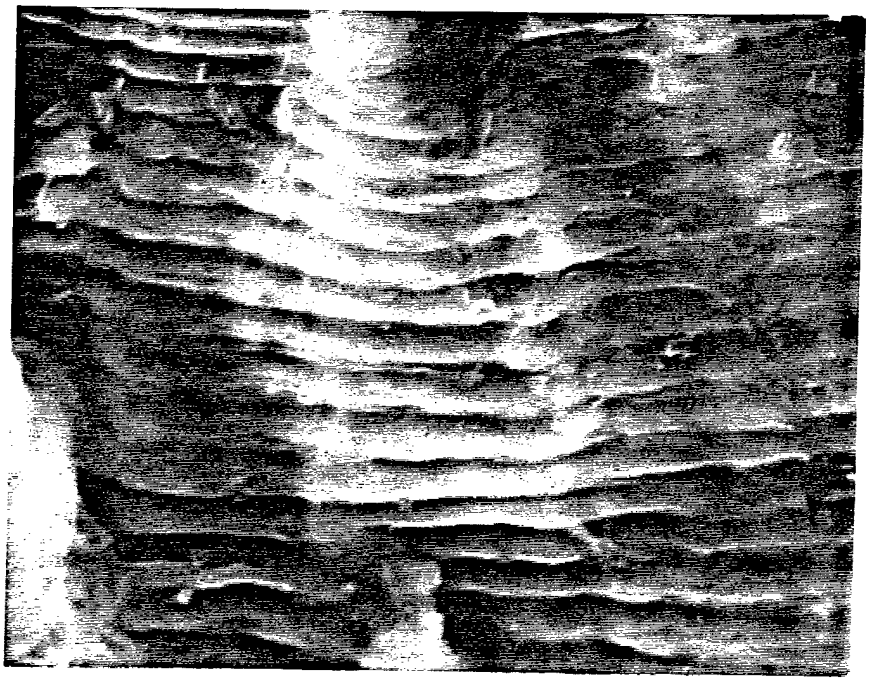

Figure 69. Striations Noted on the Surface of SIK Rod -00938 (Mag. 10kx).

Figure 70. Striations Noted on the Surface of SIK Rod -00938 (Mag. 5kx).

Figure 71. Typical Origin Noted on the Fracture Surface of SIK Rod -00973 (Mag. 200x).

Figure 72. Typical Origin Noted on the Fracture Surface of SIK Rod -00973 (Mag. 20x).

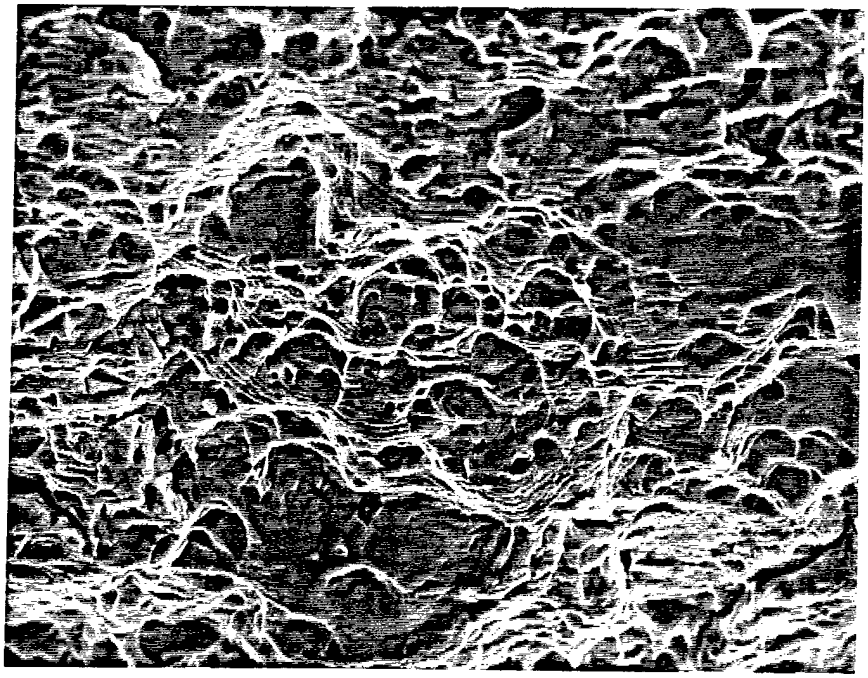

Figure 73. The Transgranular/Ductile Morphology of SIK Rod -00973 Away From the Origins (Mag. 1kx).

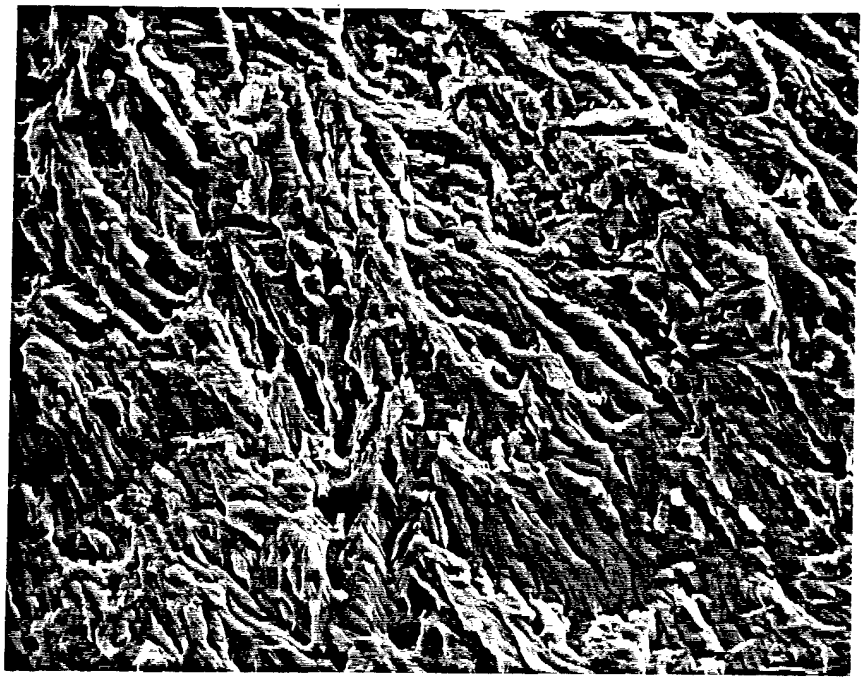

Figure 74. The Transgranular Morphology Contained Within the Fatigue Zone of SIK Tie Rod -00973 Away From the Origins (Mag. 1kx).

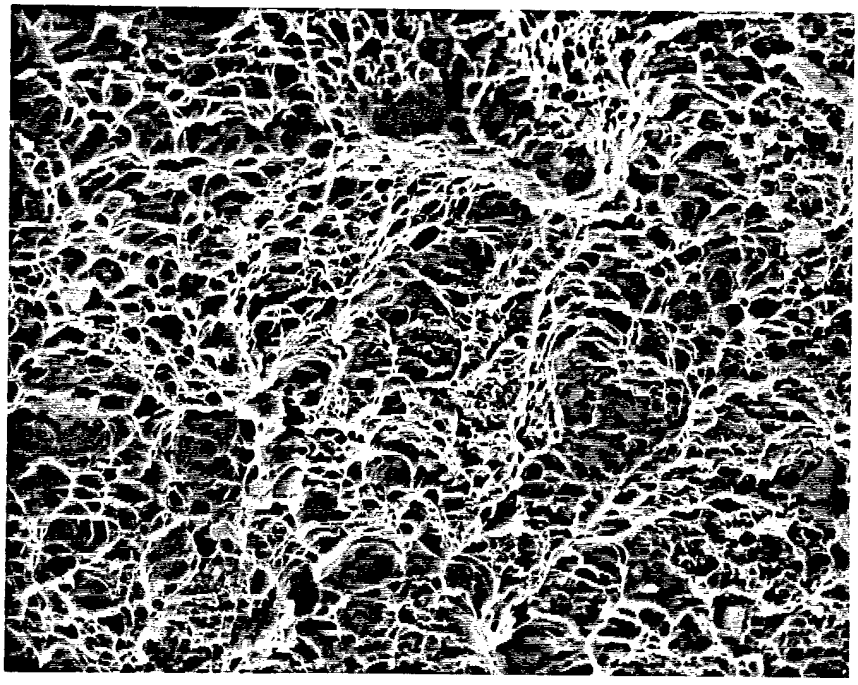

Figure 75. The Ductile Morphology of SIK Tie Rod -00973 Within the Overload Region (Mag. 1kx).

Figure 76. Typical Striations Noted on the Surface of SIK Rod -00973 (Mag. 5kx).

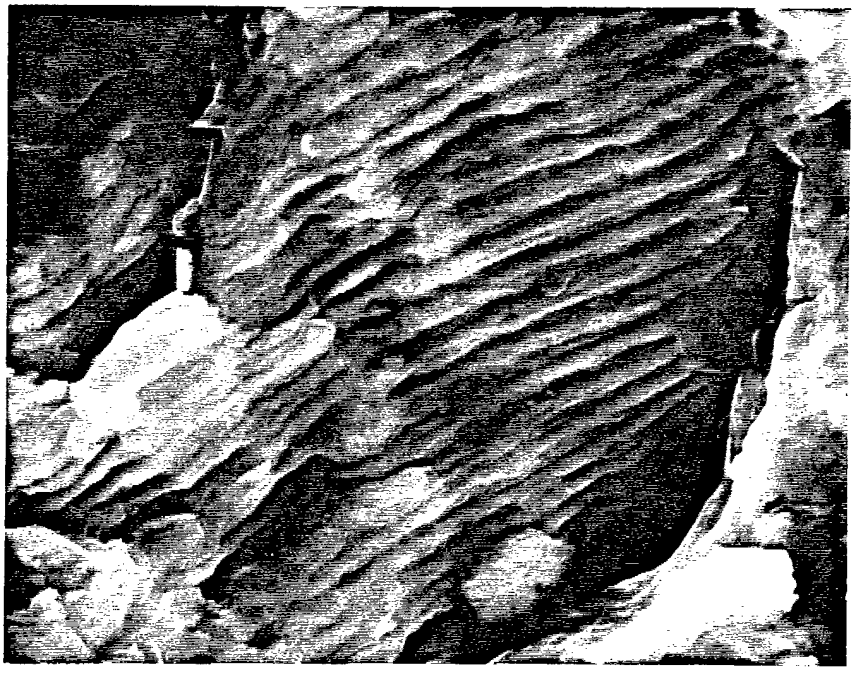

Figure 77. Typical Striations Noted on the Surface of SIK Rod -00973 (Mag. 10x).

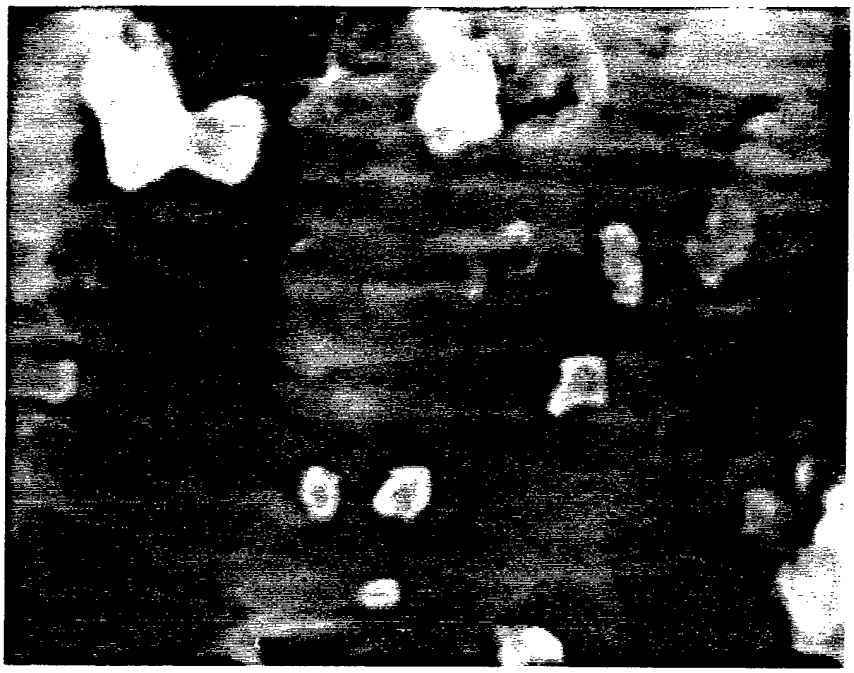

Figure 78. Typical Striations Noted on the Surface of SIK Rod -00973 (Mag. 20kx).

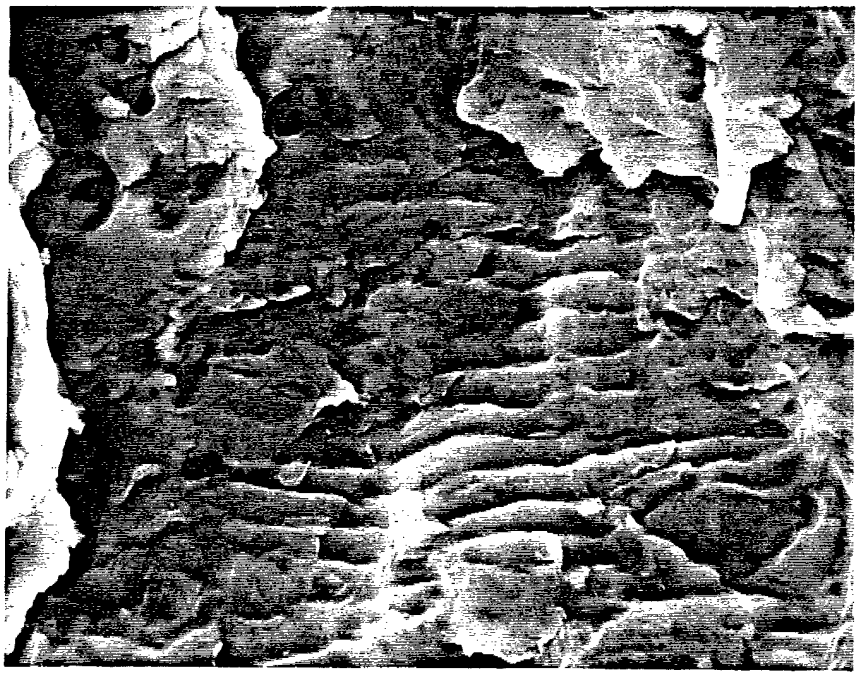

Figure 79. Typical Striations Noted on the Surface of SIK Rod -00973 Near the Shear Region (Mag. 5kx).

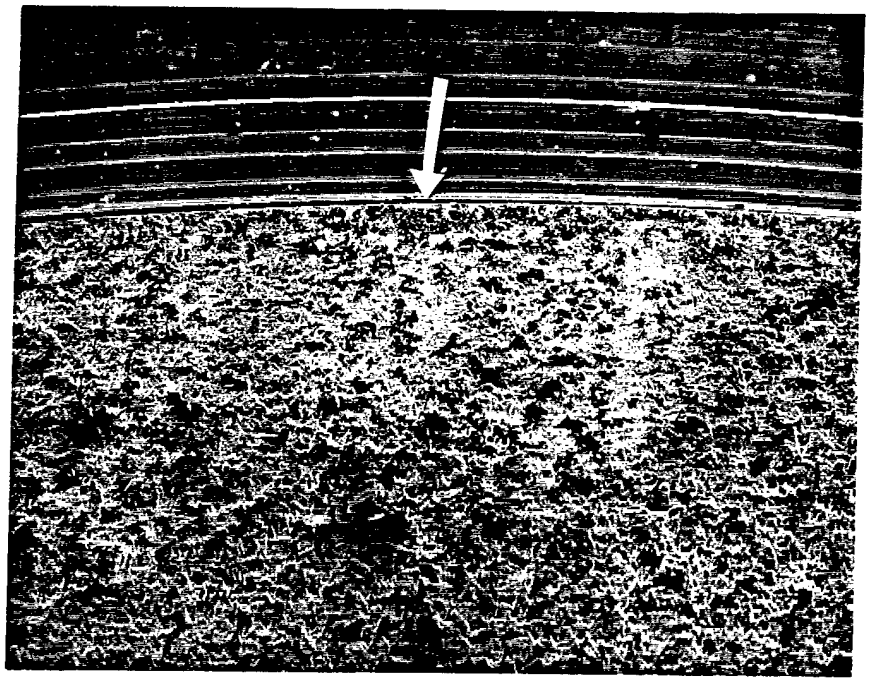

Figure 80. Typical Origin Located on the Fracture Surface of PUR Rod -174 (Mag. 50x).

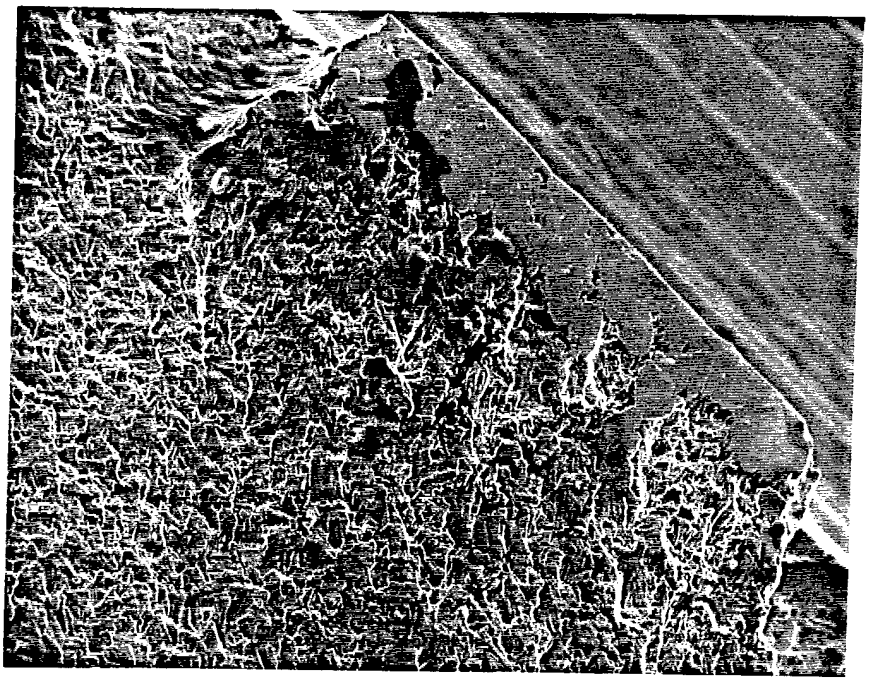

Figure 81. Typical Origin Located on the Fracture Surface of PUR Rod -174 (Mag. 150x).

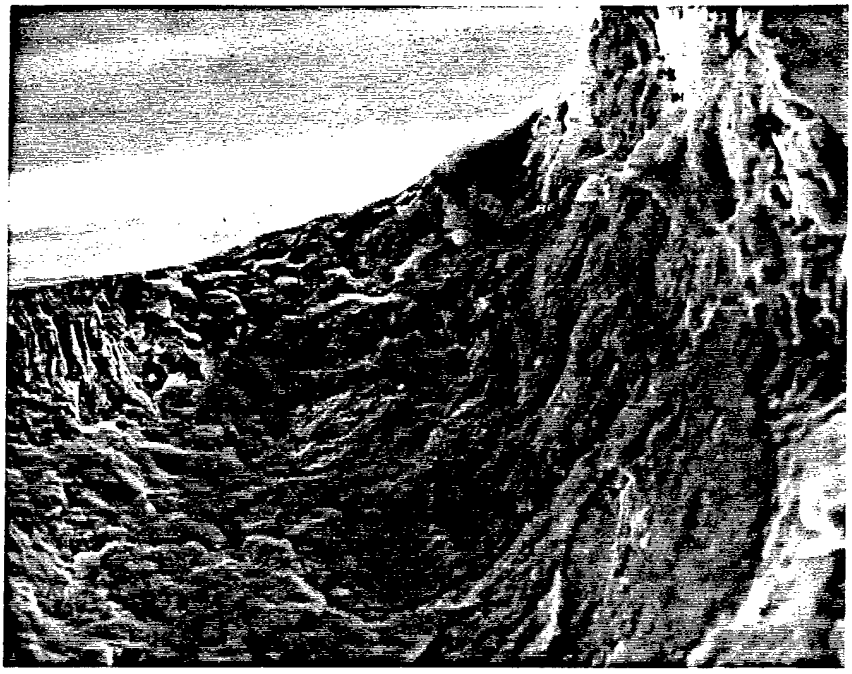

Figure 82. Detail of Origin Located on the Fracture Surface of PUR Rod -174 (Mag. 750x).

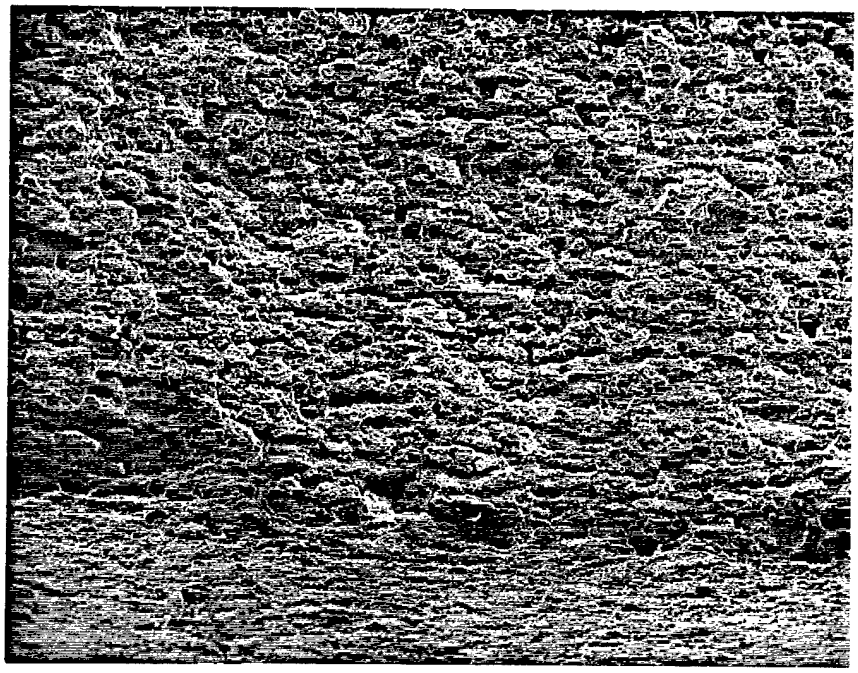

Figure 83. The Morphology of PUR Rod -174 Consisting of a Transition Zone Between Cyclic Overload and Shear (Mag. 50x).

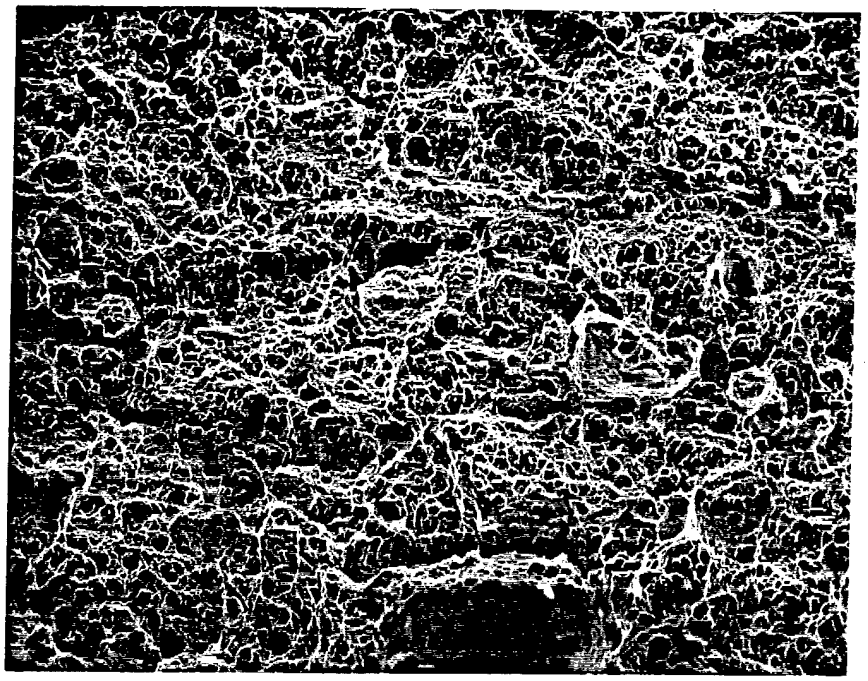

Figure 84. Cyclic Overload Morphology on the Fracture Surface of PUR Rod -174 (Mag. 200x).

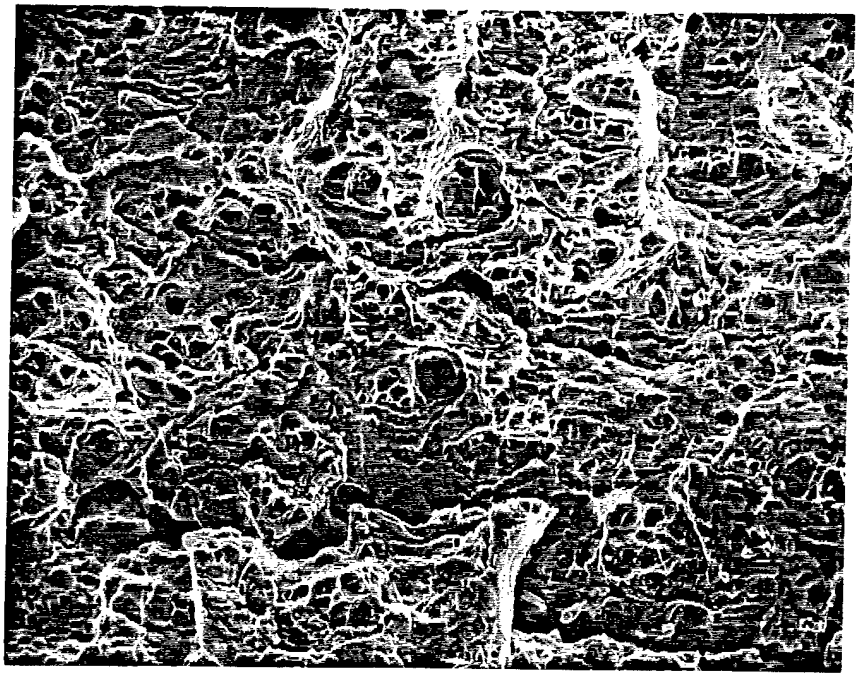

Figure 85. A Morphology Consisting of Tearing as Well as Cyclic Overload Noted on the Fracture Surface of PUR Rod -174 (Mag. 500x).

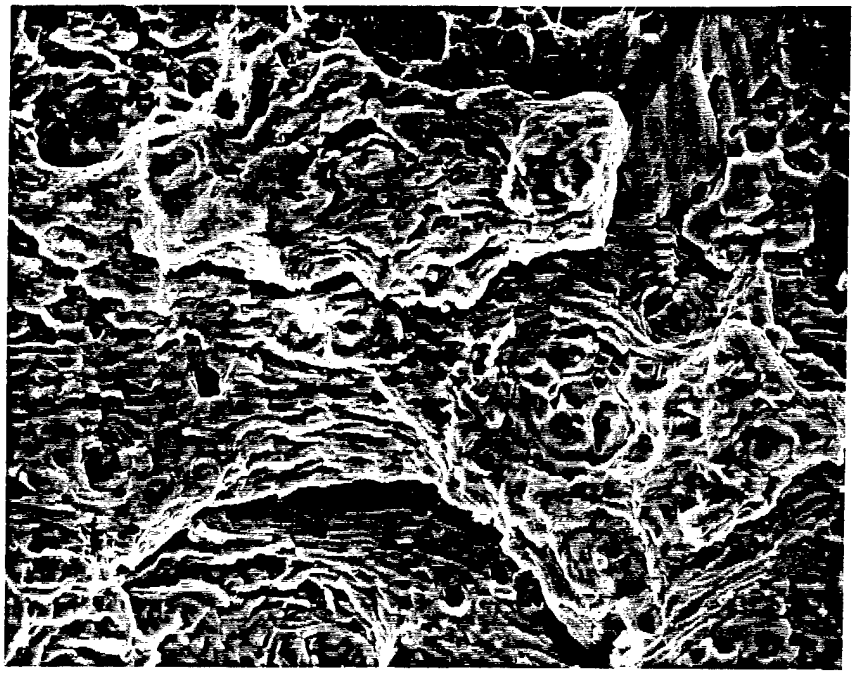

Figure 86. A Morphology Consisting of Striations, Tearing, and Ductility Observed on the Fracture Surface of PUR Rod -174 (Mag. 1kx).

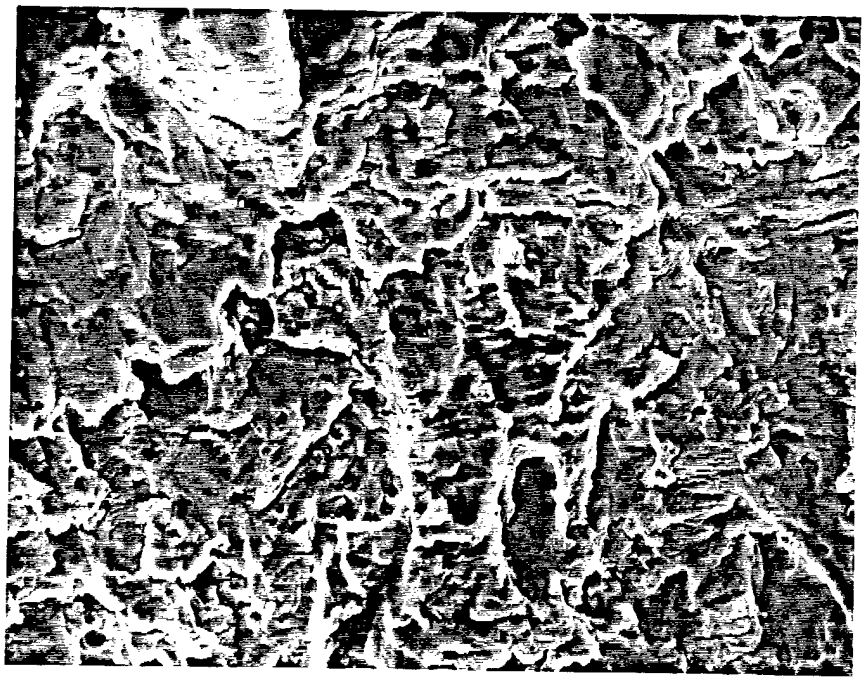

Figure 87. The Transgranular Morphology Representative of the Fatigue Zones of PUR Tie Rod -174 (Mag. 1kx).

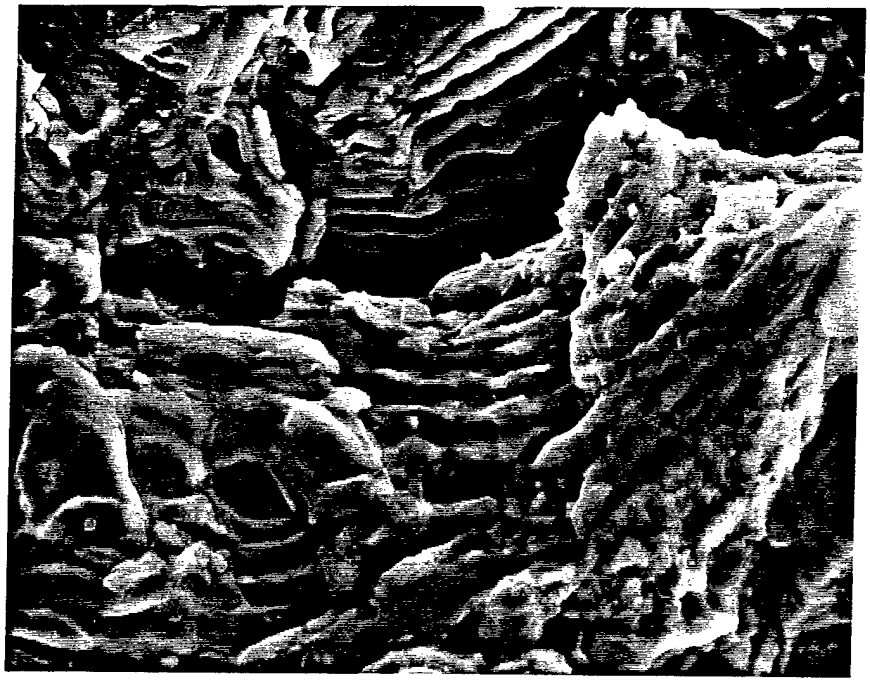

Figure 88. Striations Noted Within the Fracture Surface of PUR Rod -174 (Mag. 3kx).

Figure 89. Striations Noted Within the Fracture Surface of PUR Tie Rod -174 (Mag. 5kx).

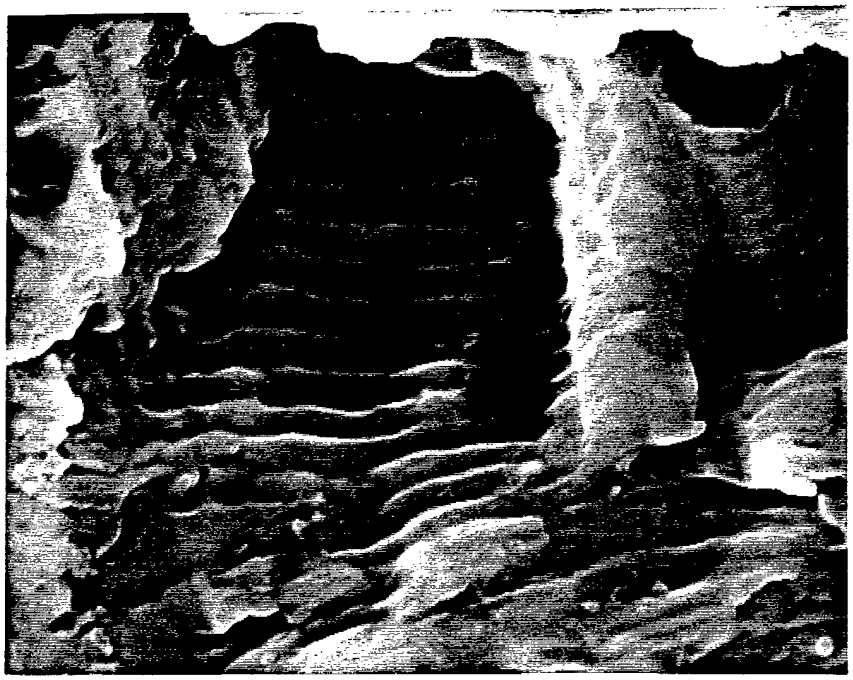

Figure 90. Striations Noted Within the Fracture Surface of PUR Rod -174 (Mag. 10kx).

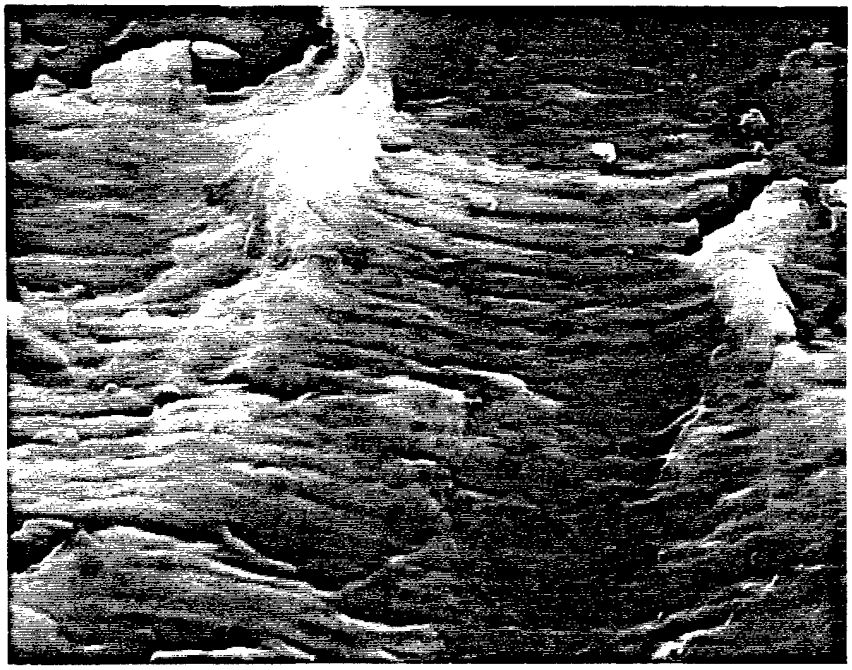

Figure 91. Striations Noted Within the Fracture Surface of PUR Rod -174 (Mag. 10kx).

Figure 92. A Typical Origin of PUR Rod -177 (Mag. 100×).

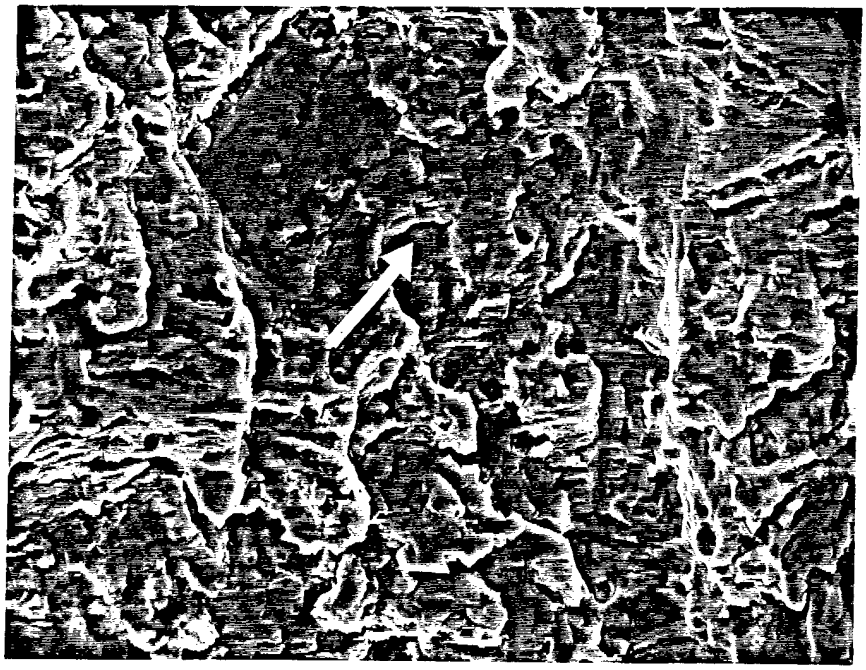

Figure 93. A Transgranular Cyclic Fatigue Morphology Observed Within the Fracture Surface of PUR Rod -177. Note the Fatigue Striations (Mag. 1kx).

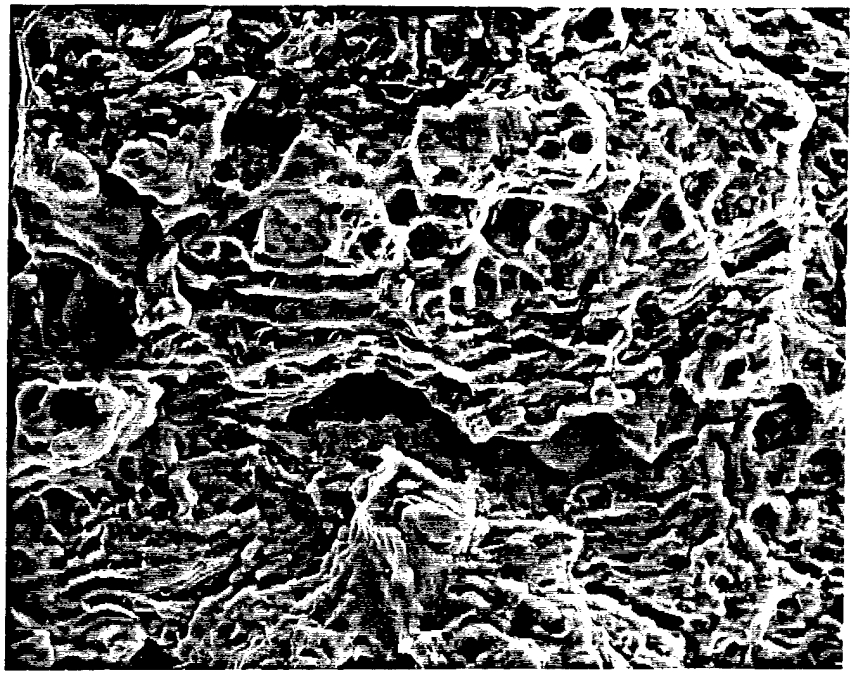

Figure 94. A Transgranular Morphology Mixed With Tearing on the Fracture Surface of PUR Rod -177 (Mag. 1kx).

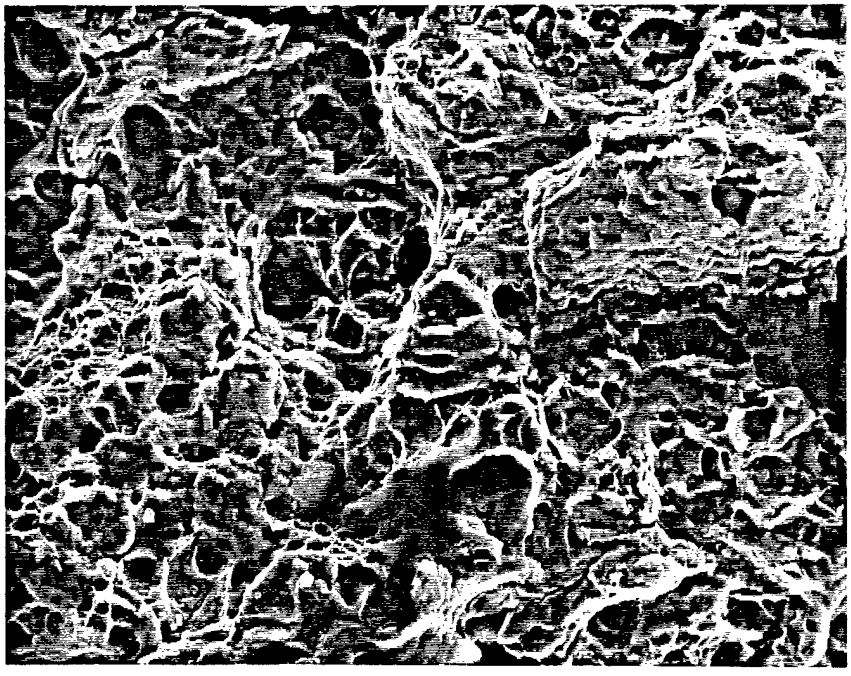

Figure 95. The Morphology of PUR Rod -177 Consisting of Striations Mixed With Ductility (Mag. 1kx).

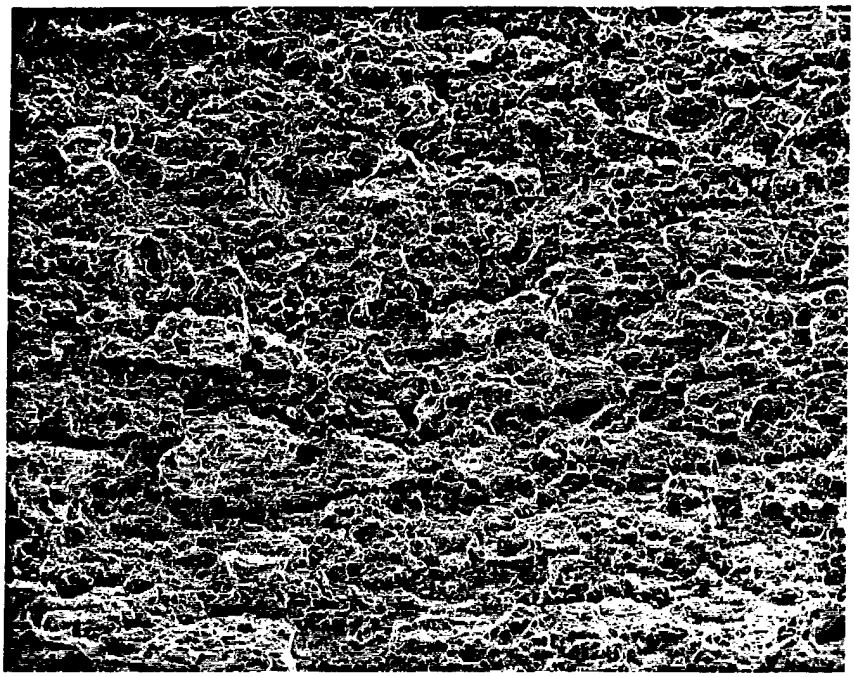

Figure 96. The Ductile Morphology of PUR Rod -177 Within the Overload Region Showing Incremental Loading (Mag. 100×).

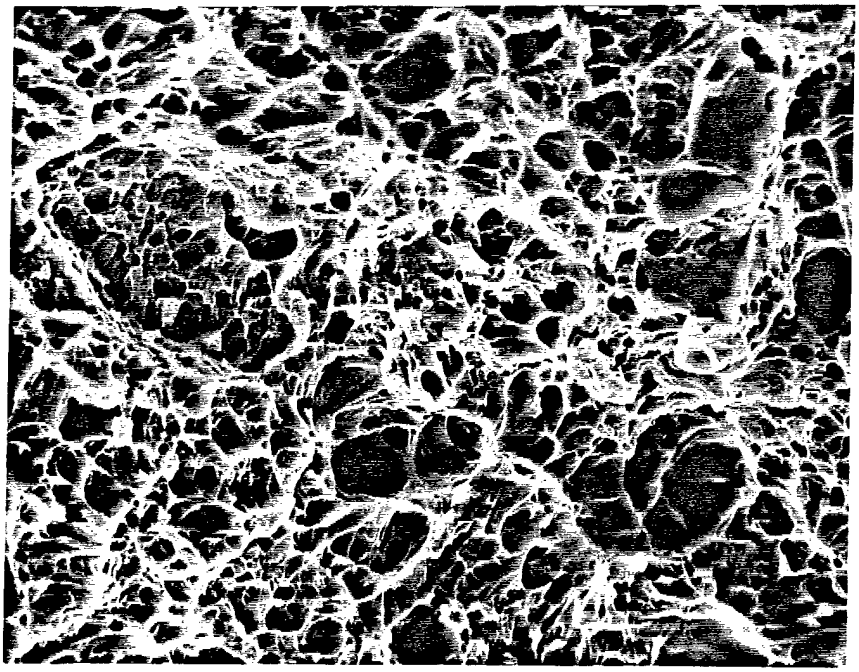

Figure 97. The Ductile Morphology of PUR Rod -177 Showing Dimples Within the Overload Zone (Mag. 2.5x).

Figure 98. Striations Noted on the Fracture Surface of PUR Rod -177 (Mag. 10kx).

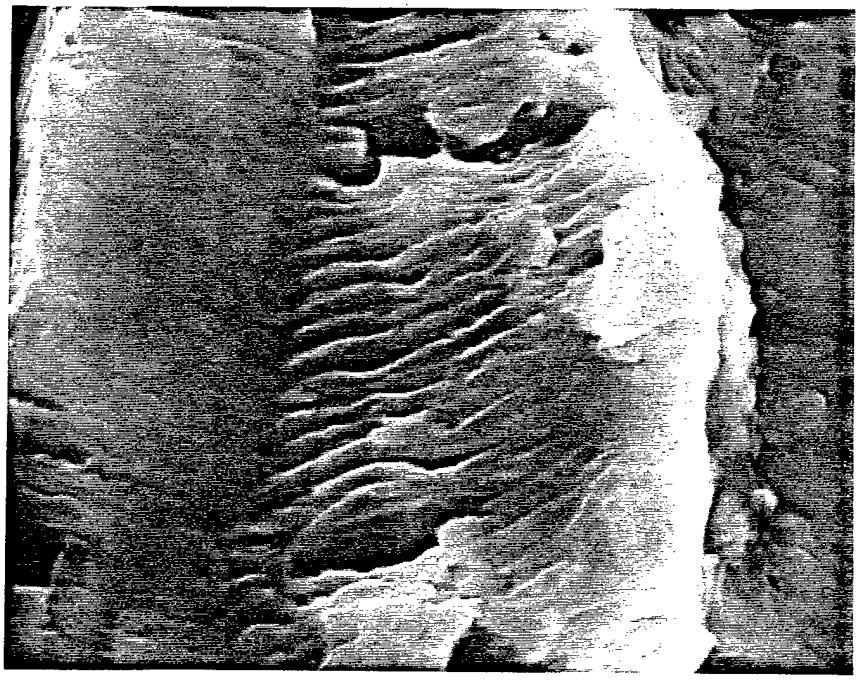

Figure 99. Additional Striations Noted on the Fracture Surface of PUR Rod -177 (Mag. 10kx).

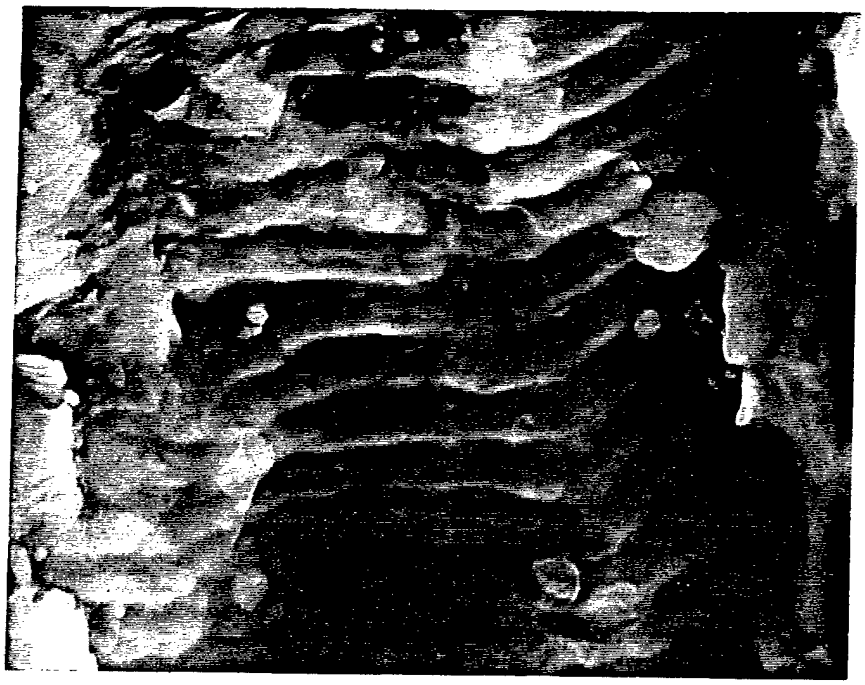

Figure 100. Striations Noted on PUR Rod -177, Note How Spacing Is Increasing From Figure 98 and 99 (Mag. 10kx).

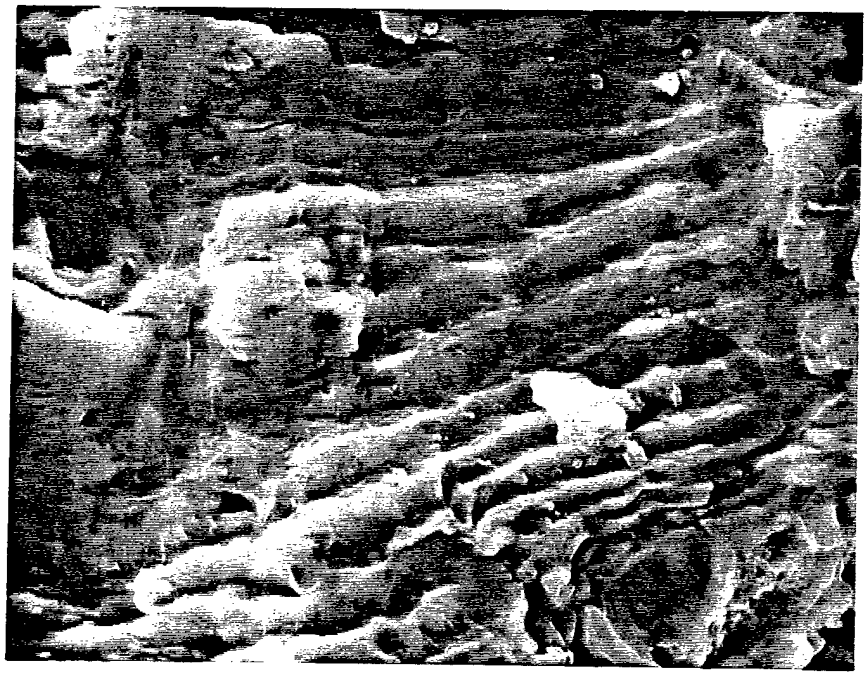

Figure 101. Striations Noted on the Fracture Surface of PUR Rod -177 (Mag. 5kx).

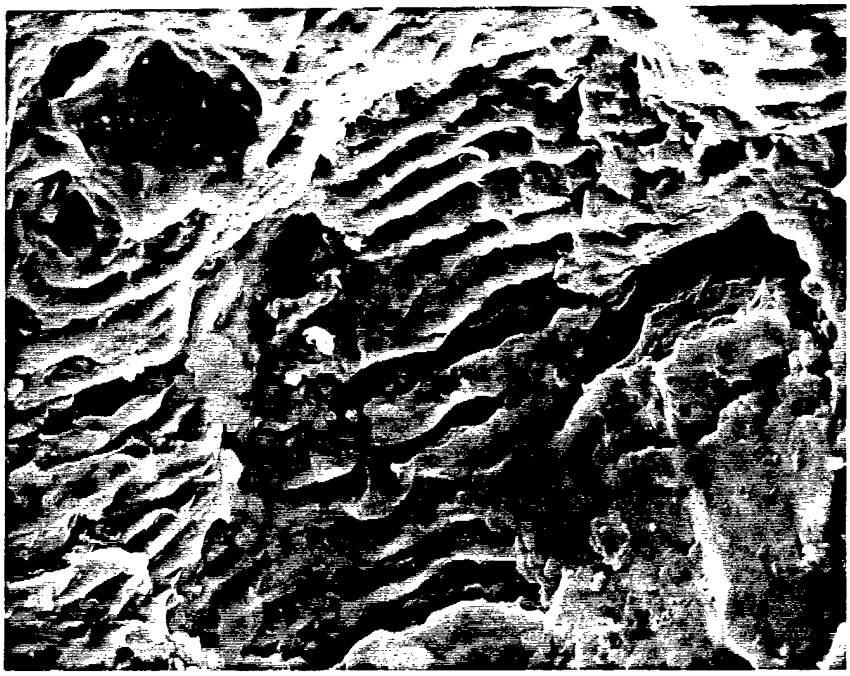

Figure 102. Striations Noted on the Fracture Surface of PUR Rod -177 (Mag. 3kx).

Figure 103. A Typical Origin on the Fracture Surface of S&S Tie Rod -2 (Mag. 150x).

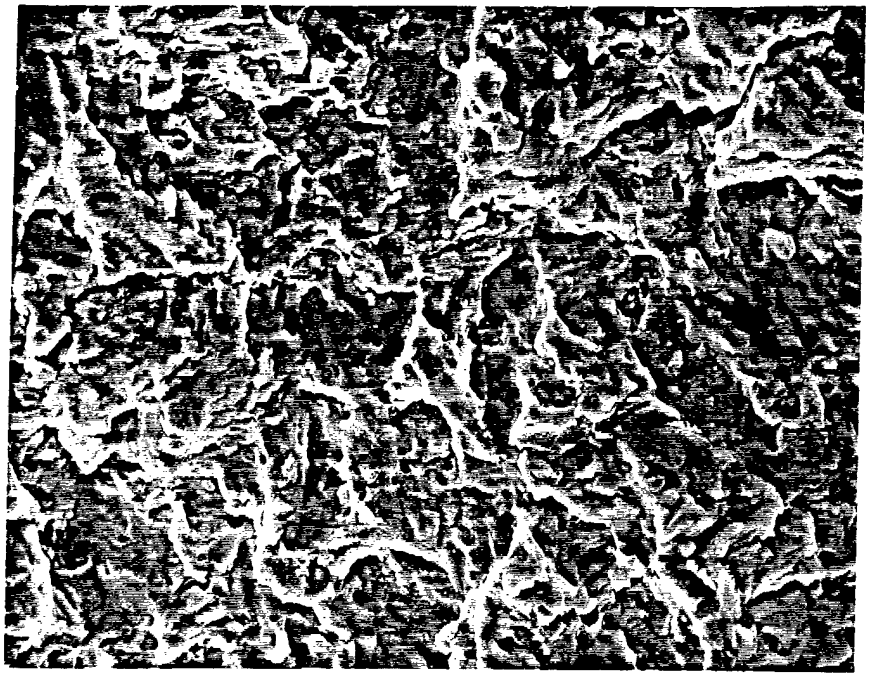

Figure 104. Typical Transgranular Morphology of S&S Rod -2. This Morphology Was Characteristic of Fatigue (Mag. 1kx).

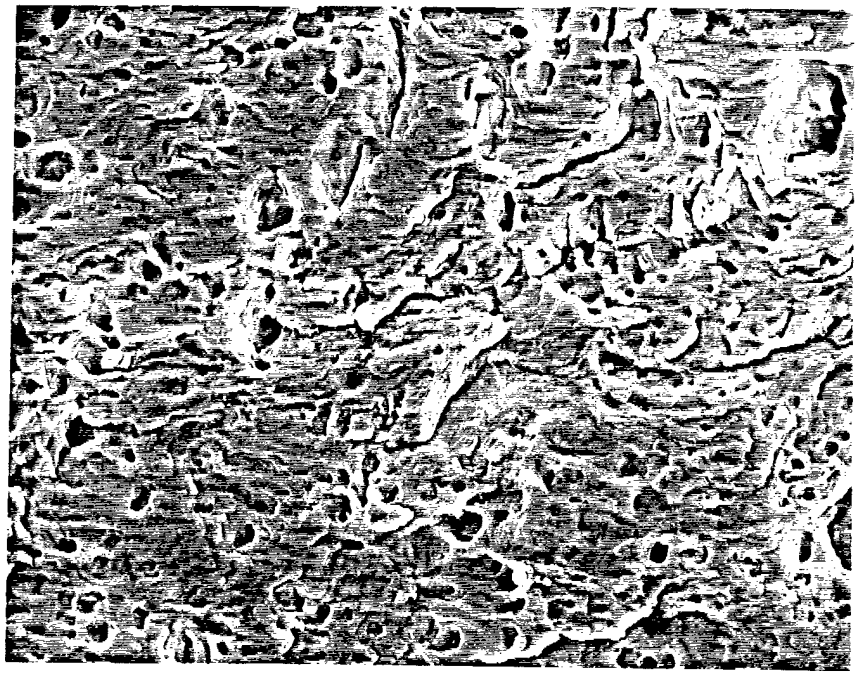

Figure 105. Directional Tearing Within the Shear Region of S&S Rod -2 (Mag. 1kx).

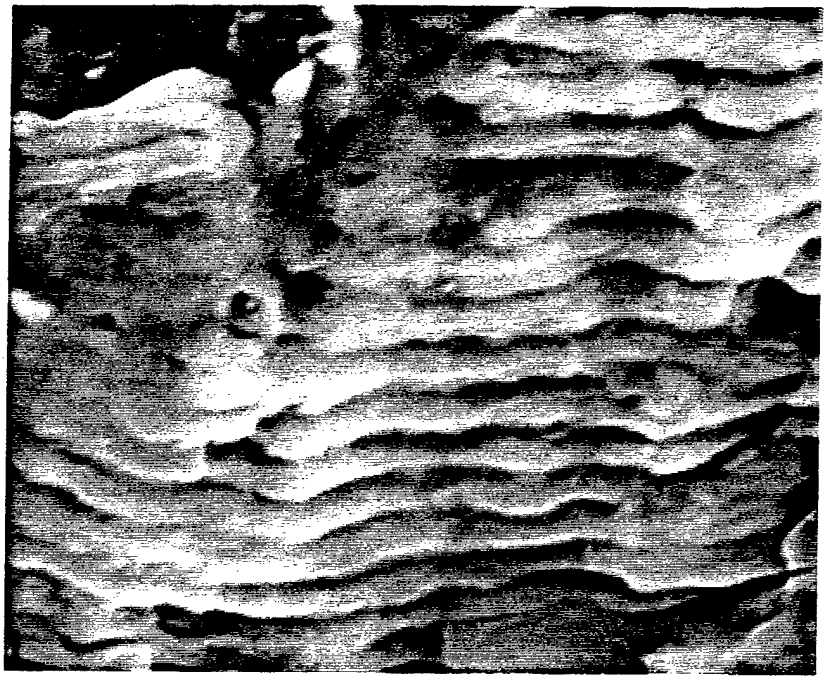

Figure 106. Typical Striations Noted on the Surface of the S&S Rod -2 (Mag. 10kx).

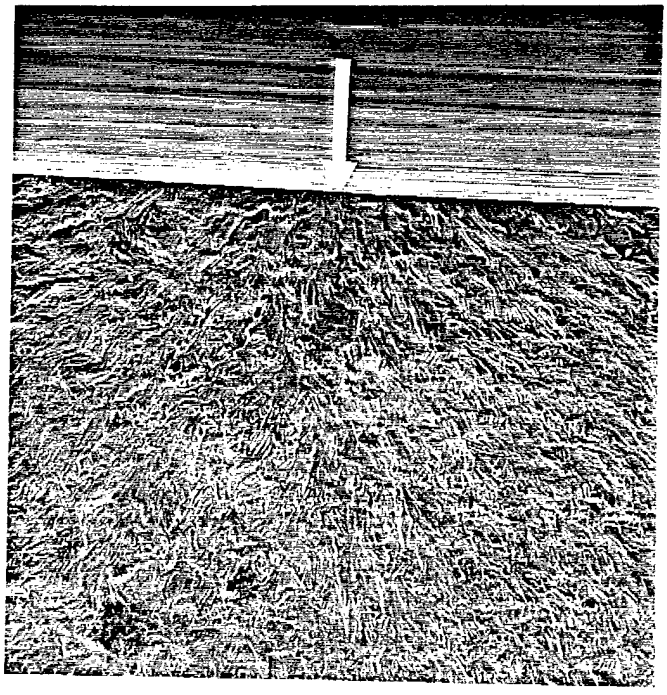

Figure 107. Typical Origin Noted on the Fracture Surface of the S&S Rod -3 (Mag. 200x).

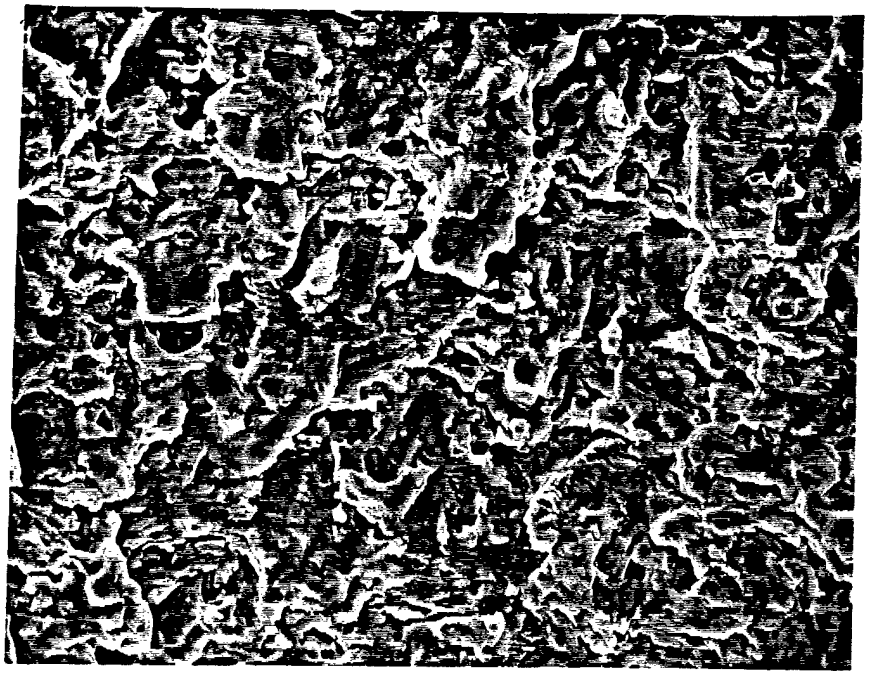

Figure 108. The Transgranular Morphology Contained Within the Fatigue Zone of the S&S Tie Rod -3 (Mag. 1kx).

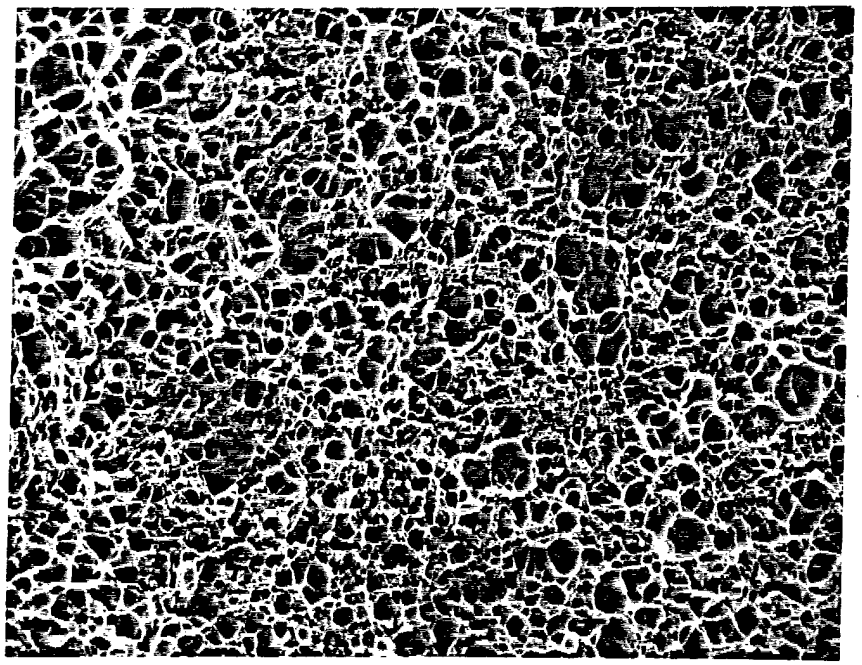

Figure 109. The Ductile Morphology of S&S Tie Rod -3 Within the Overload Region (Mag. 500x).

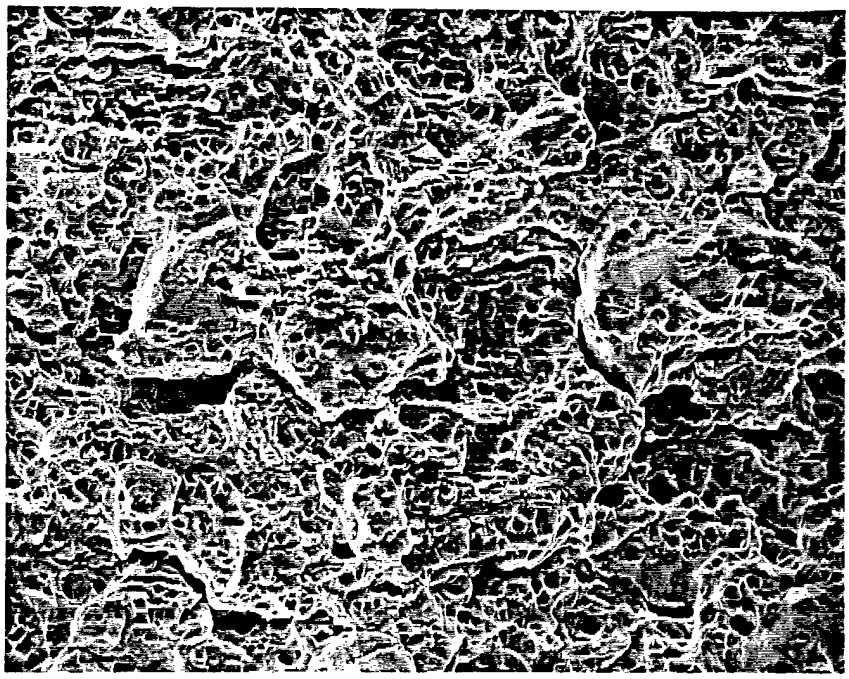

Figure 110. The Ductile Morphology of S&S Rod -3 Showing Dimples Within the Shear Region (Mag. 1kx).

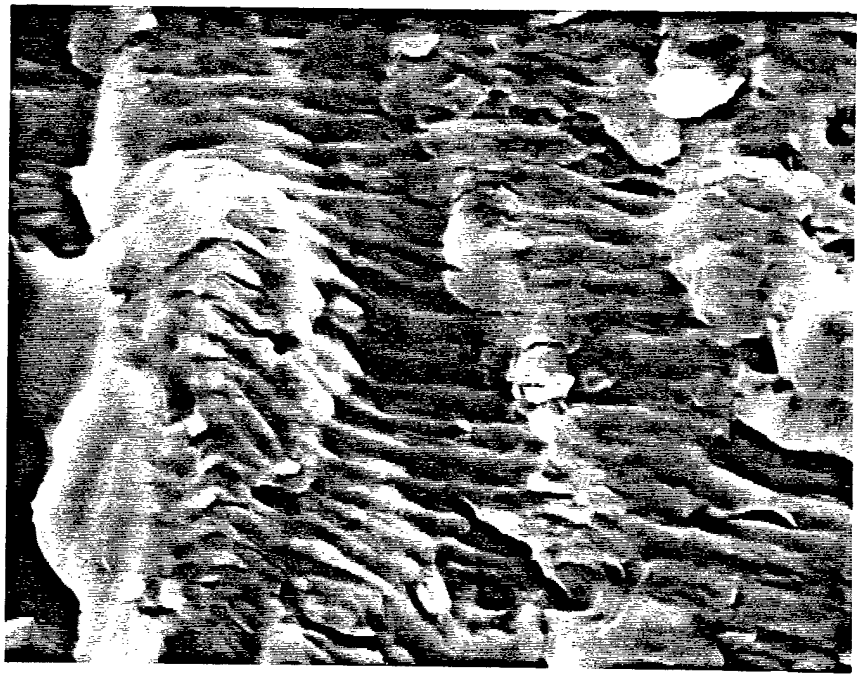

Figure 111. Typical Striations Noted on the S&S Tie Rod -3 (Mag. 5kx).

INTENTIONALLY LEFT BLANK.

12. References

1. SIK Engineering Drawing for P/N 7102-08102/103, Revision D, Sikorsky Helicopter, Stratford, CT, 16 November 1992.

2. Aerospace Material Specification (AMS) 5629. "Steel, Corrosion Resistant, Bars, Forgings, Rings, and Extrusions." Society of Automotive Engineers, Inc., Warrendale, PA, 1986.

3. Aerospace Material Specification (AMS) 2315. "Determination of Free Ferrite Content." Society of Automotive Engineers, Inc., Warrendale, PA, 1986.

4. MIL-S-8879. "Screw Threads, Controlled Radius Root With Increased Minor Diameter." Custodians Army-AR-Navy-AS, Air Force-11, Project No. THDS-0067, 25 July 1991.

5. Jasper, J. Private communication. Armco Corporation, 15 May 1996.

6. Armco Inc. "Armco PH 13-8 Mo Stainless Steel (XM-13, UNS S13800)." Product Data Bulletin No. S-24, Middletown, OH, 1964.

7. Battelle Memorial Institute. "Mechanical Property Data, PH 13-8 Mo Stainless Steel." p. 41, Columbus, OH, 1972.

8. Peckner, D., and I. M. Bernstein. "Handbook of Stainless Steels." p. 4–18, McGraw-Hill Book Company, New York, NY, 1977.

INTENTIONALLY LEFT BLANK.

Appendix:

Heat-Treatment Investigation

INTENTIONALLY LEFT BLANK.

This section is an addendum to the "Investigation of the UH-60 Main Rotor Spindle Assembly Retaining Rods, P/N 70102-08102/-103." In the previous work, it was concluded that the difference in fatigue resistance of the tie rods manufactured by Sikorsky Helicopter (SIK) and Purdy Manufacturing Corporation (PUR) was primarily attributed to heat treatment. The U.S. Army Aviation and Troop Command (ATCOM) had requested, based upon the recommendation of the U.S. Army Research Laboratory (ARL), Materials Division (MD), an effort to raise the mechanical properties of the PUR material to that of the SIK material. In this investigation, samples of the SIK and PUR tie rods were solution heat-treated and aged to the H1050 condition in the laboratory. Subsequently, mechanical test specimens were taken from the laboratory heat-treated tie rods, and additional tensile and fatigue data were obtained. Previously, since the PUR material had not been heat-treated to the "typical" H1050 condition[1] premature failure occurred during fatigue testing at a stress level of 170 ksi, with an R value of 0.1 and a frequency of 25 Hz. The SIK tie rods, which exhibited mechanical properties that met or exceeded the "typical" properties of the H1050 condition, ran out to 3 million cycles. The intent of this study was to provide additional evidence indicating that the heat-treatment operation significantly affected the fatigue properties of the precipitation hardened (PH) 13-8 stainless steel. It was hypothesized that the laboratory heat-treated PUR material would now also run out to 3 million cycles, while the SIK material would yield similar results as before, since it had already been heat-treated to the "typical" properties of the H1050 condition.

Heat-Treat Schedule

The following procedure taken from AMS 5629 was utilized to heat-treat the PUR (tie rod SN 33129-177 [-177]) and SIK (tie rod SN D504-00938 [-00938]) material to the H1050 condition. Both tie rod sections were placed vertically in the same location within the furnace.

[1] Armco Inc. "Armco PH 13-8 Mo Stainless Steel (XM-13, UNS S13800)." Product Data Bulletin No. S-24, Middletown, OH, 1964.

Solution Heat Treatment

- Heat to 1,700° F +/- 25° F for 1-hr minimum,
- air cool until the parts are warm enough to handle, and
- run samples under cold water.

Age

- Heat to 1,050° F +/- 10° F for 4 hr +/- 15 min and
- air cool.

Hardness Testing

Specification AMS 5629 requires a minimum hardness of 40 HRc for the H1050 heat-treat condition of the PH 13-8 material. Surface macrohardness was determined from Rockwell C scale measurements directly on the part utilizing a 150-kg major load. PUR tie rod -177 and SIK tie rod -00938 were used in this experiment. A total of 10 readings was obtained from each specimen. The data acquired were corrected according to the standard round work correction for cylindrical specimens. These data are presented in Table A-1, along with the hardness values obtained before heat treatment. Previously, the average hardness of the SIK -00938 tie rod was 42.2 HRc in the as-received condition, while that of PUR tie rod -177 was 40.7 HRc The data show a slight increase in hardness for the SIK material (0.5 HRc) and a significant increase for the PUR material (2.7 HRc).

Tensile Testing

A tensile specimen was fabricated from each of the two heat-treated tie rods to confirm the mechanical properties of the H1050 condition. Cylindrical rods were sectioned from the tie rods by wire EDM, and final machining was performed to achieve the dimensions presented in the main work. Table A-2 contains the results obtained, as well as the data previously collected on the tie rods in the as-received condition. The heat treatment resulted in a slight decrease in the UTS of the SIK

Table A-1. Hardness Results Before and After Laboratory Heat Treatment HRc 150-kg Major Load

SIK -00938 Before (HRc)	SIK -00938 After (HRc)	PUR -177 Before (HRc)	PUR -177 After (HRc)
41.9	42.3	40.4	42.5
41.9	42.7	40.9	43.4
43.4	42.1	41.3	43.2
41.2	42.9	41.1	43.5
42.5	42.6	41.1	43.7
41.8	43.2	40.7	43.7
40.8	42.9	39.8	43.9
43.0	42.8	40.7	42.7
42.4	42.2	40.0	43.6
43.4	43.1	40.5	43.5
Avg. 42.2	42.7	40.7	43.4

Table A-2. Tensile Properties Before and After Laboratory Heat Treatment

Specimen No.	0.2% YS (psi)	UTS (psi)	RA (%)	EL (%)
SIK - 00938 Before	201,000	203,600	64.6	14.0
SIK -00938 After	190,200	198,000	69.0	13.0
PUR -177 Before	178,200	182,700	67.6	14.4
PUR -177 After	189,800	197,500	66.3	15.0

material (from 204 ksi to 198 ksi), while the PUR material experienced a large increase in UTS (from 183 ksi to 198 ksi).

Fatigue Testing

Fatigue specimens were fabricated by the same machinist utilizing the same process and tooling in order to minimize the effects of machining. This concern was a result of the initial fatigue tests performed on actual tie rods where the failures occurred within the threads of each component. This raised questions concerning the thread dimensions, surface finish, etc., since three different manufacturers were involved in producing the parts. Two fatigue specimens were fabricated from PUR tie rod -177 and two fatigue specimens from SIK tie rod -00938 to the same dimensions as the previous work. Testing was conducted on a Model 8502 Instron servohydraulic test machine with an R value of 0.1 and a frequency of 25 Hz. As dictated by ATCOM, a stress level of 170 ksi was utilized. Table A-3 lists the fatigue test data of the heat-treated specimens and that of the tie rods in the as-received condition. Fatigue data were not generated for SIK tie rod -00938 in the as-received condition, but fatigue data on SIK tie rod -973 in the as-received condition have been included for comparative purposes. It must be noted that only a limited amount of material was available for testing from each rod. The results show that after heat-treating, the PUR material ran out to 3 million cycles, as did the SIK material. Previously, the PUR material experienced failure after 83,020 and 168,567 cycles.

Discussion

The purpose of this experiment was to determine if the heat treatment or cold-working of the threaded regions affected the mechanical properties, primarily fatigue, of the PUR and SIK tie rods. It was deduced that the laboratory heat treatment performed on the SIK material would not result in an increase in mechanical properties because previous test data obtained from this material in the as-received condition indicated that it exceeded the typical properties of the H1050 condition. In fact, the as-received SIK -00938 tie rod exhibited a UTS of 204 ksi, which is 14 ksi above the "typical" range for H1050.[1] However, the PUR material in the as-received condition, although

[1] Armco Inc. "Armco PH 13-8 Mo Stainless Steel (XM-13, UNS S13800)." Product Data Bulletin No. S-24, Middletown, OH, 1964.

Table A-3. Fatigue Results Before and After Laboratory Heat Treatment

Specimen No.	Stress (ksi)	No. of Cycles
SIK -00973 Before	170	3+ million
SIK -00973 Before	170	3+ million
PUR -177 Before	170	168,567
PUR -177 Before	170	83,020
SIK -00938 After	170	3+ million
SIK -00938 After	170	3+ million
PUR -177 After	170	3+ million
PUR -177 After	170	3+ million

meeting the minimal requirement for H1050 (175 ksi), was approximately 7 ksi below "typical" values.

Therefore, it was thought that the PUR material would experience a significant increase in mechanical properties after laboratory heat-treating was conducted. All of the test data collected on the heat-treated PUR material show an increase in mechanical properties, namely, hardness, tensile strength, and fatigue. Based upon this data, it can be stated with confidence that heat treatment played a significant role in the failure of the PUR tie rods to meet the fatigue performance test requirements.

The variation in the amount of cold-working within the threaded regions of the tie rods could not be verified as a cause of the difference observed in the mechanical performance. All of the specimens fabricated were created in such a way as to eliminate any variation in the amount of cold-working on the surfaces of the specimens. However, in the original work, the laboratory mechanical testing still showed differences in the mechanical performance. The work within this appendix only furthers this argument. All of the data acquired demonstrate that the variation in the amount of cold-

working in the threaded regions was not a significant contributor to the difference in mechanical properties.

Conclusions

- The laboratory heat-treated PUR and SIK material subjected to fatigue testing at a stress level of 170 ksi with an R value of 0.1 and a frequency of 25 Hz both exceeded 3 million cycles.

- Heat treatment appears to be the primary factor for the premature fatigue failures of the PUR tie rods.

- Variation in the cold-working within the threaded regions of the original components does not appear to significantly affect the mechanical performance.

NO. OF COPIES ORGANIZATION

2 DEFENSE TECHNICAL INFORMATION CENTER
DTIC DDA
8725 JOHN J KINGMAN RD
STE 0944
FT BELVOIR VA 22060-6218

1 HQDA
DAMO FDQ
DENNIS SCHMIDT
400 ARMY PENTAGON
WASHINGTON DC 20310-0460

1 DPTY ASSIST SCY FOR R&T
SARD TT F MILTON
RM 3EA79 THE PENTAGON
WASHINGTON DC 20310-0103

1 OSD
OUSD(A&T)/ODDDR&E(R)
J LUPO
THE PENTAGON
WASHINGTON DC 20301-7100

1 CECOM
SP & TRRSTRL COMMCTN DIV
AMSEL RD ST MC M
H SOICHER
FT MONMOUTH NJ 07703-5203

1 PRIN DPTY FOR TCHNLGY HQ
US ARMY MATCOM
AMCDCG T
M FISETTE
5001 EISENHOWER AVE
ALEXANDRIA VA 22333-0001

1 PRIN DPTY FOR ACQUSTN HQS
US ARMY MATCOM
AMCDCG A
D ADAMS
5001 EISENHOWER AVE
ALEXANDRIA VA 22333-0001

1 DPTY CG FOR RDE HQS
US ARMY MATCOM
AMCRD
BG BEAUCHAMP
5001 EISENHOWER AVE
ALEXANDRIA VA 22333-0001

NO. OF COPIES ORGANIZATION

1 INST FOR ADVNCD TCHNLGY
THE UNIV OF TEXAS AT AUSTIN
PO BOX 202797
AUSTIN TX 78720-2797

1 USAASA
MOAS AI W PARRON
9325 GUNSTON RD STE N319
FT BELVOIR VA 22060-5582

1 CECOM
PM GPS COL S YOUNG
FT MONMOUTH NJ 07703

1 GPS JOINT PROG OFC DIR
COL J CLAY
2435 VELA WAY STE 1613
LOS ANGELES AFB CA 90245-5500

1 ELECTRONIC SYS DIV DIR
CECOM RDEC
J NIEMELA
FT MONMOUTH NJ 07703

3 DARPA
L STOTTS
J PENNELLA
B KASPAR
3701 N FAIRFAX DR
ARLINGTON VA 22203-1714

1 USAF SMC/CED
DMA/JPO
M ISON
2435 VELA WAY STE 1613
LOS ANGELES AFB CA
90245-5500

1 US MILITARY ACADEMY
MATH SCI CTR OF EXCELLENCE
DEPT OF MATHEMATICAL SCI
MDN A MAJ DON ENGEN
THAYER HALL
WEST POINT NY 10996-1786

1 DIRECTOR
US ARMY RESEARCH LAB
AMSRL CS AL TP
2800 POWDER MILL RD
ADELPHI MD 20783-1145

NO. OF
COPIES ORGANIZATION

1 DIRECTOR
US ARMY RESEARCH LAB
AMSRL CS AL TA
2800 POWDER MILL RD
ADELPHI MD 20783-1145

3 DIRECTOR
US ARMY RESEARCH LAB
AMSRL CI LL
2800 POWDER MILL RD
ADELPHI MD 20783-1145

ABERDEEN PROVING GROUND

4 DIR USARL
AMSRL CI LP (305)

NO. OF COPIES	ORGANIZATION
2	COMMANDER US ARMY MATERIEL CMD AMCSCI AMCQA P S J LORBER 5001 EISENHOWER AVENUE ALEXANDRIA VA 22333-0001
4	CDR HQ AMCCOM AMSMC PCA WM J WELLS AMSMC QAM I G SMITH AMSMC ASR M B KUNKEL J HOUSEMAN ROCK ISLAND IL 61299-6000
7	CDR US ARMY ATCOM AMSAV ECC E BUELTER R LAWYER AMSAV EFM F BARHORST K BHANSALI AMSAV E C SMITH AMCPM AAH D ROBY B KENNEDY ST LOUIS MO 63120-1798
4	CDR CORPUS CHRISTI ARMY DEPOT AMSAV MRPD N HURTA L NERI MAIL STOP 55 SDSCC QLM D GARCIA C WILSON MAIL STOP 27 CORPUS CHRISTI TX 78419-6195
1	CDR US ARMY ARDEC AMSTA CCS C A SEBASTO BLDG 1 PICATINNY ARSENAL NJ 07806-5000

NO. OF COPIES	ORGANIZATION
	ABERDEEN PROVING GROUND
10	DIR USARL AMSRL WM MD S GRENDAHL BLDG 4600

INTENTIONALLY LEFT BLANK.

REPORT DOCUMENTATION PAGE

Form Approved
OMB No. 0704-0188

1. AGENCY USE ONLY *(Leave blank)*	2. REPORT DATE	3. REPORT TYPE AND DATES COVERED
	January 1998	Final, April 1996 - Present

4. TITLE AND SUBTITLE
Investigation of the UH-60 Main Rotor Spindle Assembly Retaining Rods
P/N 70102-08102/-103

5. FUNDING NUMBERS
N/A

6. AUTHOR(S)
Scott M. Grendahl

7. PERFORMING ORGANIZATION NAME(S) AND ADDRESS(ES)
U.S. Army Research Laboratory
ATTN: AMSRL-WM-MD
Aberdeen Proving Ground, MD 21005-5066

8. PERFORMING ORGANIZATION REPORT NUMBER
ARL-TR-1585

9. SPONSORING/MONITORING AGENCY NAMES(S) AND ADDRESS(ES)

10.SPONSORING/MONITORING AGENCY REPORT NUMBER

11. SUPPLEMENTARY NOTES

12a. DISTRIBUTION/AVAILABILITY STATEMENT
Approved for public release; distribution is unlimited.

12b. DISTRIBUTION CODE

13. ABSTRACT *(Maximum 200 words)*

The U.S. Army Research Laboratory (ARL) was tasked by the U.S. Army Aviation and Troop Command (ATCOM) to perform a metallurgical examination of main rotor spindle assembly retaining rods fabricated from precipitation hardened (PH 13-8 Mo) stainless steel by three different manufacturers. These components were subjected to prior spectrum load fatigue testing in order to qualify an alternate source. One of the manufacturer's components exhibited only half the fatigue resistance of the other two. The results of fatigue testing (of coupons sectioned from the original rods) showed a dramatic difference between the rods. Metallography was utilized to examine the microstructure and grain size. The structure of each rod was consistent with the prior treatment, and the grain size met the governing requirement. The amount of delta (free) ferrite within the structure varied slightly from rod to rod, but was well within the specified limits. The threads of each rod were examined metallographically, since this was the area of failure as a result of the spectrum load fatigue testing. Although differences in the surface profile of the threads from the different manufacturers were noted, there was no evidence of gross abnormalities such as tear out or chatter. The chemical analysis of each rod varied, but each composition met the governing requirements. Based upon the results of reheat treating, it was concluded that an inadequate prior heat treatment sequence was performed by the manufacturer.

14. SUBJECT TERMS
UH-60, tie rod, PH 12-8, Mo stainless steel, fatigue, mechanical testing

15. NUMBER OF PAGES
106

16. PRICE CODE

17. SECURITY CLASSIFICATION OF REPORT	18. SECURITY CLASSIFICATION OF THIS PAGE	19. SECURITY CLASSIFICATION OF ABSTRACT	20. LIMITATION OF ABSTRACT
UNCLASSIFIED	UNCLASSIFIED	UNCLASSIFIED	UL

INTENTIONALLY LEFT BLANK.

USER EVALUATION SHEET/CHANGE OF ADDRESS

This Laboratory undertakes a continuing effort to improve the quality of the reports it publishes. Your comments/answers to the items/questions below will aid us in our efforts.

1. ARL Report Number/Author ARL-TR-1585 (Grendahl) Date of Report January 1998

2. Date Report Received _____

3. Does this report satisfy a need? (Comment on purpose, related project, or other area of interest for which the report will be used.) _____

4. Specifically, how is the report being used? (Information source, design data, procedure, source of ideas, etc.) _____

5. Has the information in this report led to any quantitative savings as far as man-hours or dollars saved, operating costs avoided, or efficiencies achieved, etc? If so, please elaborate. _____

6. General Comments. What do you think should be changed to improve future reports? (Indicate changes to organization, technical content, format, etc.) _____

CURRENT ADDRESS

Organization

Name E-mail Name

Street or P.O. Box No.

City, State, Zip Code

7. If indicating a Change of Address or Address Correction, please provide the Current or Correct address above and the Old or Incorrect address below.

OLD ADDRESS

Organization

Name

Street or P.O. Box No.

City, State, Zip Code

(Remove this sheet, fold as indicated, tape closed, and mail.)

(DO NOT STAPLE)

DEPARTMENT OF THE ARMY

OFFICIAL BUSINESS

NO POSTAGE
NECESSARY
IF MAILED
IN THE
UNITED STATES

BUSINESS REPLY MAIL
FIRST CLASS PERMIT NO 0001,APG,MD

POSTAGE WILL BE PAID BY ADDRESSEE

DIRECTOR
US ARMY RESEARCH LABORATORY
ATTN AMSRL WM MD
ABERDEEN PROVING GROUND MD 21005-5066